

NPS ARCHIVE
1959
PEARSON, M.

DESIGN, ANALYSIS AND TEST OF A
D C SERVOMECHANISM UTILIZING DIRECT DRIVE

MARTIN PEARSON
AND
DONALD W. TARDIF

LIBRARY
U.S. NAVAL POSTGRADUATE SCHOOL
MONTEREY, CALIFORNIA

DESIGN, ANALYSIS AND TEST
OF A DC SERVOMECHANISM
UTILIZING DIRECT DRIVE

by

Martin Pearson

//

Major, United States Marine Corps

Donald W. Tardif

Major, United States Marine Corps

Submitted in partial fulfillment
of the requirements
for the degree of
MASTER OF SCIENCE
IN
ELECTRICAL ENGINEERING

United States Naval Postgraduate School
Monterey, California

1959

NES ARCHIVE

1959

PEARSON, M.

Thesis
~~PBN~~

DESIGN, ANALYSIS AND TEST
OF A DC SERVOMECHANISM
UTILIZING DIRECT DRIVE

* * * * *

Martin Pearson

and

Donald W. Tardif

DESIGN, ANALYSIS AND TEST
OF A DC SERVOMECHANISM
UTILIZING DIRECT DRIVE

by

Martin Pearson

and

Donald W. Tardif

This work is accepted as fulfilling
the thesis requirements for the degree of
MASTER OF SCIENCE
IN
ELECTRICAL ENGINEERING
from the
United States Naval Postgraduate School

ABSTRACT

The direct drive DC motor as a component part of a servomechanism system utilized in stabilized platform control offers a great deal of promise from the standpoint of system accuracy and performance. The authors have endeavored to develop means of predicting system performance and of improving the response characteristics of this type of control system. From investigations conducted at the Dalmo Victor Company, Belmont, California, and at the United States Naval Postgraduate School, Monterey, California, it is the opinion of the authors that direct drive DC motors used in servo systems provide the servo engineer with two principle advantages over the conventional AC servo motor used in the same application. These are:

1. Backlash elimination caused by gear train assemblies.
2. Servo resonance reduction caused by springy shafts.

The investigation pointed out a glaring weakness in the current state of the art in regard to power amplification. Although well-known for many years, the absence of a suitable DC power amplifier greatly restricts the use of equipment of this type. It is felt that the development of the power transistor will alleviate this problem. The authors feel strongly that when the amplifier problem is solved, the direct drive DC motor will replace the AC motor in many servo applications.



The authors gratefully acknowledge the advice and assistance provided by Dr. R.C.H. Wheeler of the United States Naval Postgraduate School.

TABLE OF CONTENTS

CERTIFICATE OF APPROVAL	i
ABSTRACT	ii
TABLE OF CONTENTS	iv
LIST OF ILLUSTRATIONS	v
CHAPTER	
I Introduction	1
II Historical Review and Statement of the Problem	4
III Preliminary Analysis and Design: Torque Motor and Servo System	19
IV Direct Drive Torque Motors	47
V Intermediate Analysis and Design; Torque Motor and Servo System	101
VI Evaluation of the Closed Loop System	112

LIST OF ILLUSTRATIONS

Chapter	Figure	Title	Page
II	1	Parallel Gear Trains Driven by Two Motors to Eliminate Backlash	6
	2	Parallel Gear Trains Driven by a Single Motor With Gear Trains Wound Up so that They Will Continuously Load Each Other	7
	3	Parallel Gear Trains With Motors Energized so that One Drives One Direction and One the Other	9
	4	Simplified Gear Train with a Single Shaft which Can Twist as Load is Applied	10
	5	System of Fig. 4 with Load Inertia Referred Back to the Motor	12
	6	Simple Motor Drive with Output Position θ_M	14
	7	Frequency Response of an Actual System with the Transfer Function Given by EQ 5	17
	8	(A) Normal Power Drive With Gearing to Reduce Motor Speed from 2000RPM to 5 RPM	19
	(B) Direct Drive in Which Motor Moves Load Without the Use of a Gear Train	21	
III	1	Generalization of Output Torque in Direct Drive DC Motors	21
	2	Logarithmic Plot, Motor Alone	27
	3	Single Axis Inertial Space Stabilization System Using a Direct Drive DC Torque Motor to Position the Controlled Member	29
	4	Servo Block Diagram Representation of Fig. 3	30

Chapter	Figure	Title	Page	
III	5	Logarithmic Plot, Motor-Load Combination	31	
	6	Servo Block Diagram of Compensated System	33	
	7	Logarithmic Plot, Motor-Load Combination Lead Compensated	35	
	8	Servo Block Diagram: Lead-Tachometer Compensated System	37	
	9	Logarithmic Plot, Motor-Load Combination Lead-Tachometer Compensated	40	
	10	Logarithmic Plot, Preliminary Design	42	
	11	MN Chart Lead-Tachometer Compensated System	43	
	12	M&N Versus W Lead-Tachometer Compensated System	44	
	13	Transient Response Preliminary Design	46	
	IV	1	Rotor Current Versus Torque (Manufacturer's Data)	48
		2	Cutaway View of Torque Motor T2108A	54
		3	Plot of generated voltage versus angular velocity	59
		4	Plot of $(E - IR)$ versus angular velocity for motor-load combination	62
5		Motor bracket for torque measurements (front view)	66	
6		Motor bracket for torque measurements (rear view)	67	
4B		Mounting bracket for motor, tachometer and synchro pickoffs	63	
4A		Motor disassembled	64	

Chapter	Figure	Title	Page
	7	Plot of stalled (output) torque versus armature current.	70
	8	Plot of stalled (output) torque versus armature current.	72
	9	Plot of stalled (output) torque versus armature current.	75
	10	Types of friction torque.	78
	11	Plot of coulomb and viscous friction versus speed.	80
	12	Plot of output torque versus speed (steady state).	84
	13	Plot of output torque versus speed (steady state).	87
	14	Plot of output torque versus armature current.	88
	15	Plot of output torque versus armature current.	89
	16	Recording of motor-load combination transient response.	91a
	17	Picture of motor transient.	94
	18	Mechanical low frequency oscillator	95
	20	Frequency response of motor without load.	98
	21	Inertia load and gears (physical dimensions).	99
V	1	Plot of r and ϕ versus angular speed.	103
	2	Plot of r and ϕ versus angular speed for intermediate design.	106
	3	MN chart for intermediate design.	107
	4	Plot of M and N versus angular speed for intermediate design.	108
	5	Plot of transient response of intermediate design.	110

Chapter	Figure	Title	Page
VI	1	Block diagram of closed loop system.	113
	2	Laboratory setup of closed loop system.	114
	3	Circuit diagram of DC power amplifier	116
	4	Circuit diagram of phase splitter.	117
	5	Circuit diagram of AC amplifier in tachometer loop.	118
	6	Circuit diagram of demodulators.	120
	7	Circuit diagram of lead network and filters.	121
	8	Block diagram of 5 cps system	122
	9	Plot of data for determining position gain.	125
	10	Velocity gain evaluation.	126
	11	Filter and lead net zero frequency gain.	126
	12	Plot of data for determining torque gain constant.	127
	13	Dead zone.	128
	14	Accelerometer nomograph	129
	15	Schematic of solartron in position loop.	130
	16	Transient response of final closed loop system (15 cps).	132
	17	Frequency response of final closed loop system.	134



CHAPTER I

INTRODUCTION

The use of the AC motor is widespread in applications where the continuous positioning type of a servo is used. Of equal use is the standard gear train assembly whereby the load is coupled to the torque producing source. Much has been written about these conventional methods of servo control, and the state of the art is probably as advanced as it will ever be. The engineer who is vexed by the practical problems of the non-linearity introduced by backlash when using these conventional methods is usually content to obtain high precision instrument gearing, drive the load through this sophisticated system and then hope that the load follows within the accuracy required. Another problem introduced by the gear train assembly is mechanical resonance which may cause the servo to oscillate in an unruly manner when the gain is increased.

High performance servo control systems demand more smoothly operating power drives without these normally attendant backlash and resonance problems. Although it has been known for some time that direct drive DC torque motors in this application can solve most of the problems mentioned above, little has been done in the mathematical treatment of such systems and the correlation with actual tests.

The objective of this paper, then, is to report on the design, analysis, and test of a position servo utilizing a

direct drive DC motor for use in single axis stabilized platform control.

Chapter II is an historical review and statement of the problem. It is intended that this chapter will point out the requirements for the study.

Chapter III presents the preliminary analysis and design. Included is a mathematical treatment of the torque motor alone and a comprehensive study of the servo system, including compensation, and culminates in a preliminary design. Calculations are based on manufacturer's characteristics for system components.

Chapter IV includes a detailed discussion of the torque motor and its use in the application described. Results of motor tests are presented and these experimentally obtained characteristics are compared with the manufacturer's characteristics.

Chapter V presents the intermediate design of the servo system based on the experimentally obtained data for system components.

Chapter VI includes the experimental verification of the intermediate design and an analysis and discussion of the results obtained. A final design is presented based on the experimental data and this design is compared with both the preliminary and intermediate designs.

An explanation of the approach to this problem appears worthwhile. At the time the authors were ready to begin

experimental work on the motor, difficulties were encountered in the construction of a suitable amplifier and motor-mounting facilities. In view of the relatively short period reserved for a thesis investigation, it was decided to proceed with a preliminary analysis based on the manufacturer's data rather than to waste valuable time in awaiting proper facilities. As facilities became available an intermediate analysis was made based on actual motor characteristics obtained through experimentation. Then as the amplifier was completed, the servo loop was closed and a final design was obtained.

The analysis includes a number of figures and charts which are numbered consecutively within each chapter. Unless otherwise noted, the figures discussed refer to those within the chapter under consideration.

CHAPTER II

HISTORICAL REVIEW AND STATEMENT OF THE PROBLEM

General

The principal non-linearity introduced into a servo system by the conventional gear train assembly is caused by backlash. Gear trains also contribute to mechanical resonance problems which are difficult to predict and may cause the servo to oscillate at various frequencies or gain settings. A brief discussion of these difficulties and current methods of control or elimination are included in this chapter.

Backlash Elimination

Techniques generally applied to remove backlash from instrument power gearing now find applications to servo systems. Split gears are an obvious remedy. Their use does reduce backlash (if they are made with stiff enough spring constants) but will add to the friction load and provide additional resonance effects. In addition, their expense and short life have all contributed to the general reluctance on the part of engineers to consider their use on a wide scale.

Split gears also must have wider gear faces for two reasons:

- (1) Each half of the gear must be capable of driving the full torque requirement.
- (2) If the split gear is not to open up under the load, it must continually have a loading equivalent to the peak torque capability of the drive at the mesh in question.

These wide gears, of course, increase the friction load and contribute to the weight and bulk of the system, an important consideration in this day of miniturization.

The parallel gear train approach shown in Figure 1 is sometimes used. Here two motors are electrically connected in series, each driving the load through a separate gear train. The pinion gears are placed nearly 180 degrees apart on the full gear in order to eliminate as much as possible the opening of the full gear mesh due to the torque of the pinions. This arrangement also removes side thrust from the bearing supporting the load. Furthermore, care is taken to insure that the two gear trains do not mesh identically at the same time. Here again, two motors and associated power requirements may negate the value of the approach by increasing the weight and bulk.

Figure 2 shows another approach in which two gear trains are driven in parallel from a single motor. Before the common mesh at the motor end is completed, the gear trains are wound up so that they will continually load each other.

This method has the same disadvantages as split gears, giving high friction and continual high tooth face loading. In fact, two identical sets of ship propulsion gears are often tested in this way in order to obtain the high tooth-face loading required without using undue amounts of power. Even if this method could eliminate backlash, the increased friction would probably introduce a non-linearity of greater magnitude than the one eliminated.



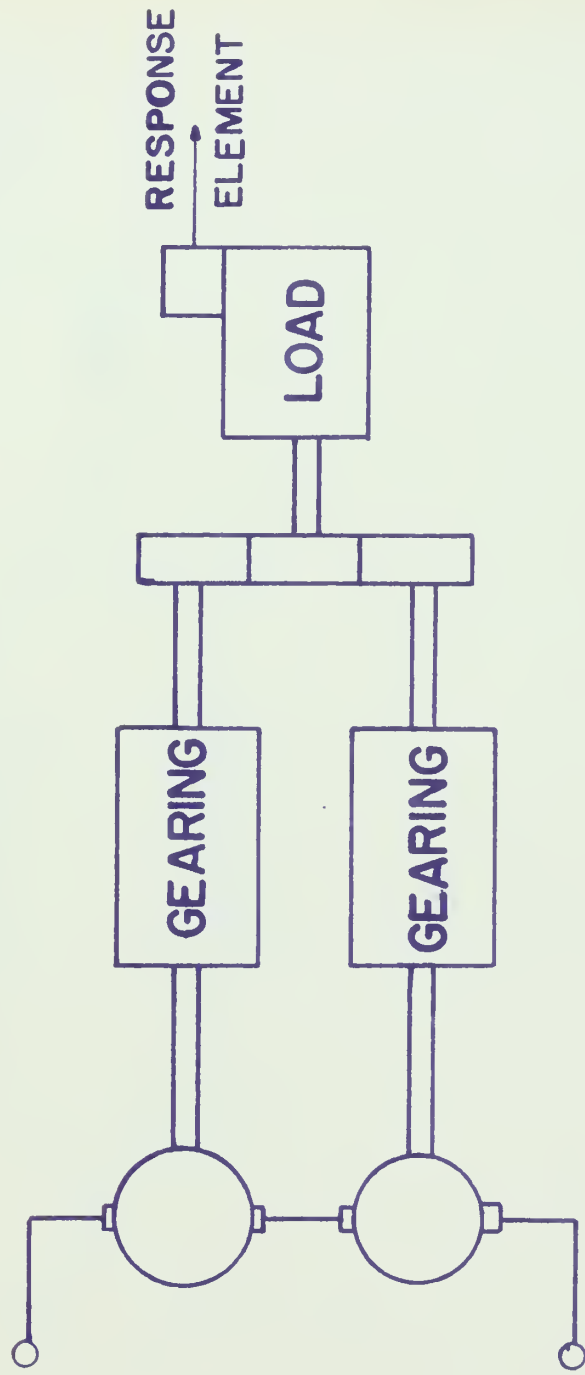


FIG 1 - PARALLEL GEAR TRAINS DRIVEN BY TWO MOTORS
TO ELIMINATE BACKLASH



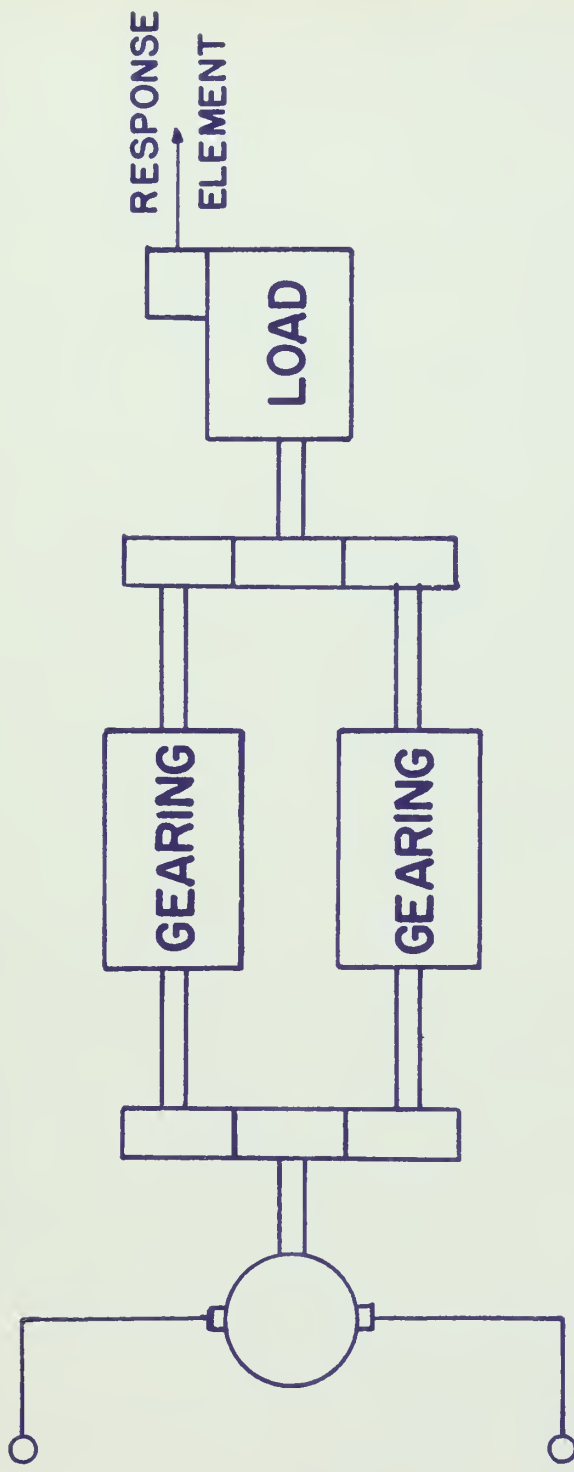


FIG 2 - PARALLEL GEAR TRAINS DRIVEN BY A SINGLE MOTOR WITH GEAR TRAINS WOUND UP SO THAT THEY WILL CONTINUOUSLY LOAD EACH OTHER

A final method of eliminating backlash that has had some use is shown in Figure 3. Here the motors are separately controlled, one driving the load clockwise and the other driving counter-clockwise. At standstill each motor draws the same amount of idling power, but for creeping speeds the power in one motor is decreased while that in the other is increased. Note that, when driving at high speeds, say, in a counter-clockwise direction, some precaution must be taken to prevent the clockwise drive motor from acting as a generator and dissipating most of the developed power in its armature circuit. Thus the armature circuit for either motor must have a low impedance when driving but a high impedance when being driven. This may be virtually impossible to attain but even if such a system were a reality, it would have the same disadvantages of the techniques mentioned above.

Servo Resonance

While the limitations imposed on servo performance by gearing backlash are more or less easily understood, the problem of resonance and its location in the system and subsequent analysis has not been given a great deal of attention. This is due to the fact that resonance is almost impossible to predict with any degree of accuracy. Yet, a predominant source of mechanical resonance in many systems is the gear train. Figure 4 shows an oversimplified gear train being driven by a motor and having a single shaft which can twist as load is applied. By referring the load to the

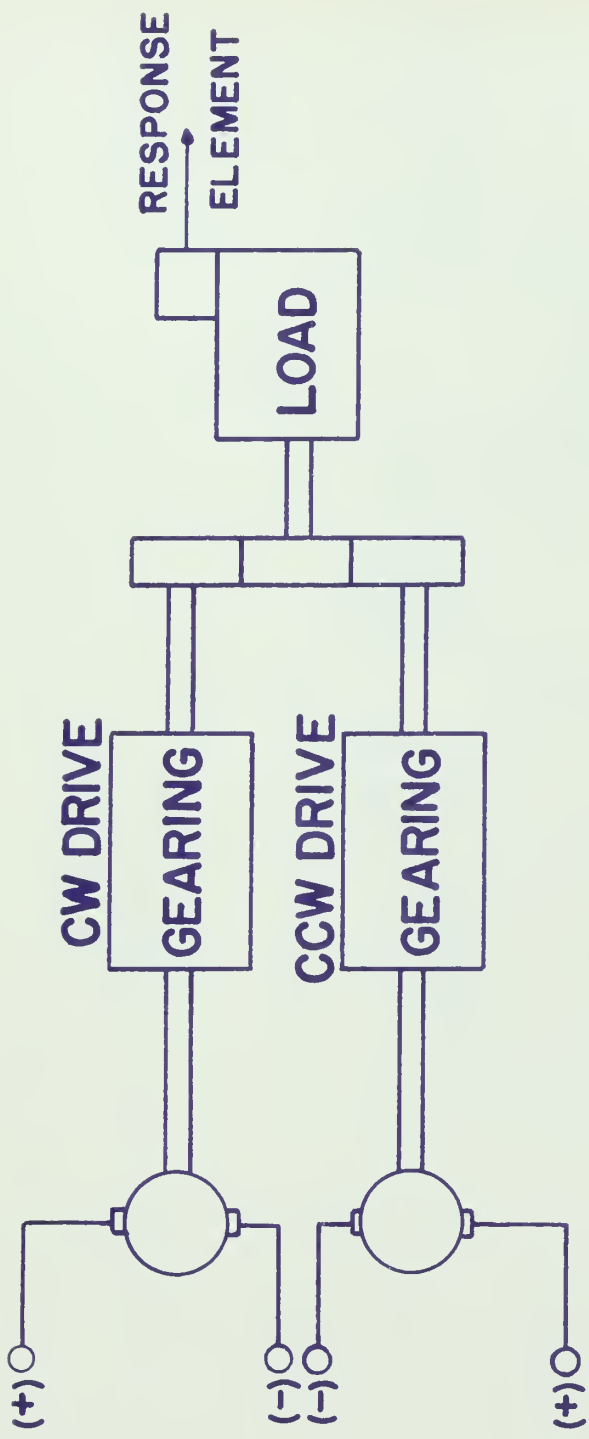


FIG 3- PARALLEL GEAR TRAINS WITH MOTORS ENERGIZED SO THAT ONE DRIVES ONE DIRECTION AND ONE THE OTHER

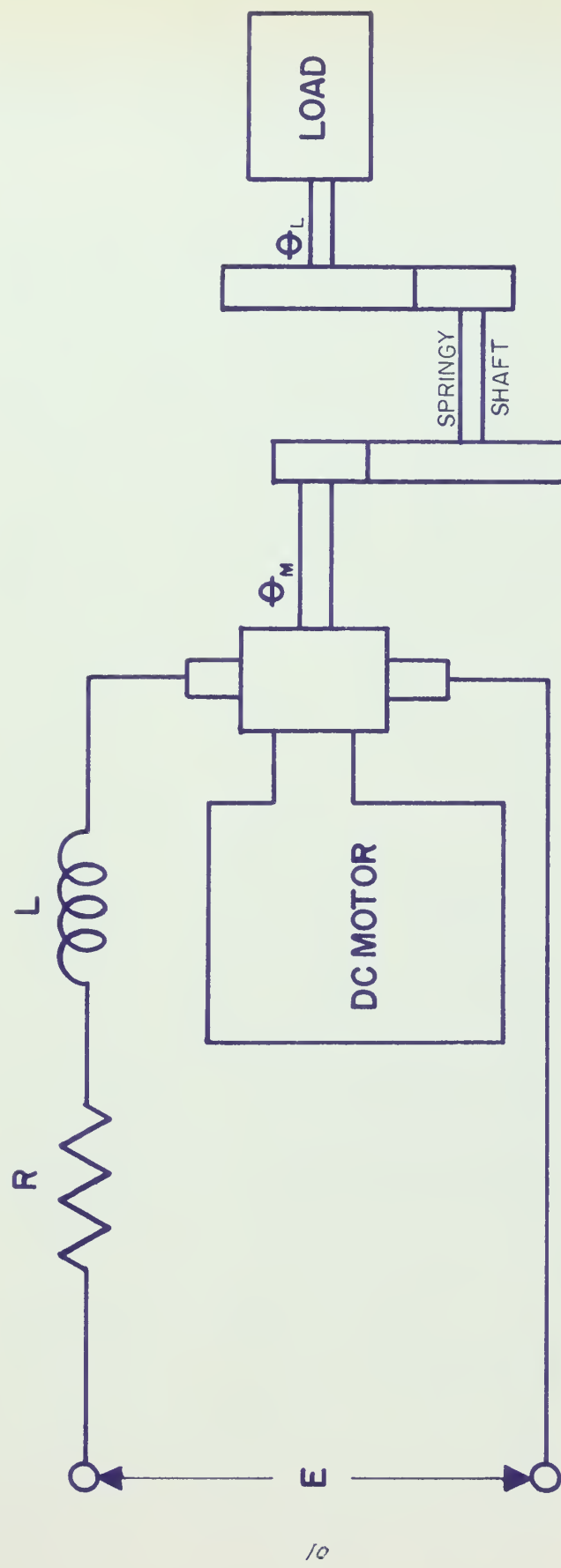


FIG 4 – SIMPLIFIED GEAR TRAIN WITH A SINGLE SHAFT WHICH CAN TWIST AS LOAD IS APPLIED

drive by use of the square of the gear ratio, the system of Figure 4 may be further simplified to produce Figure 5. The only viscous damping shown is between the load and ground.

When analyzing servo resonance, of primary interest is the motor transfer function which gives the relationship between the load shaft position or motor shaft position and armature applied voltage; this function will be found by considering first θ_L and then θ_m as the shaft position of interest. θ_L is of interest when considering systems where the response element, usually a synchro pickoff, is driven from the load when the load is separated from the motor by instrument gearing. θ_m is the shaft of interest when the pickoff is driven directly from the motor shaft. Typical units are shown in parenthesis.

E = applied voltage (volts)

R = armature resistance (ohms)

L = armature inductance (henries)

K = spring constant of shaft (lb.in./radian)

J_M = inertia of motor plus inertia of gearing on the motor end of the spring shaft (lb.in.sec.²)

J_L = inertia of load plus inertia of gearing on the load end of the spring shaft (lb.in.sec.²)

β = viscous damping (lb.in./radian/sec.)

θ_m = position of the motor end of the spring shaft (radians)

θ_L = position of the load end of the spring shaft (radians)

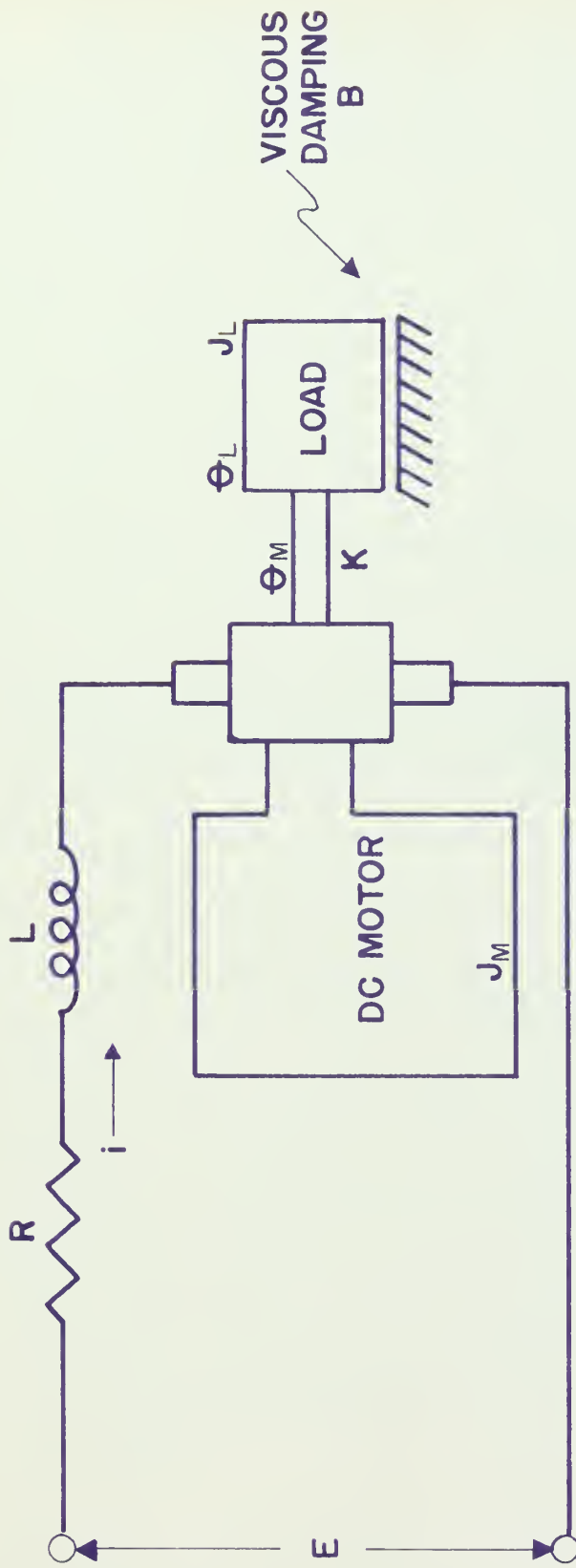


FIG 5- SYSTEM OF FIG 4 WITH LOAD INERTIA REFERRED BACK TO THE MOTOR

K_v = back emf constant of motor (volts/rad/sec)

K_t = torque constant of motor (.lb.in./amp.)

Three basic equations may be written as follows, the first being a voltage equation, the second and third being torque equations:

$$(1) E = i(R + SL) + K_v S \theta_M$$

$$(2) K_t i = J_M S^2 \theta_M + J_L S^2 \theta_L + B S \theta_L$$

$$(3) K(\theta_M - \theta_L) = J_L S^2 \theta_L + B S \theta_L$$

From these equations, the transfer function θ_L/E is found to be:

$$(4) \frac{\theta_L}{E} = \frac{K_t / (K_t K_v + BR)}{S^4 \left[\frac{J_L J_M L}{K(K_t K_v + BR)} S^4 + \frac{J_L J_M R + B J_M L}{K(K_t K_v + BR)} S^3 + \frac{J_L K_t K_v + B J_M R + J_M L K + J_L L K}{K(K_t K_v + BR)} S^2 + \frac{B K_t K_v + J_M R K_t J_L R + K B L}{K(K_t K_v + BR)} S + 1 \right]}$$

$\frac{\theta_M}{E}$ is found to be

$$(5) \frac{\theta_M}{E} = \frac{K_t \left[\left(\frac{J_L S^2}{K} \right) + \left(\frac{B S}{K} \right) + 1 \right]}{S (K_t K_v + BR) \left(\text{SAME QUARTIC AS } \frac{\theta_L}{E} \right)}$$

The following analysis concerning equations (4) and (5) is included to emphasize four important points:

1. Springy shafts complicate transfer functions.
2. Synchro pickoffs driven from the load (where the load is separated from the motor by a gear train assembly) contribute to the mechanical resonance problems.

3. Phase shift at the lower and middle frequencies as a result of gear backlash and springy shafts cannot be tolerated in high performance servo systems.
4. The above problems are largely eliminated when direct drive DC motors are used in servo systems.

Comparison of equations (4) and (5) indicates that they both have the same denominator, but the numerator of equation (5) has a quadratic that does not appear in equation (4). The significance of this quadratic is very important, as will be shown. But first, for further comparison, the usual motor transfer function uncluttered with spring shafts and other complications is given (refer to Figure 6). This transfer function will be derived in Chapter III.

J = inertia of motor, gearing, load

$= J_L + J_M$ in absence of springy shaft (lb.in.sec.²)

θ = motor position = $\theta_m = \theta_L$ in absence of springy shaft (radians)

$$(6) \quad \frac{\theta}{E} = \frac{1}{K_v S \left[\frac{JL}{K_v K_t} S^2 + \frac{JR}{K_v K_t} S + 1 \right]}$$

The methods for providing feedback are relatively simple and well known for a system of this type. If the system is similar to Figure 5, however, the motor transfer function is no longer simple, being either equation (4) or (5). Location of the synchro pickoff (hereafter referred to as the response element) so that it moves exactly with θ_m will give the trans-

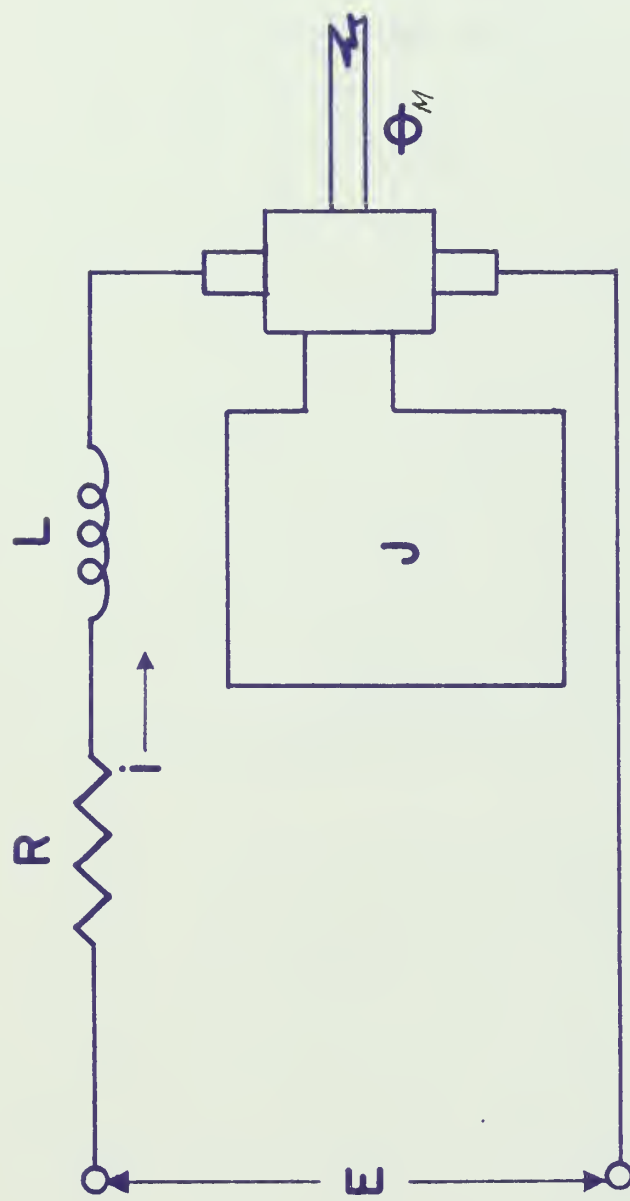


FIG 6 – SIMPLE MOTOR DRIVE WITH OUTPUT POSITION Φ_M

fer function of equation (5). Even though the transfer function is rather complex, the maximum ultimate phase shift is 270 degrees due to the presence of the quadratic in the numerator; the same as for equation (6) and, although performance may be slightly compromised due to the resonance effects, the servo may still be stabilized in a straight-forward manner. But if the response element is mounted on the end of the springy shaft opposite the motor so that it moves with θ_L , the transfer function of equation (4) applies. This will give an additional 180 degrees of phase shift for a total of 450 degrees. This phase shift will not in itself cause instability but does interfere with the performance of the system by producing a large phase lag at both the lower and the higher frequencies. In gyro stabilized systems this problem is critical because the systems are required to operate at frequencies ranging from 0 to 200 radians per second.

Of course, it is realized that the values of phase shift quoted above refer to infinite frequencies. However, a detailed examination of the transfer functions presented as equations (4) and (5) with typical values substituted for the parameters therein, reveals a large amount of phase shift at the lower frequencies, approaching 180 degrees. Where the pickoff is driven from the motor shaft, the phase shift at lower frequencies is not quite as great but still too large to tolerate.

While it is difficult to generalize, the limiting mechanical resonance of a system is often in the gear train and may be caused by shaft twisting, shaft bending and deflection, bearing deflection, split gears or other effects. Building a system with the response element driven directly from a motor shaft will render the transfer function of equation (5). This type system is satisfactory if one is willing to accept the mechanical resonance problems because the phase shift at higher frequencies can be compensated for. The frequency response of an actual system built in this manner is shown in Figure 7, except that the transfer function used is $S\theta_m/E$ instead of θ_m/E . For comparison, the same plot with the load disconnected from the gear train is also given. Note that the resonance effects disappear. A system built according to Figure 1, 2, or 3 with a load speed response element will invariably produce the transfer function of equation (4) together with its problem of large phase shifts at the lower frequencies in addition to the resonance problems.

In reality, for the newer, truly high performance systems, use of methods outlined in Figures 1, 2, and 3 (and other similar methods not illustrated) to overcome the problems of conventional designs have proven to be gap-filler approaches. Like all such expedients making use of presently available knowledge, they do not solve the problem to the complete satisfaction of the servo design engineer. What really is

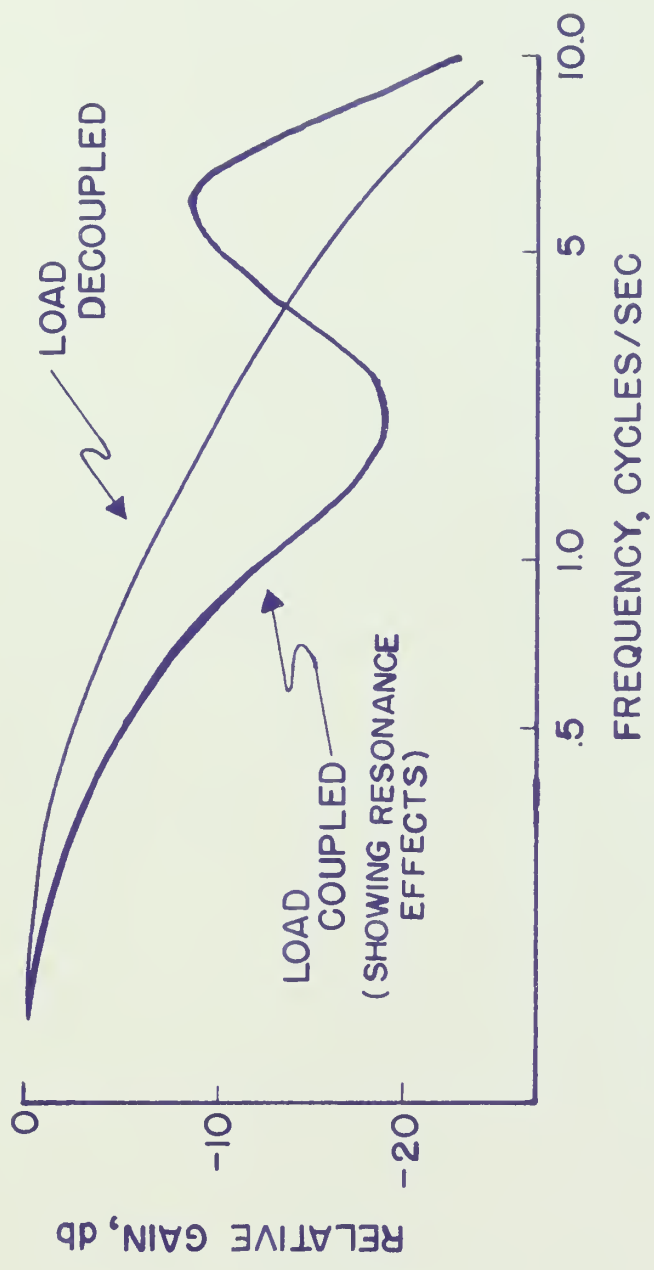


FIG 7 - FREQUENCY RESPONSE OF AN ACTUAL SYSTEM WITH THE TRANSFER FUNCTION GIVEN BY EQ 5

needed is the complete elimination of the gear train as illustrated by Figure 8. If this can be done, both resonance and backlash effects can be completely disregarded and the system can be described by equation (6). This, of course, is the substance of this thesis and the basis upon which the following chapters are built.

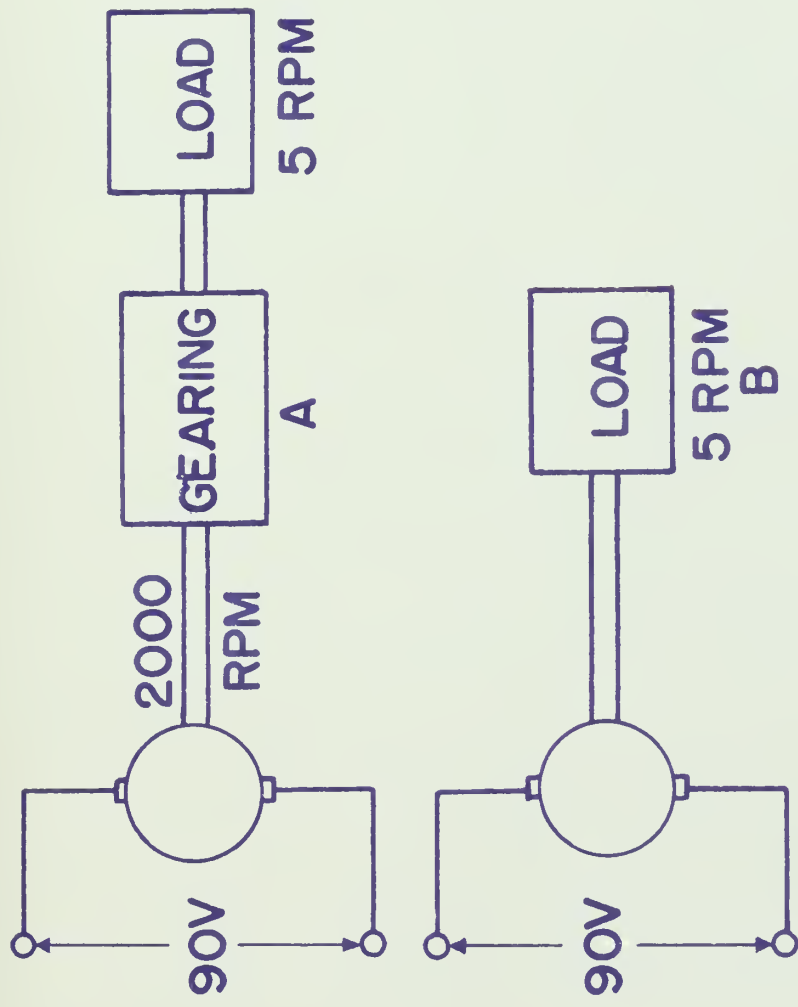


FIG 8 (A) NORMAL POWER DRIVE WITH GEARING TO REDUCE MOTOR SPEED FROM 2000 RPM TO 5 RPM
 (B) DIRECT DRIVE IN WHICH MOTOR MOVES LOAD WITHOUT THE USE OF A GEAR TRAIN

CHAPTER III

PRELIMINARY ANALYSIS AND DESIGN: TORQUE MOTOR AND SERVO SYSTEM

Based on the advice and recommendations of the Servo Department, Dalmo Victor Company, Belmont, California, an experienced company in the field of stabilized platforms, involving servo control, the design requirements and goals of the system under consideration were stipulated as follows:

1. Requirements of Load

- a. Single axis platform
- b. Continuous rotation
- c. Load inertia: $50 \text{ lb.in.}^2 = .13 \text{ lb.in.sec.}^2$
- d. Mass unbalance and gimbal friction small
- e. Maximum velocity: 2 rad/sec.
- f. Maximum velocity: 1 millirad/sec.
- g. Maximum acceleration: 20 rad./sec.²

2. Position Loop

- a. Static accuracy 1.5 milliradian
- b. Gain crossover frequency: 15 cps
- c. Gain of loop at 1 cps: 40 db
- d. Smooth tracking at 1 millirad/sec.

3. Stabilization Loop

- a. Static accuracy: 1.5 millirad or better

Dalmo Victor Company, Belmont, California to provide:

- (1) Mechanical design and construction of gimbal drive.
- (2) Design and construction of servo amplifier.

(3) Torque motor T-2108A (Inland Motor Corporation,
Pearl River, New York.)

Mathematical Analysis - Motor Transfer Function

Of primary consideration is the motor transfer function which gives the relationship between motor shaft position and armature applied voltage. Figure 1 indicates the equivalent circuit when the load is attached to the motor shaft.

E = applied voltage (volts) (input signal)

R = armature resistance (ohms)

L = armature inductance (henries)

\mathcal{E}_b = back electromotive force (volts)

T = motor torque (in.lbs.)

i = current (amperes)

J_L = load inertia (lb.in.sec.²)

J_m = motor inertia (lb.in.sec.²) (load and Motor)

J = $J_L + J_m$ (total inertia)

θ = output shaft position (radians)

K_t = torque constant motor (in.lb/amp.)

K_v = back emf constant (volt/rad/sec.)

B = motor friction, viscous

A = step input, A magnitude

Proceeding in the conventional manner and using the La Place Transformation, the motor-load transfer function can be derived as follows:

The back emf is proportional to speed,

$$1. \quad \mathcal{E}_b = K_v S \theta$$

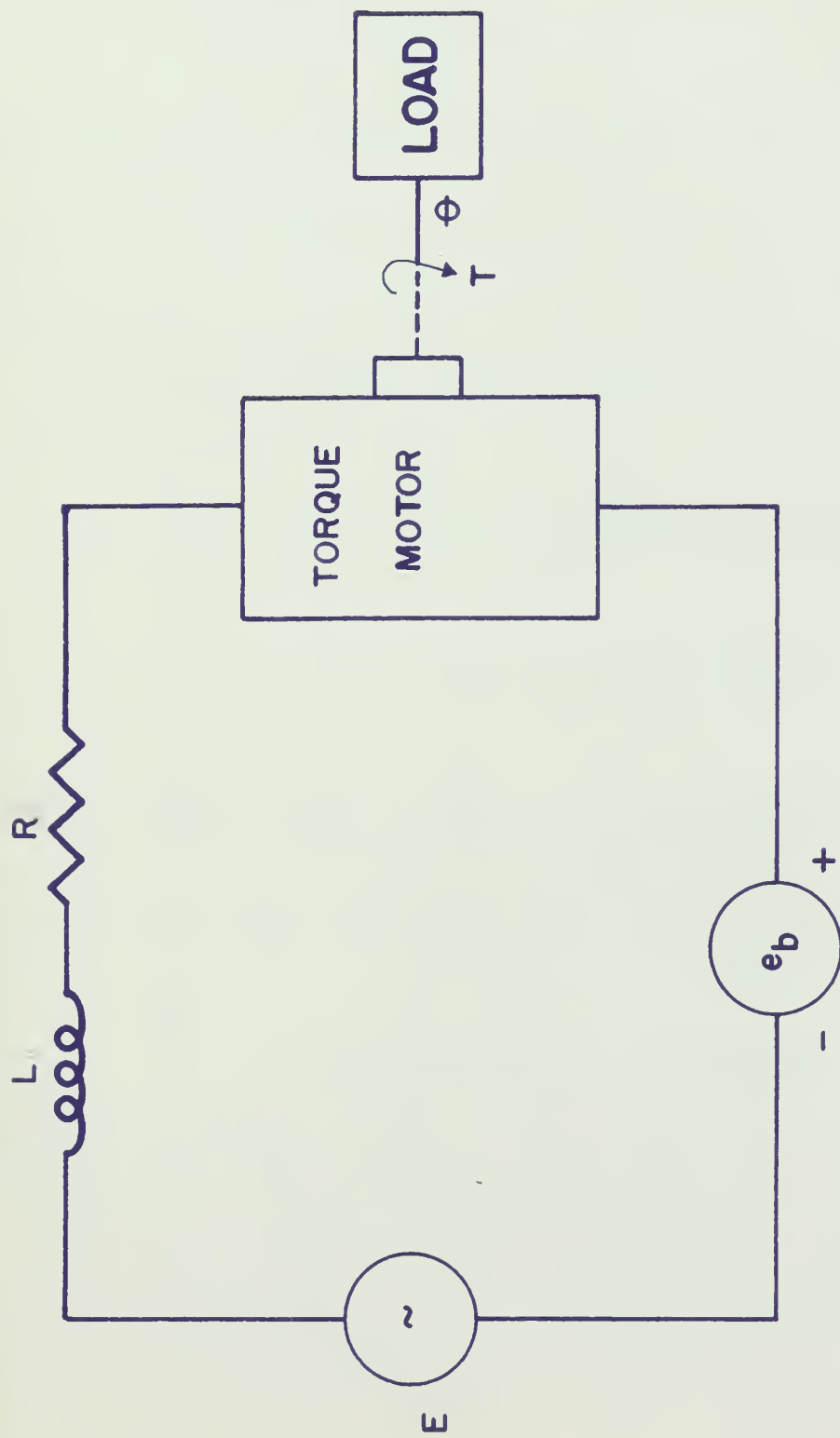


FIG 1 GENERALIZATION OF OUTPUT TORQUE IN DIRECT DRIVE D.C. MOTORS

and torque is proportional to current.

$$2. T = K_t i$$

The torque absorbed by the load,

$$2a. T = (JS^2 + BS) \theta_o$$

The armature current depends on effective voltage,

$$3. i = \frac{E - \ell_b}{R + SL}$$

Simplifying and substituting,

$$4. K_t \left(\frac{E - K_v S \theta_o}{R + SL} \right) = S^2 J \theta_o + BS \theta_o$$

and

$$5. K_t E = [S^3 J L + (JR + BL) S^2 + (K_t K_v + BR) S] \theta_o$$

$$6. K_t E = S [S^2 J L + (JR + BL) S + (K_t K_v + BR)] \theta_o$$

thus,

$$7. \frac{\theta_o}{E} = \frac{K_t}{S [S^2 J L + (JR + BL) S + (K_t K_v + BR)]}$$

simplified, the motor-load transfer function becomes:

$$8. \frac{\theta_o}{E} = \frac{\frac{K_t}{J L}}{S [S^2 + S \left(\frac{JR + BL}{J L} \right) + \left(\frac{K_v K_t + BR}{J L} \right)]}$$

Motor Time Constants

In the past, servo motors have been designed with armatures shaped like right circular cylinders (i.e., axially long but small in diameter). This design minimizes motor inertia and consequently the motor inertial time constant.

Examination of the denominator quadratic of equation

(8) will illustrate this fact.

$$9. S^2 + S \left(\frac{JR+BL}{JL} \right) + \left(\frac{KR K_t + BR}{JL} \right)$$

Factoring the quadratic:

$$\frac{- \left(\frac{JR+BL}{JL} \right) + \sqrt{\left(\frac{JR+BL}{JL} \right)^2 - 4 \left(\frac{KR K_t + BR}{JL} \right)}}{2}$$

which is:

$$\left[S + \frac{JR+BL}{2JL} + \sqrt{\left(\frac{JR+BL}{2JL} \right)^2 - \left(\frac{BR+KR K_t}{JL} \right)} \right] \left[S + \frac{JR+BL}{2JL} - \sqrt{\left(\frac{JR+BL}{2JL} \right)^2 - \left(\frac{BR+KR K_t}{JL} \right)} \right]$$

The term $\left(\frac{JR+BL}{2JL} \right)^2$ is much greater than the term $\left(\frac{BR+KR K_t}{JL} \right)$

and thus the factor in the first brackets above becomes

$\left(S + \frac{R}{L} + \frac{B}{J} \right)$. In general, the term $\frac{R}{L} \gg \frac{B}{J}$ and thus the first factor becomes $\left(S + \frac{R}{L} \right)$.

The second factor is determined by the difference of two nearly equal values. Applying the binomial expansion theorem to the radical and evaluating the result, the factor reduces to $\left(S + \frac{BR+KR K_t}{JR+BL} \right)$. Since $JR \gg BL$, the factor can be simplified to $\left(S + \frac{BR+KR K_t}{JR} \right)$.

Equation 8 becomes:

$$\frac{\theta_0}{E} = \frac{\frac{K_t}{JL}}{S \left(S + \frac{R}{L} \right) \left(S + \frac{BR+KR K_t}{JR} \right)}$$

which is:

$$\frac{\theta_0}{E} = \frac{\frac{K_t}{BR+KR K_t}}{S \left(\frac{L}{R} S + 1 \right) \left(\frac{JR}{BR+KR K_t} S + 1 \right)}$$

Since $K_v K_t \gg BR$, (as later verified by experimentation) equation 8 becomes:

$$10. \frac{\theta_o}{E} = \frac{1}{K_v S \left[\left(\frac{JR}{K_v K_t} S + 1 \right) \left(\frac{L}{R} S + 1 \right) \right]}$$

The first time constant, $\frac{JR}{K_v K_t}$, is the inertial time constant and is a measure of time required for motor to come up to speed, the motor reaching 63 per cent of speed in one time constant. The second time constant $\frac{L}{R}$, called the electrical time constant, is inductive and is a measure of time required for current to build up to final level in the armature. This latter time constant is always smaller than the inertial time constant, however, both should be kept at a minimum for optimum system performance.

Prior to a mathematical treatment of the motor-load combination, it was decided to obtain the motor transfer function alone. Based on the data presented in the manufacturer's characteristics handbook the following information was obtained:

<u>List of Standardized Ratings</u>	<u>T-2108A</u>
Peak Torque, lb.in.	3.72
Sensitivity, lb.in./amp.	7.92
DC Resistance at 25°C, ohms	193
Self Inductance, henries	.10
Temperature Rise per Watt, °C	5.3°

List of Standardized Ratings (cont.)T-2108A

Max. Permissible Temp., $^{\circ}\text{C}$	135 $^{\circ}$
Total Friction, max, lb.in.	.096
Back EMF, volts/rad./sec	.90
Viscous Damping, lb.in./rad./sec.	
Zero impedance source	.036
Infinite impedance source	.012
Ripple Torque, lb.in.	
At low torque levels	0
At peak rated torque	.36
Rotor Inertia, lb.in.sec. ²	6.96 $\times 10^{-4}$
Weight, lb.	.85

The motor transfer function is:

$$11. \frac{\theta_o}{E} = \frac{1}{K_v S \left[\left(\frac{J_m R}{K_v K_t} S + 1 \right) \left(\frac{L}{R} S + 1 \right) \right]}$$

Substituting known values:

$$12. \frac{\theta_o}{E} = \frac{1}{.95 \left[\left(\frac{6.96 \times 10^{-4} \times 193}{.9 \times 7.92} S + 1 \right) \left(\frac{1}{193} S + 1 \right) \right]}$$

$$13. \frac{\theta_o}{E} = \frac{1.11}{S(0.01885 + 1)(5.18 \times 10^{-4} S + 1)}$$

Special note should be made of the inertial time constant above. Chapter IV will present the time constant based on experimental data.

Figure 2 represents a logarithmic plot of this transfer function with corners marked. The plot of r_{db} is asymptotic since accuracy is not required for this presentation.

Motor-Load Time Constants

Substituting the values obtained from the manufacturer's characteristics for this motor and the load inertia from the design goals, the following transfer function is obtained:

$$14. \frac{\theta_o}{E} = \frac{1.11}{5[(3.525+1)(5.18 \times 10^{-4}S+1)]}$$

An analysis of this transfer function is warranted. If the steady state solution of equation (14) is found by first substituting jw for the operator S and then substituting high values of frequency for W , it is found that the maximum phase shift approaches 270 degrees. This indicates that feedback will be required to stabilize the system which will use this motor as the torque producing source. The inertial time constant of 3.52 seconds is relatively long and consequently adversely affects system performance. This time constant can be significantly reduced by reducing the load inertia or armature resistance. The latter course of action is the only acceptable one and can be easily realized. An examination of similar torque motors reveals most of them possess values of armature resistance on the order of 5 per cent to 10 per cent of this motor.

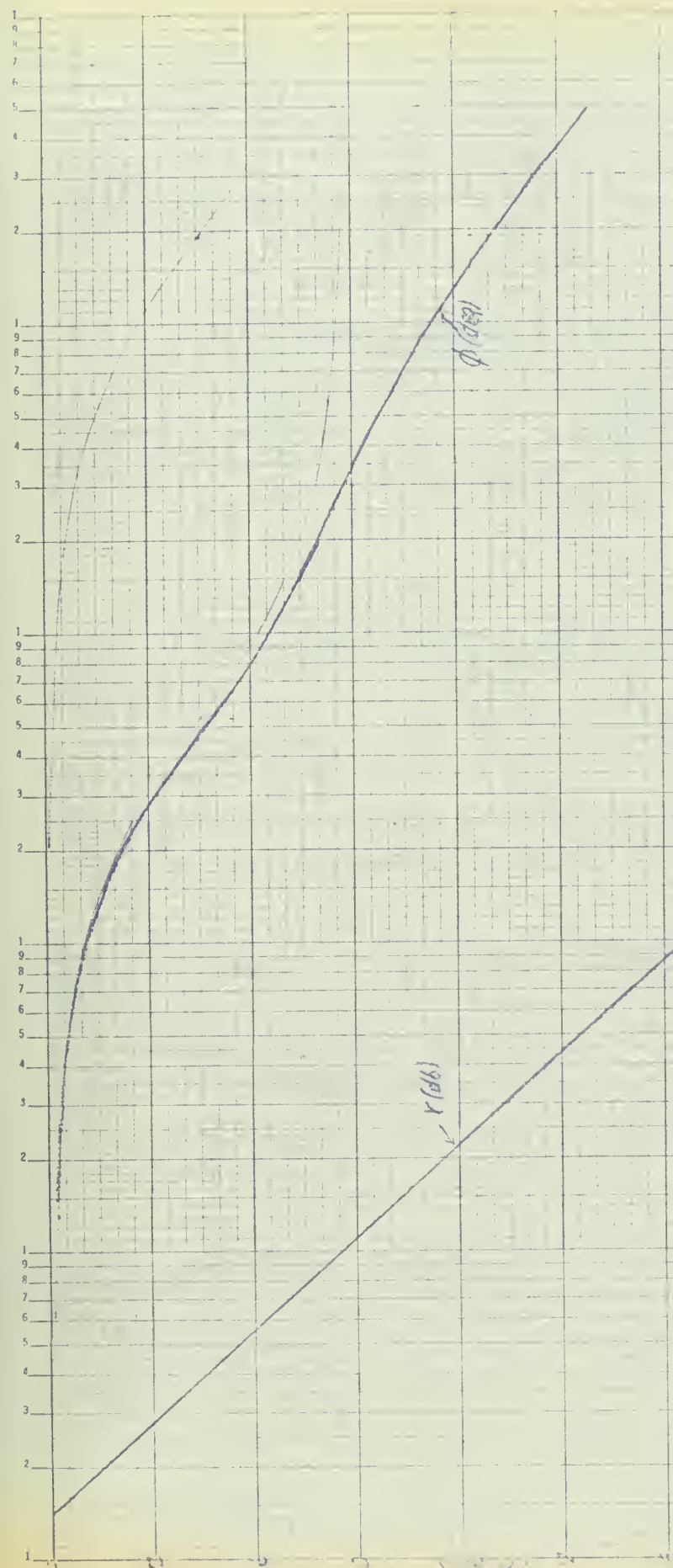


Fig 2
 Y AND t VS t
 FACTOR ALONE
 1/11
 E. S. C. GEORGE STANLEY STID

SECOND ORDER
 EXPONENTIAL TYPE
 CONSTANT $\alpha = 10^{-2}$

FIRST ORDER
 EXPONENTIAL TYPE
 $\alpha = 53.2$

100

Of special interest is the fact that the friction and motor inertia in direct drive motors is so small as to be insignificant when compared to other values used in the transfer function. In addition, the electrical time constant is so small that it may be disregarded entirely.

Mathematical Analysis - Closed Loop Transfer Function

Consider the case of a single-axis stabilized platform driven by the direct drive torque motor described above, where the base of the structure is subject to all the motions of the carrier to which it is attached. To stabilize the controlled member, it is necessary only to keep it stationary with respect to inertial space. Figure 3 represents a functional schematic of such a single-axis inertial space stabilization system, stabilized by an integrating gyro unit. It is to be emphasized that the final system used in this investigation did not utilize a DC generator, however, this fact does not alter the validity of what follows.

Figure 4 represents the servo block diagram of this schematic. Assume also that the amplifier gain is unity. Figure 5 represents the logarithmic plot of such a system. Again, the plot of r_{db} is asymptotic.

Analysis of this logarithmic plot reveals that the design goals are not met; i.e., the gain crossover frequency is much less than the 100 radians per second required. In addition none of the criteria as specified by The American Society of Mechanical Engineers (ASME) are satisfied, namely:

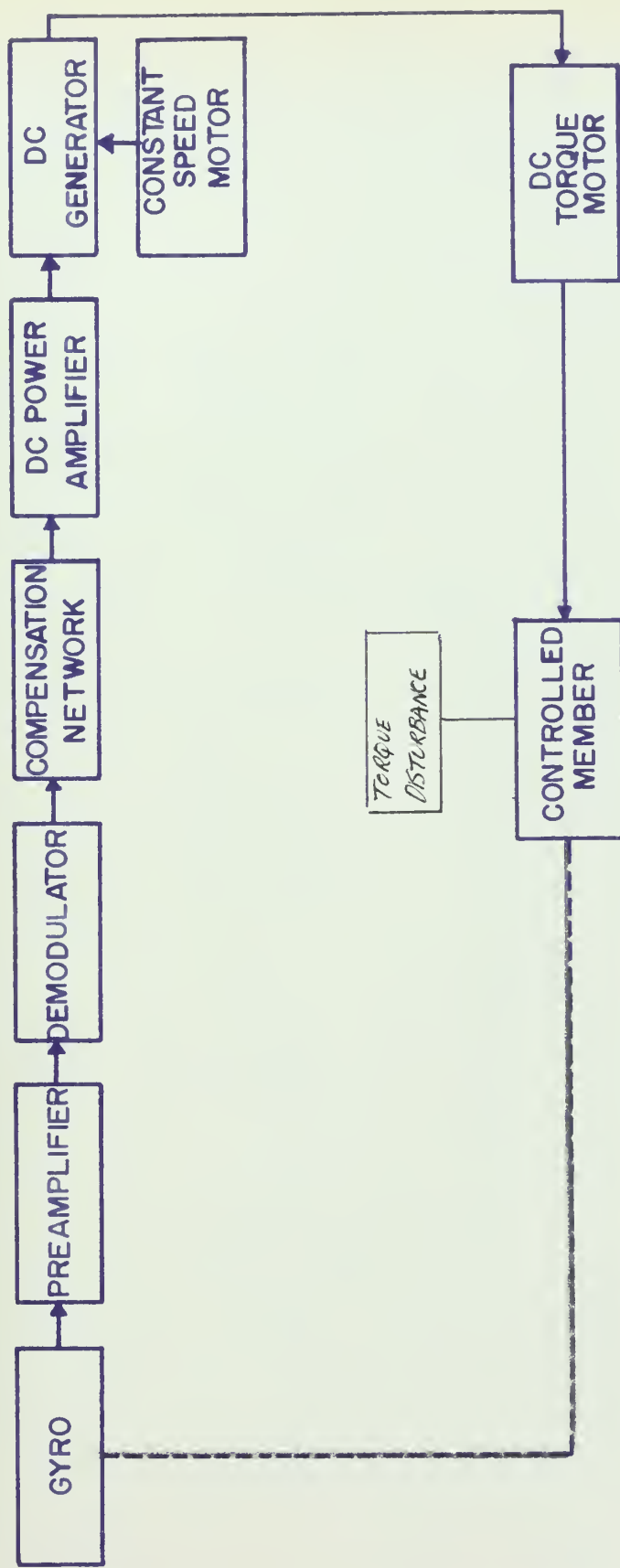


FIG 3- SINGLE AXIS INERTIAL SPACE STABILIZATION SYSTEM
USING A DIRECT DRIVE DC TORQUE MOTOR TO POSITION THE
CONTROLLED MEMBER

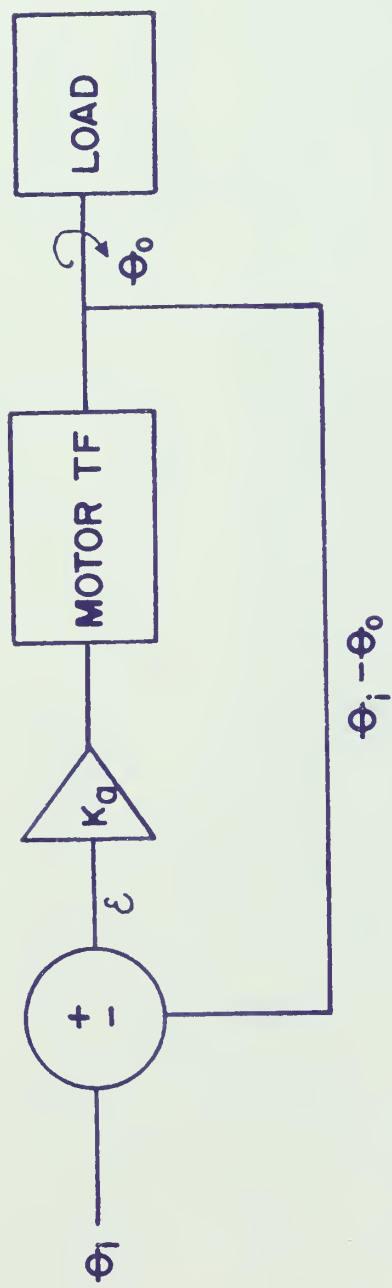
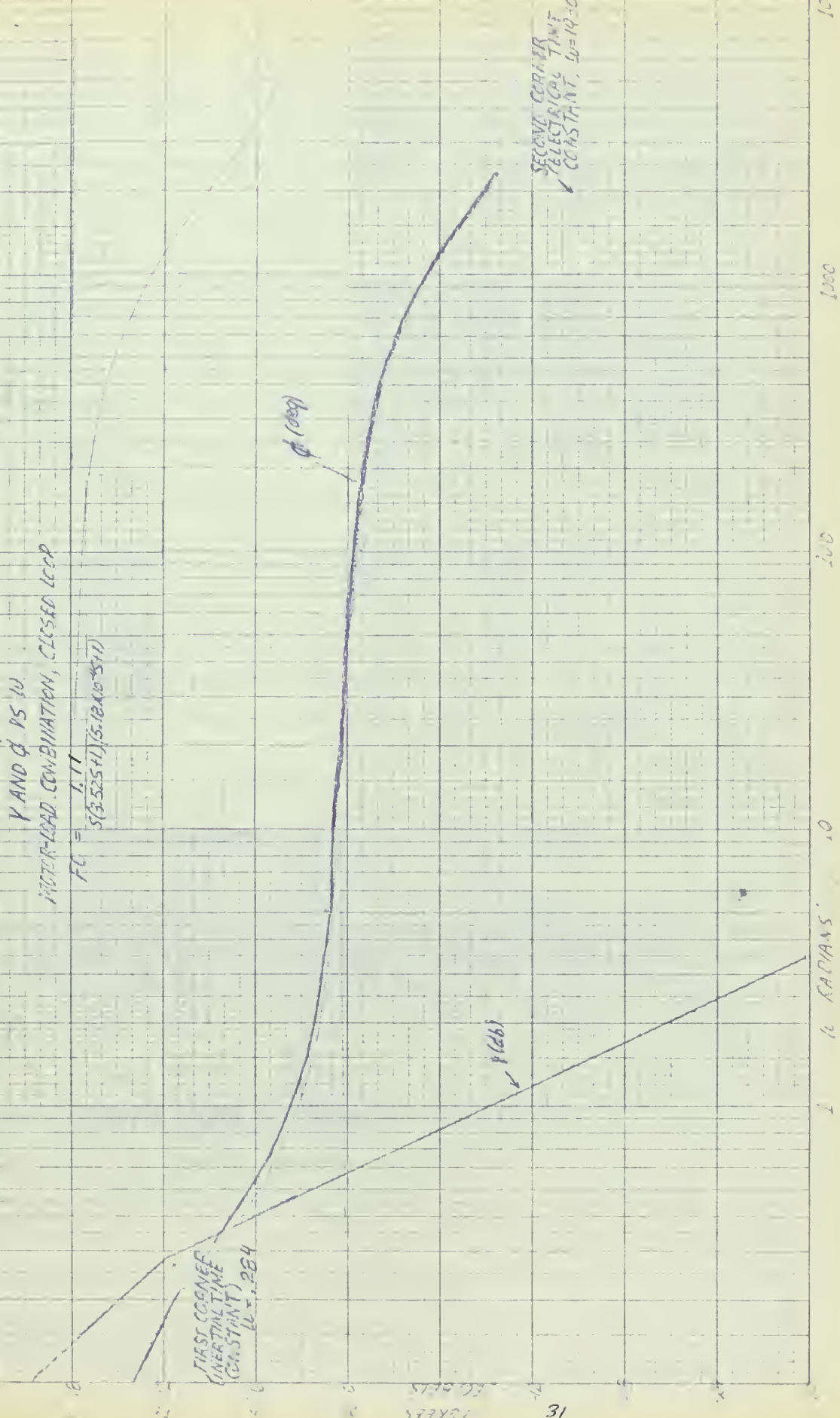


FIG 4 SERVO BLOCK DIAGRAM REPRESENTATION OF FIG 3

FIG 5



1. That the gain asymptote slope at crossover be -6 db per octave and that the slope of the gain asymptotes segments immediately before and after the crossover be -12 db per octave.
2. PM = 30° minimum
3. GM = 8 db minimum

Increase in gain, K_a , would probably insure that the servo system could meet some of the design specifications but the amount of gain would be prohibitive and ASME criteria would not be met.

From the appearance of the logarithmic plot, the importance of the so called compensation networks become apparent. Even with a higher gain, the phase lag at lower frequencies is too great. A lead compensation network was added to the system as evidenced by Figure 6.

A lead network is a device having a transfer function locus in the first quadrant because its phase angle is then positive or leading and causes the compensated system locus to advance in phase with respect to the original system. The position of the pole and zero configuration affects the shape of the gain curve since it causes the gain curve to change slope; first at a + 6 db per octave slope and then at a - 6 db per octave slope. Since crossover parameters were specified, it was a relatively simple matter to chose a lead network that would insure three things:

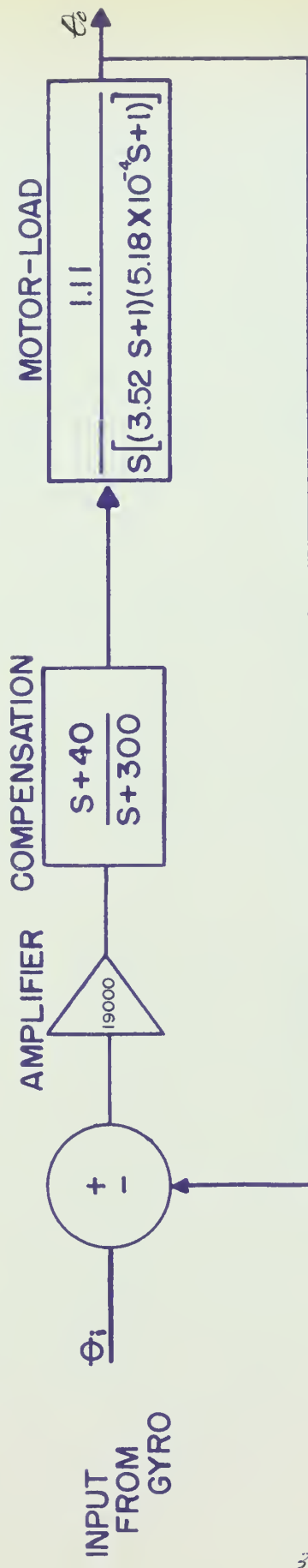


FIG 6 – SERVO BLOCK DIAGRAM OF COMPENSATED SYSTEM

1. Gain crossover approximately 100 radians per second.
2. Gain curve slope at crossover; -6 db per octave.
3. Gain curve crossover to occur at the geometric mean of the pole-zero configuration which produces the -6 db slope.

The proper shape to the gain curve was met with lead network $\frac{5+40}{5+300}$ and amplifier gain of 19,000.

The open loop transfer function, $\frac{F_o}{E}$ (with unity feedback) hereinafter referred to as F_o is:

$$\begin{aligned}
 14a. \quad F_o &= \frac{19000 (5+40) 1.11}{5[(3.525+1)(5.18 \times 10^{-4}5+1)](5+300)} \\
 &= \frac{2810 (.0255+1)}{5[(3.525+1)(5.18 \times 10^{-4}5+1)(.00335+1)]}
 \end{aligned}$$

Figure 7 is a logarithmic plot of this system and illustrates how design goals and ASME criteria are met. Of particular interest is the excellent phase margin and gain margin of this theoretical system. However, the lead network reduces the gain of the system by the ratio $\frac{W_n}{W_p} = .133$ and in order to meet the design goal of 40 db gain at 1 cycle, a prohibitive amount of amplifier gain is required (19,000). This system is considered unacceptable.

FIRST CORNER
ELECTRICAL VARS
CONSTANTS $\mu = 264$

FIG. 7
LEAD COMPENSATED SYSTEM
 2810 (0.5551)
 $\text{FO} = 5(2.5251)(4.13 \times 10^{-954})(0.002250)$

DESIGN LEVEL
40dB GAIN
 $40^{\circ} 6.28$

LEAD
CORNER
 $\mu = 40$

30°
PHASE
MARGIN

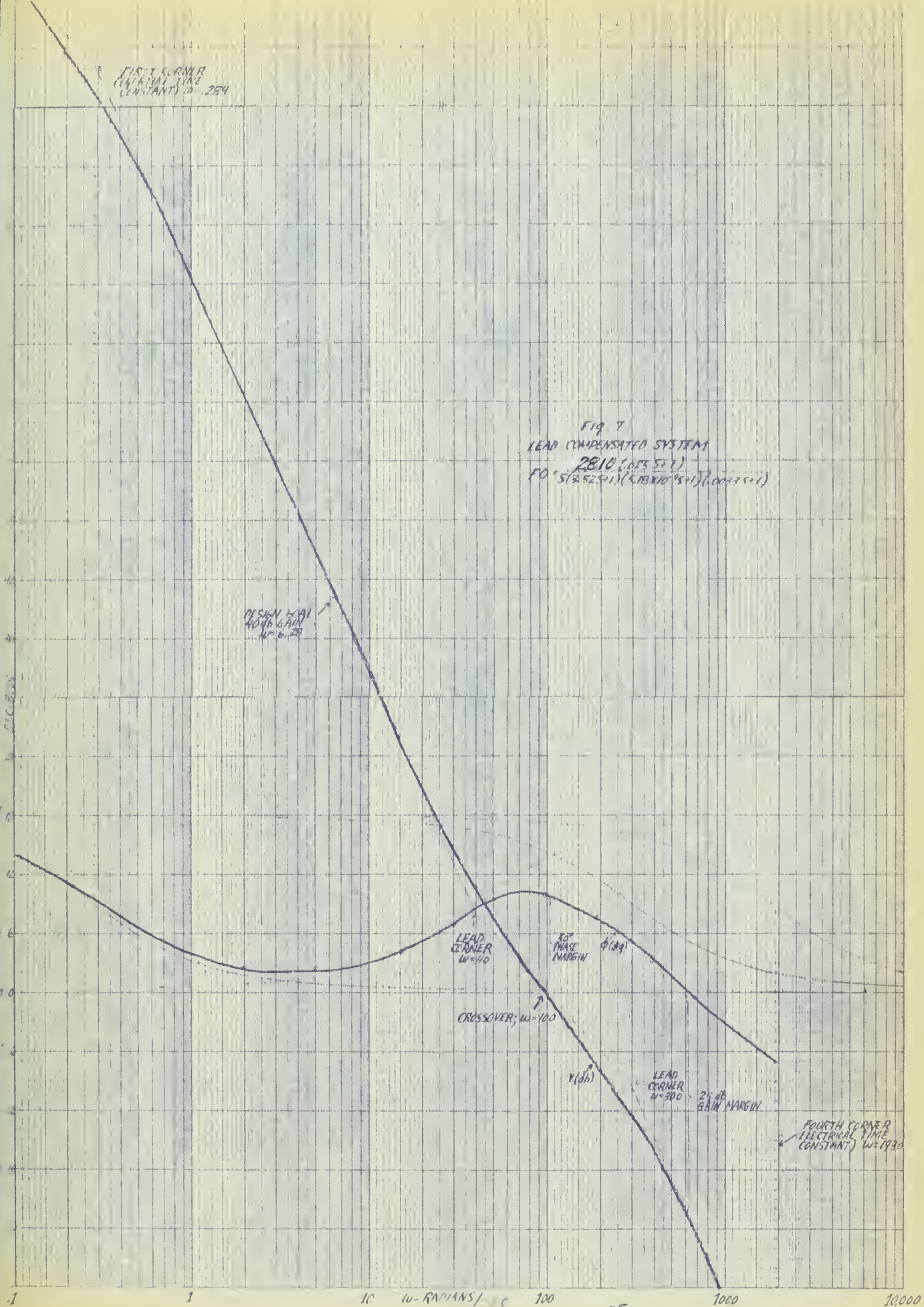
CROSSOVER; $\mu = 100$

$\mu(10)$

LEAD
CORNER
 $\mu = 900$

25dB
GAIN MARGIN

FOURTH CORNER
ELECTRICAL VARS
CONSTANT) $\mu = 1930$



A reanalysis of the problem is now in order. Of concern is the fact that in order to obtain the design goals, the amplifier gain is prohibitively high. An attempt will be made to shape the magnitude curve in such a manner as to meet the design and ASME criteria and reduce the gain requirements. The corner obtained from the inertial time constant (3.52 sec.) must be eliminated or moved to higher value of W . This can be done by use of tachometer feedback with a lead network in the main feed path. Figure 8 illustrates the block diagram of such a system.

The open loop transfer function for a system with tachometer feedback is obtained in the following manner:

$$F_o = \frac{G(s)}{1 + hSG(s)}$$

F_o signifies the open loop transfer function, $G(s)$ corresponds to the networks (motor and compensation) in the main feed path. The factor h represents the tachometer feedback constant.

As previously explained on page 32, a lead network $\frac{5+60}{5+400}$ was chosen as that required to properly shape the magnitude curve insofar as crossover frequency and slope at crossover were concerned.

The tachometer constant and the other poles were obtained by development and solution of the following equations:

$$15. F_o = \frac{\frac{1.11 Ka (s + W_N)}{s(3.52s + 1)(5.18 \times 10^{-4}s + 1)(s + W_D)}}{1 + hS \left[\frac{1.11 Ka (s + W_N)}{s(3.52s + 1)(5.18 \times 10^{-4}s + 1)(s + W_D)} \right]}$$

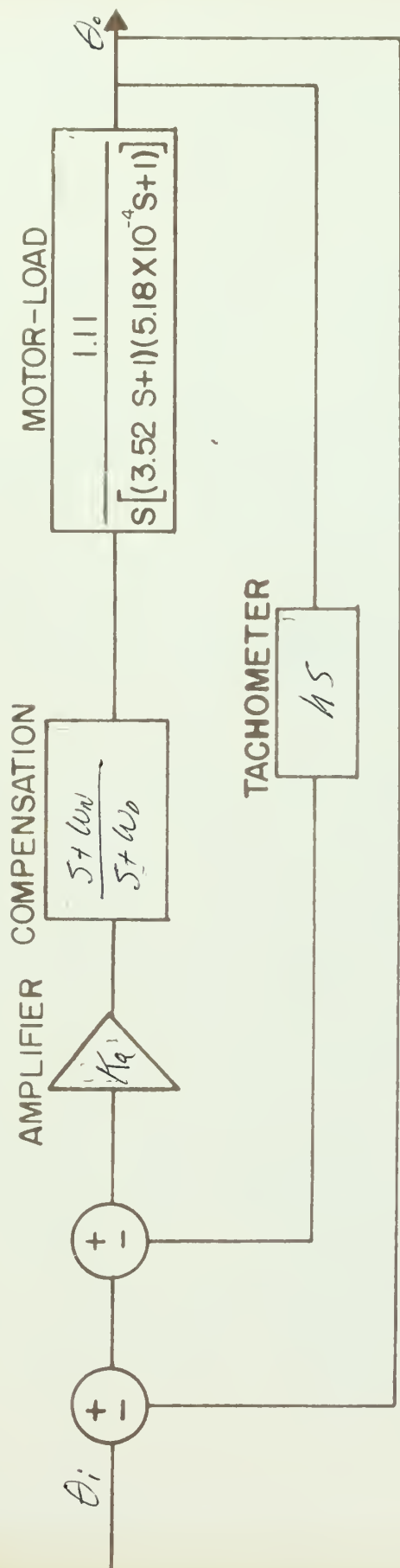


FIG 8 - SERVO BLOCK DIAGRAM: LEAD-TACHOMETER COMPENSATED SYSTEM

Simplifying,

$$15a. F_o = \frac{603 Ka (5 + W_N)}{5[5^3 + 5^2(W_D + 1933) + 5(1933 W_D + 548 + 603 h Ka) + (548 W_D + 603 h Ka W_N)]}$$

The lead network will reduce the gain by the ratio $\frac{W_N}{W_D} = \frac{60}{400} = .15$. Thus, $(.15 \cdot 1.11 \cdot Ka)_{db} = 56.5_{db}$ (the gain in d.b. at 1 radian per second) $Ka = 5558$.

Substituting the value for the amplifier gain and the lead network constants in equation 15a:

$$16. F_o = \frac{33.5 \times 10^5 (5 + 60)}{5[5^3 + 23335^2 + (773,748 + 33.5 \times 10^5 h)5 + (219,200 + 201,060,000 h)]}$$

Since the addition of tachometer feedback changes the corners on the logarithmic plot (this can be noted by examination of equation 16) and thus effectively changes the time constants of the motor and W_D of the lead network, it was decided to specify the first and second corners (the most important since they determine the slope of the gain curve at crossover and also the crossover frequency) and then solve the resultant characteristic equation for the tachometer constant and the remaining corners. Examination of the logarithmic plot, Figure 7, reveals that the first corner at 15 radians per second appears to give the magnitude curve

the proper shape. Of course, the second corner at 60 radians per second has already been specified by the numerator of the lead network and a quick plot of this data reveals that crossover will occur at approximately 100 radians per second with -6 db per octave slope.

Solving the resultant cubic equation, which can be factored as $(5+a)(5+b)(5+15)$ results in the following identities:

$$15+a+b = 2333$$

$$15a+15b+ab = 773,748 + 33.5 \times 10^5 h$$

$$15ab = 219,200 + 201,060,000 h$$

Solution of these three equations with three unknowns reveals the following values:

Roots (corners) at -15, -600, -1715

h (tachometer constant) = .07194

As mentioned above, the addition of tachometer feedback can effectively change the value of W_D used in the lead network. In this case the value of W_D was changed from -400 to -600.

These corners were plotted on a logarithmic diagram, Figure 9. ASME criteria and design goals are met except that crossover frequency of 160 radians is somewhat too high.

In order to correct this, the magnitude curve is moved down until crossover occurs at 100 radians. The amplifier gain is now 4673 and the open loop transfer function is

FIG. 9
LEAD-TACHOMETER SYSTEM

$$FO^+ = \frac{917(-0.1675+i)}{5(1.06675+i)(0.01075+i)(0.00585+i)}$$

recalculated using this value. Pole locations change only slightly but tachometer changes by 16 percent to .0856. The reason for these changes can easily be explained by examination of equation 15a which illustrates how a change in K_a modifies two terms in the characteristic equation.

Figure 10 represents the corrected log plot.

Figure 11 represents the M-N chart for this system.

Figure 12 is a plot of M and N versus W.

Transient Response

Using conventional servo theory, the closed loop transfer function, F_c , is obtained in the following manner:

$$F_c = \frac{F_o}{1+F_o}$$

$$17. F_c = \frac{33.5 \times 10^5 (s+60)}{s^4 + 2333s^3 + 1,014,680s^2 + 14,679,435s + 201,000,000}$$

Solving the quartic in the manner prescribed on page 91, Brown and Campbell, the roots of the characteristic equation are:

$$-8.78 \pm j 9.43, -1716.5, -595.9$$

Factored, the closed loop transfer function appears as,

$$18. F_c = \frac{33.5 \times 10^5 (s+60)}{(s+8.78+j 9.43)(s+8.78-j 9.43)(s+1716.5)(s+595.9)}$$

Calculation of the transient response is represented by

FIG. 10
LEAD-TACHOMETER SYSTEM,
PRELIMINARY DESIGN.

$$FB = 775 \times (1675 + 1)$$

$$37,04675 + 1 \times 001675 \times 1 \times 0058541$$

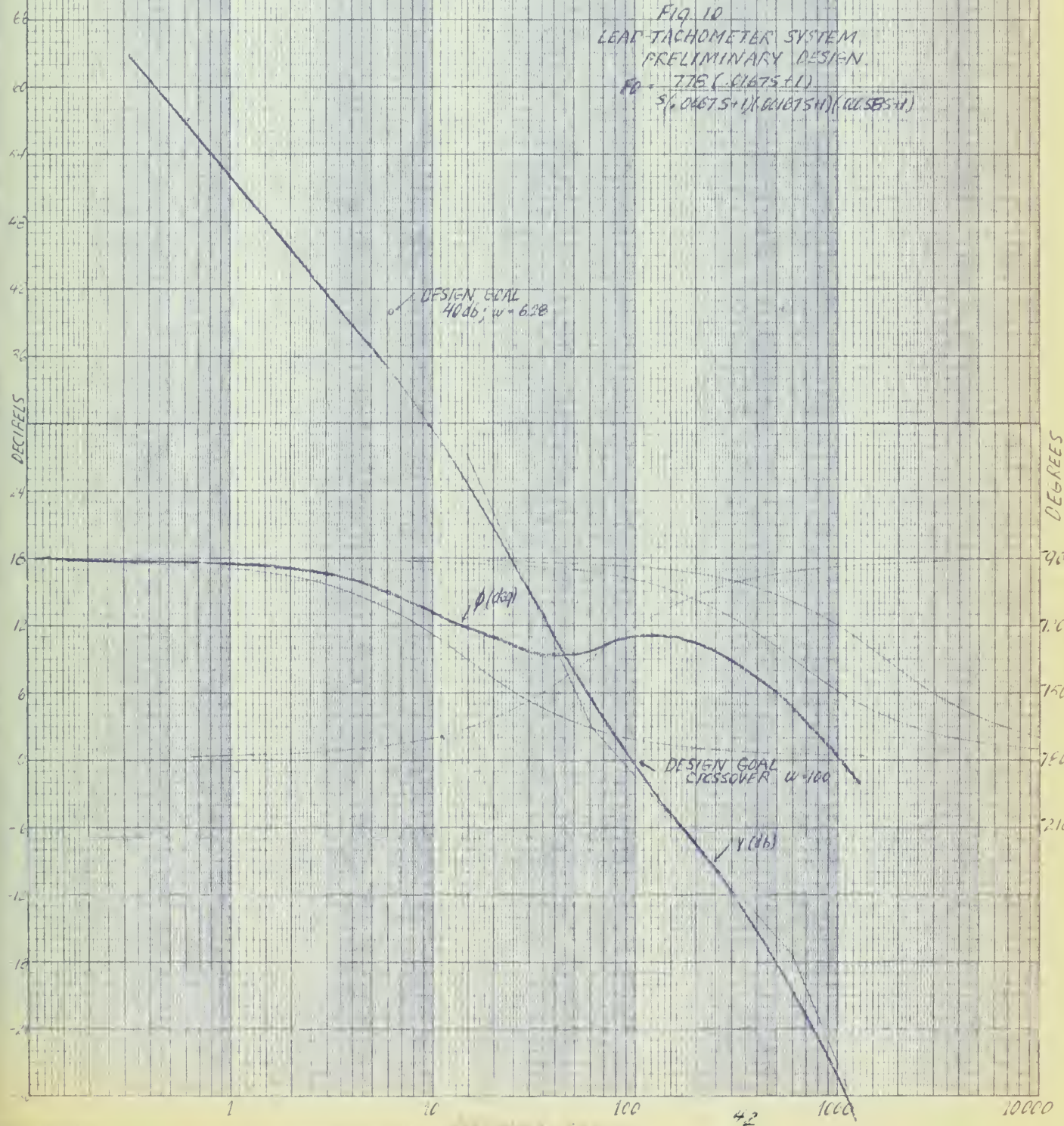
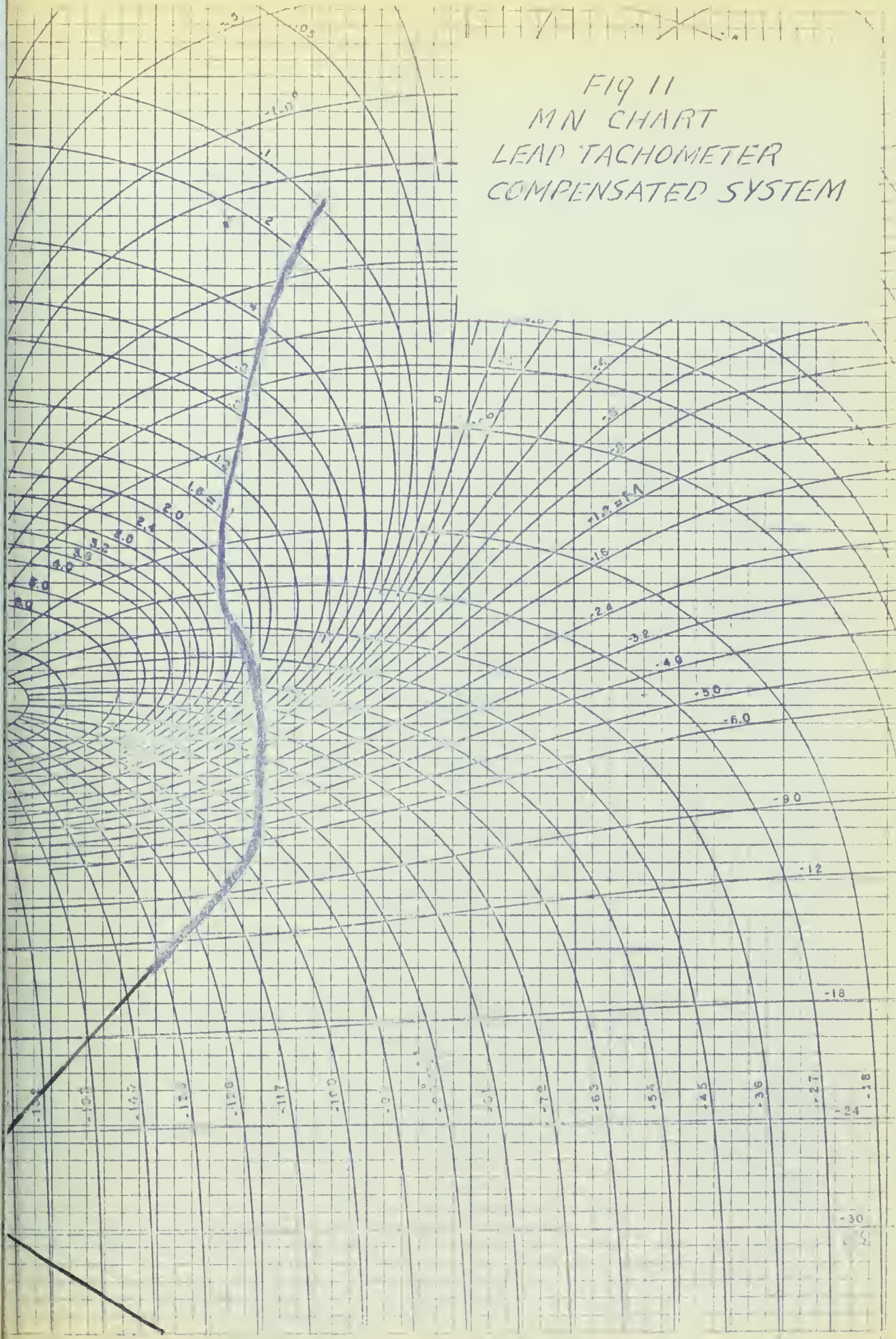
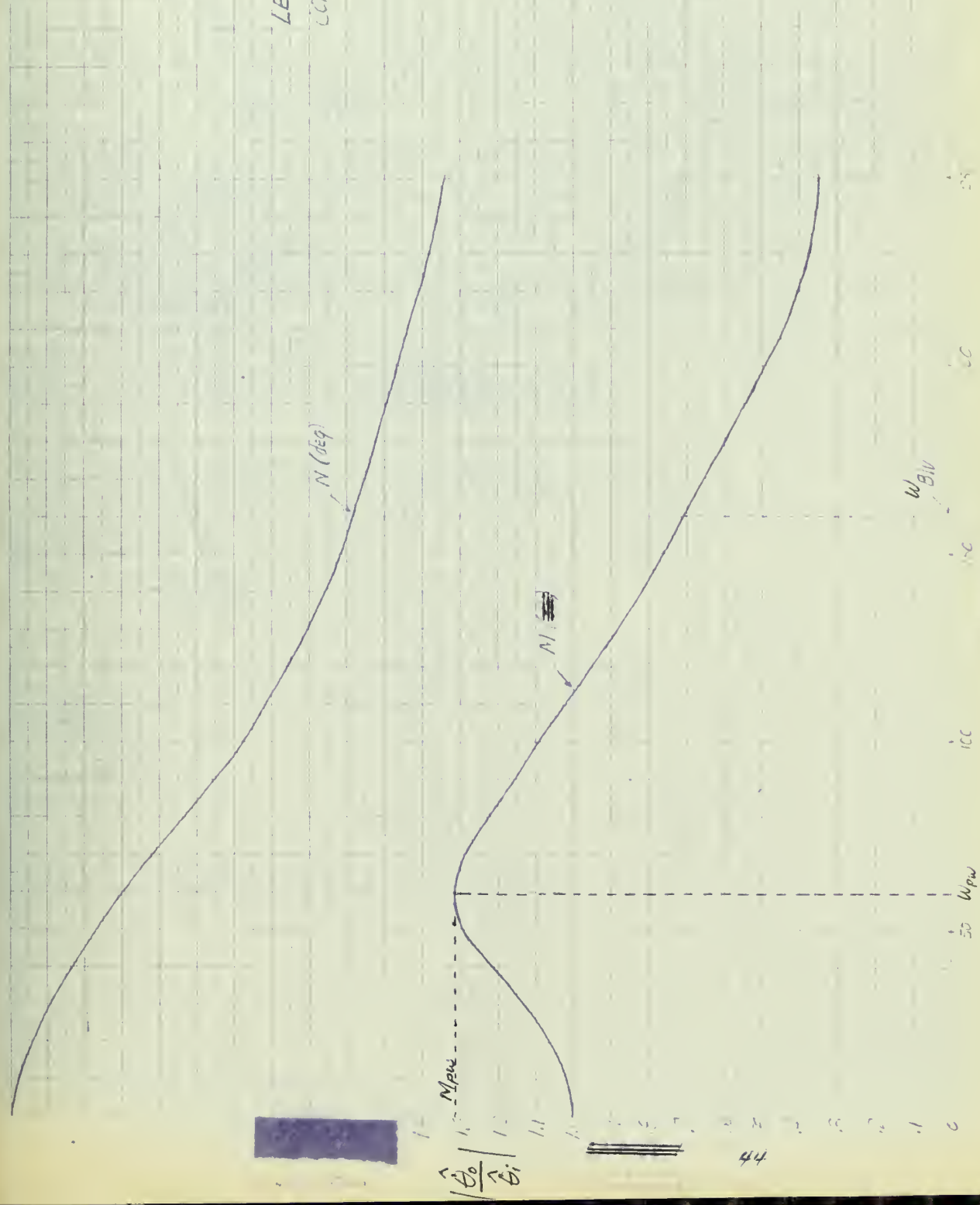


FIG 11
MN CHART
LEAD TACHOMETER
COMPENSATED SYSTEM



5/27/61

Fig 12
 N_{AVG} vs W
 LEAD-TACHOMETER
 COMPENSATED SYSTEM



the following equation obtained by the residue method:

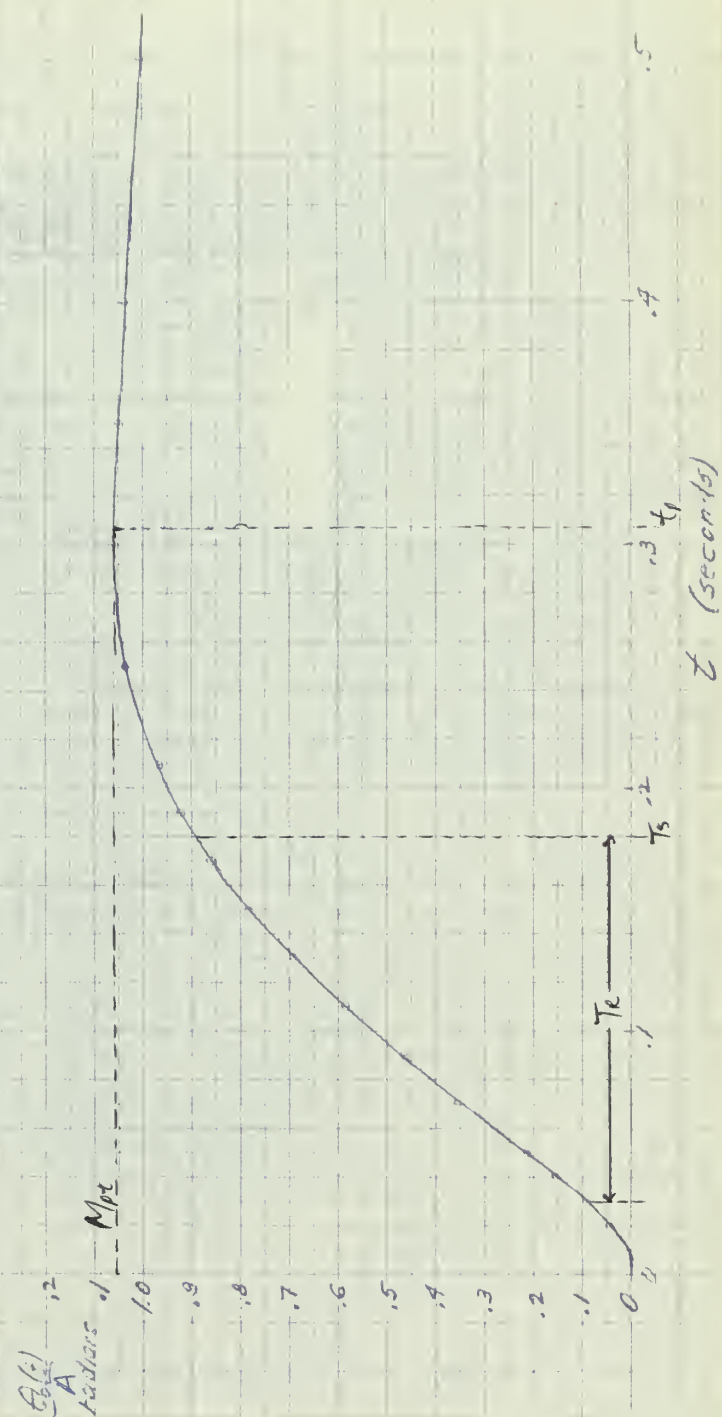
$$19. \frac{\theta_o(t)}{A} = 11.224 e^{-8.18t} \sin(9.43t - 2.14) + .00101 e^{-1716.5t} + .008 e^{-595.9t}$$

The last two terms can be neglected due to their insignificant size for times greater than .001 second.

Figure 13 represents the transient response plot for this system. The following is a tabulation of the pertinent data represented by this preliminary system, a system design to meet all specifications.

M_{pw} (Magnitude, peak, frequency basis)	= 1.32 radians
W_{pw} (Frequency of M_{pw})	= 60 radians/sec
M_{pt} (Magnitude, peak time basis)	= 1.06 radians
T_p (Time of M_{pt})	= .306 seconds
WBW (Bandwidth, frequency basis)	= 160 radians/sec
T_R (Rise Time)	= .155 seconds
T_S (Settling Time)	= .18 seconds

Fig 13
TRANSIENT RESPONSE
PRELIMINARY DESIGN



CHAPTER IV

DIRECT DRIVE TORQUE MOTORS

A DC torque motor for this direct drive servo application was chosen for the following reasons:

- a. High angular acceleration
- b. High peak torque per unit volume
- c. Minimum control and total power input
- d. Rapid electrical response
- e. Optimum shape for compact systems

In any high performance control system and specifically in stabilization and tracking system servos where size, weight, power requirements, and response times must be minimized and where high resolution is both necessary and desirable, direct drive DC torque motors have proven to have many outstanding advantages.

Principle among these is their high torque to output inertia ratio. This important figure of merit is a measure of the acceleration capabilities of a motor, a critical factor in systems of this type. For example, a system requiring a peak torque of 60 ounce-inch could use the motor chosen in this investigation, the Inland Motor Company T2108A which has a torque to inertia ratio of 5350 radians per second squared. A gear train servo motor for the same requirement would have a torque to inertia ratio at the output shaft on the order of 1/10 this value or less. Figure 1 is a performance curve for this motor as given by the

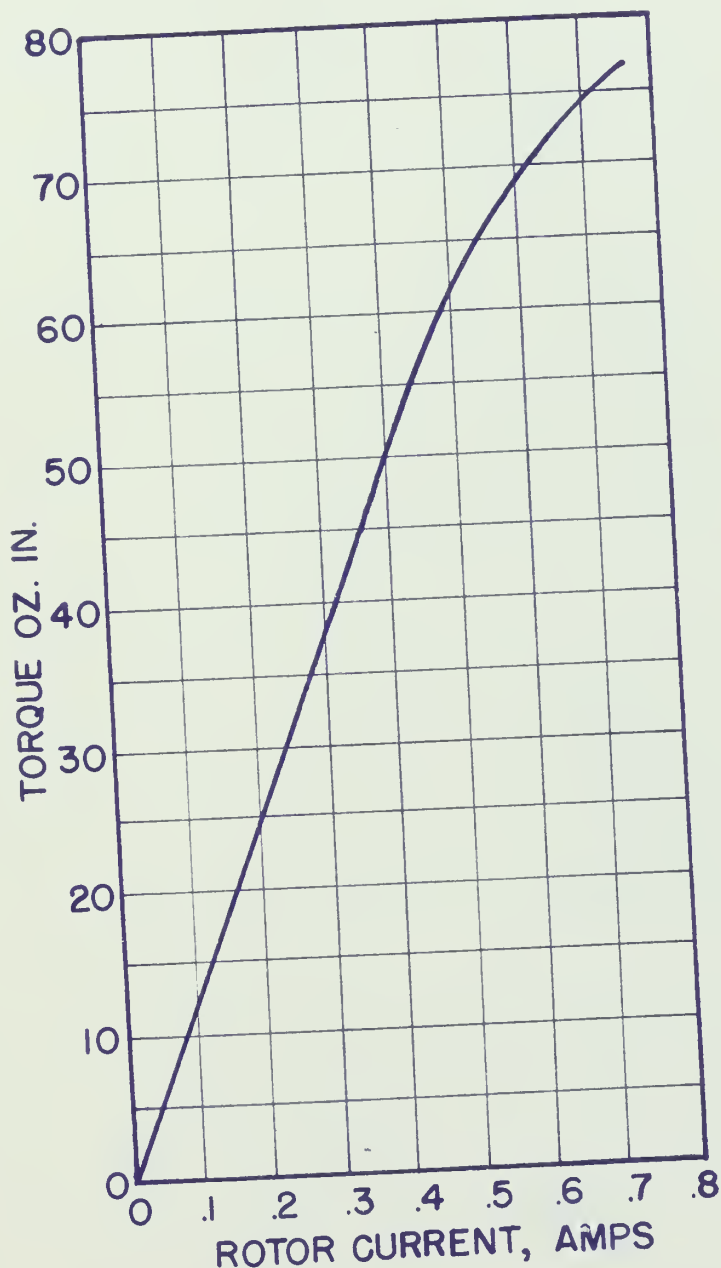


FIG 1 - ROTOR CURRENT VS TORQUE
(MANUFACTURER'S DATA)

manufacturer. Of interest here is the excellent linearity of this motor representing a torque constant slope of 125 inch-ounce per ampere.

Many other important advantages result from the direct drive characteristic. Of interest in this investigation is the absence of backlash effects in servos with direct drive motors together with the absence of any measurable ripple effects in the motor itself, which, except at very high torque levels, allows use of high loop gain to obtain fast servo response time and excellent resolution. In stabilization systems with direct drive, error is introduced to the stabilized member only through friction, whereas with gear drive, base motion accelerates the motor through the gears thereby adding acceleration error. Gears also greatly increase the friction errors.

Total friction torque of the smaller direct drive units is not more than 2 per cent of maximum torque. The ratio is even less for the larger units with peak torque output greater than 3 pound-feet. This fact, of course, simplifies analysis by reducing the complexity of transfer functions when friction is disregarded.

A complete line of DC torque motors ranging from a unit 2 inches in diameter and 1/2 inch thick, producing 0.1 pound-foot peak torque to units producing over 100 pound-feet torque are now standard items. Even larger units are available. Recent trade literature reveals that a unit with peak torque rating of 3000 pound-feet will soon be manufactured for an antenna drive application. This literature reveals plans

for performances in the realm of 100,000 pound-feet for antennae of the 80 to 100 feet diameter size.

It is felt that servo engineers should chose DC rather than AC torquers for direct drive applications because DC units require substantially less input power to obtain a given torque, much smaller size for a given maximum torque, and can have a faster torque versus time response. High level saturation of the rotor core by the permanent magnet field and use of a maximum number of poles can reduce control winding self inductance to negligible levels.

Speed of Operation

Most torque motors are designed for essentially stand still operation. However, speeds up to 100 revolutions per minute rarely present difficulty. Speed is limited by the voltage between one commutator bar and the next when the current is being reversed by commutation.

The limiting voltage is a function of the amount of iron in the circuit, number of coil turns, speed of rotation and resistance of the brushes. Generally, the higher the resistance of the brush the better the commutation, but there is a limit to the brush resistance that can be tolerated in servo applications because higher resistances add uncertainty to the loop by increasing the inertial time constant. Increasing the number of commutator bars so that the number of turns between bars is decreased also improves commutation.

When the maximum number of bars have been used due to space restriction and brushes with the maximum resistance tolerable have been installed, speed can no longer be increased without derating torque. Very small units can run intermittently at speeds of several thousand revolutions per minute operated at less than peak torque and up to one thousand revolutions per minute intermittently at peak torque. For example, the motor used in this investigation was operated at speeds in excess of one thousand revolutions per minute for at least two hours. Speed limits of larger units are considerably less. For example, speeds in the region of 500 revolutions per minute are beyond reach of most 10 and 20 foot-pound standard units.

Motor Control Power

Specifically designed rotary amplifiers are generally used to drive the torquers. With good design they can be made to provide very fast response consistent with that of torquers. However, in some cases these rotary amplifiers introduce time constants into the system which degrade the performance. Magnetic amplifiers and gas tube amplifiers can also be used in conjunction with these torquer motors.

Vacuum tube drives provide the fastest type of control. They have the disadvantages associated with relatively high power electronic systems however. These problems are being sidestepped in some cases with use of high power transistors as switches in a high frequency pulse-width type amplifier. So far, however, these transistor units are limited to use with

smaller torquers. For example, engineers at the Dalmo-Victor Corporation attempted for some seven weeks to develop a transistor amplifier for use in this investigation. Although the effort failed due to the high voltages required, it is felt that with the newer, higher-powered transistors recently marketed, success could have been realized.

Torquer Design

The first direct drive DC torquers made were designed for stabilization systems such as gyro control units. Since the torquers were to mount directly on the stabilization gimbals where space and weight are severe limitations, a major objective was to make them as small as possible. The major problem to be solved was ripple - the torquers were not even feasible if their torque varied substantially with rotation. Skewed rotors with the proper proportion of slots to the number of stator slots would minimize ripple, the difficult aspect of the problem was to accomplish this in a minimum sized unit.

The size of the rotor was reduced by mounting the commutator directly on the winding. The commutator bars actually went through the slots. After the bars were connected to the windings the whole rotor was encapsulated. The commutator ended up taking no appreciable space beyond that of the wound core, except for the insulation of the bars. The bar arrangement appears to be something like that of a barrier where the windings have been turned away. The Inland Motor Company doesn't turn away the windings however.

They simply add more bars and connect the windings to them. This was the principal reason why an Inland Torque Motor was chosen over other manufacturers for this investigation. The Inland Motor Company also saved space in the stator. Normally field poles in DC machines have substantial tooth tips to the pole face and, to achieve a low speed voltage to commutated coils, the space between the poles is relatively large both circumferentially and radially. By using Alnico-V magnets in the field, Inland was able to eliminate the slots and the spaces between the poles in the field. Simply having a highly saturated bridge of magnetic material going from one pole to the next resulted in a reduction in outside diameter on the field assembly without sacrificing anything to the ripple problems: There were no slots on the inside of the field that could conspire with the rotor slots to cause ripple.

The very thin bridge that connects one pole to the next is, of course, thoroughly saturated by the permanent magnet field, but the amount of flux through this path is relatively slight.

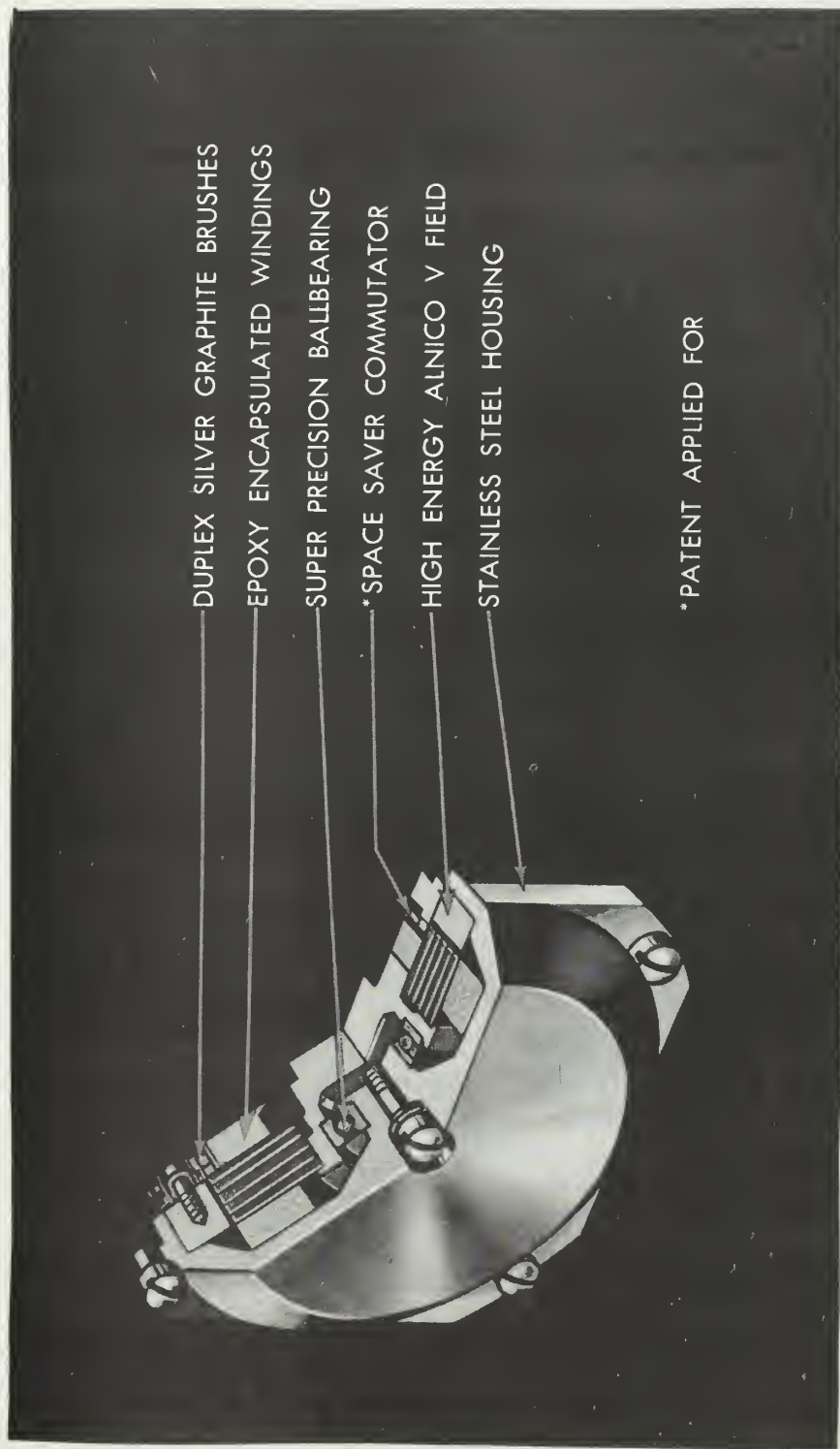
The combination of these rotor and stator designs and a rather small brush rigging made possible by the commutator configuration results in a much smaller torque motor than produced before. Furthermore, the stator is very simple and easy to produce and no complex skewing for either the stator or the rotor is required. Best of all, ripple effects are

negligible. There is no measurable reluctance torque effect with rotation and no change in the per ampere sensitivity with rotation. However, there is a slight change in input resistance as the brushes move from bar to bar resulting in a small variation in per volt sensitivity, and armature reaction causes an additional ripple at very high torque levels. Figure 2 is a cutaway view of the T2108A torque motor used in conjunction with this investigation.

Motor Tests

The purpose of the motor tests in this investigation were twofold. First, correct data was necessary in order to predict system performance. Second, a correlation between manufacturers data and actual data was required in order to form an experience base to be used in future preliminary designs of this type.

The parameters numerically evaluated in the motor test program were armature resistance R , electromotive force constant K_v (back electromotive force), friction, torque constant K_t (sensitivity), armature inductance L , time constants, and inertia J . In addition to the tests on the motor alone, tests were made with the load inertia as well as with the tachometer, synchro and gear which were to be included in the final closed loop system. Parameters, whenever practical, were evaluated by more than one method in order to verify results.



Measurement of Resistance R^1

The armature resistance was measured with an impedance bridge at the brush terminals. An average value was taken for the resistance measured at several positions of the armature. The average resistance was 165 ohms, compared with 193 ohms given by the manufacturer.

Measurement of Inductance L^1

The impedance bridge was used for this measurement. The self-inductance was measured for several armature positions for the permanent magnetic field motor with armature in place. The average inductance was .15 henries compared to .1 henries given in the manufacturer's data.

Measurement of the Motor Back emf Constant K_v

This constant was evaluated by driving the motor mechanically as a generator as well as running as a motor.

A dynamometer² was used to drive the motor mechanically while the speed and generated voltage were measured.³ A Model 311, Simpson VTVM was used with input impedance of 22 megohms for recording voltage and the Jagabi chronometric tachometer was used for speed measurements. The motor was run through a range from 100 rpm to 1000 rpm which was considered to include the closed loop operating speed range. Higher speeds were not used for this reason as well as to minimize commutator brush wear which the manufacturer cautioned would occur at higher speeds. Motor speed was set by adjusting the hydraulic coupling unit between the dynamometer

drive motor and the dc torque motor being tested.

The data obtained in this test is tabulated in Table I and the generated voltage versus speed data is plotted in Figure 34. The motor was driven in both directions as shown by the two curves.

The motor back emf constant K_V has units of volts per unit of rotation per unit of time or in this case, volts per radian per second. It represents the slope of the generated voltage versus speed curves of Figure 2 which are noted to approximate a straight line. From the average of the two curves representing the different motor directions the value of K_V was determined to be .883 volts/radian/second which correlates favorably with the manufacturer's figure of .90.

The second method of evaluating K_V employed Kirchoff's Law equation, $E = IR = K_V \omega^1$. In this evaluation a range of voltages were applied to the motor while speed and armature current were recorded for each voltage. Using the previously determined value of armature resistance of 165 ohms, the IR drop was calculated. Table II contains the data obtained during the tests. The first set of data was for the motor with a 50 pound-inch squared inertia disk load but no tachometer, synchro or gears. The second set of data is for the motor with the tachometer, synchro and gears but no load. Figure 48 shows the mounting arrangement for the tachometer, synchro and gears. To assemble, the motor shaft is inserted through the hole in the gear located in the motor housing.

TABLE I
Back emf Constant (K_V) and Viscous Friction Data

RPM	ω rad/sec	E Gen	weight grams	weight ounces	arm inches	Torque in-oz
Clockwise						
86	8.9	7.6	7.02	0.25	7.3	1.82
252	26.4	23.2	7.02	0.25	8.6	2.15
465	48.7	42.5	7.02	0.25	9.9	2.48
536	56.0	48.8	28.03	1.0	2.6	2.60
600	62.8	54.5	28.03	1.0	2.7	2.70
644	67.4	58.2	28.03	1.0	2.7	2.70
736	77.0	66.2	28.03	1.0	2.8	2.85
832	87.0	75.2	28.03	1.0	2.9	2.90
899	94.1	80.5	28.03	1.0	3.0	3.00
1008	105.3	90.5	28.03	1.0	3.2	3.20
Counterclockwise						
102	16.7	9.6	7.02	0.25	6.6	1.65
184	192.5	17.1	7.02	0.25	7.3	1.82
339	35.5	32.0	7.02	0.25	8.2	2.05
489	51.2	46.5	7.02	0.25	9.5	2.38
615	64.1	57.5	7.02	0.25	10.0	2.50
726	75.9	68.2	28.03	1.0	2.0	2.75
889	93.1	83.5	28.03	1.0	3.0	3.00
955	99.9	89.5	28.03	1.0	3.1	3.10
1008	105.2	93.7	28.03	1.0	3.2	3.20

100

80

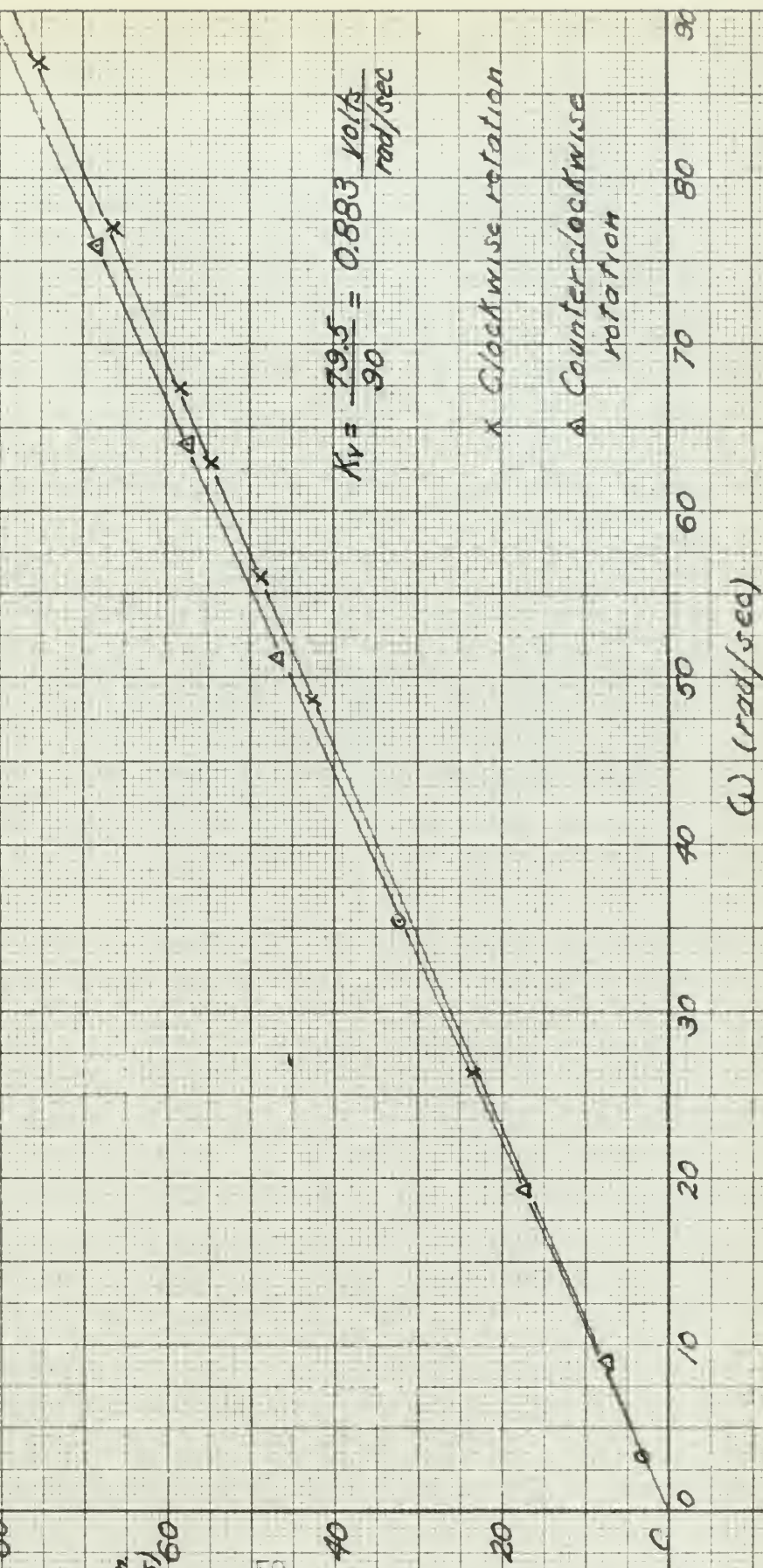
Egen
(volts/60)

50

40

20

0

FIG. 3
Egen. vs. ω 

\times Clockwise rotation
 \times Counter-clockwise
rotation

ω (rad/sec)

Table II

Determination of K_V from expression $E-IR=K_V$

E	$E-IR$	IR	E-IR	RPM	rad/sec
$J=50 \text{ # -in}^2, R=165 \text{ ohms}$					
10	.0195	3.22	6.78	84	8.79
20	.023	3.79	16.21	218	22.80
30	.026	4.28	25.72	355	37.15
40	.029	4.78	35.22	491	51.35
50	.032	5.28	44.72	636	66.50
No Load					
5	.0105	1.73	3.27	26.1	2.7
10	.0122	2.01	7.99	25.0	9.9
15	.0131	2.16	12.84	159.0	16.6
20	.0140	2.31	17.69	236.0	24.7
25	.0145	2.39	22.61	313.0	32.7
30	.0152	2.51	27.49	388.0	40.6

The gear is fastened to the shaft with screws in the three holes shown on the gear and motor shaft. The motor is then fastened in the housing with four screws. Figure 4A shows the motor disassembled. To assemble the motor, the rotor is placed in the stator and fastened with a nut and bolt through the center. The ring holding the brushes is then placed on top of the stator and fastened with screws.

The plot of the $(E - IR)$ versus speed data of Table II is shown on Figure 4. The widely scattered points, as noted on the figure were from the dynamic torque test with the inertia disk load as illustrated in Figure 5. This test was undertaken to determine what effect motor loading would have on the slope of the $(E - IR)$ versus speed curve or the value of K_v .

The slope of the line or K_v is .661 as compared to .883 by the first evaluation or .90 from the manufacturer's data. The value .661 was used in the theoretical calculations in predicting the servo response as it was the only value available at the time. The data from driving the motor is considered more reliable because only two quantities were measured whereas in the Kirchoff's Law method, current was the third quantity. The accuracy of the VTVM is stated by the manufacturer as ± 3 per cent of full scale for DC voltages. Assuming an error as large as 5 per cent, the value of K_v is considered not sufficiently changed to warrant a more accurate meter. One justification is the use of an average



50

40

$(E-IR)$
(volts)

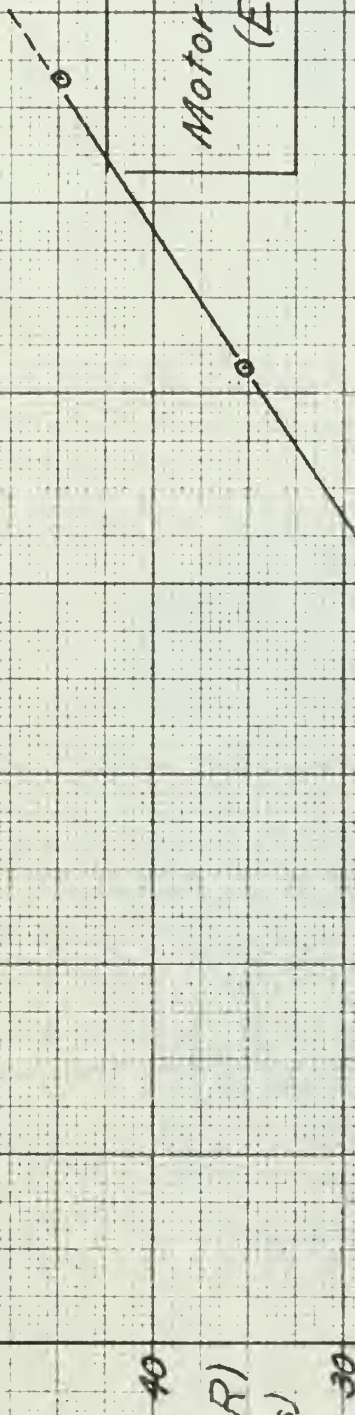
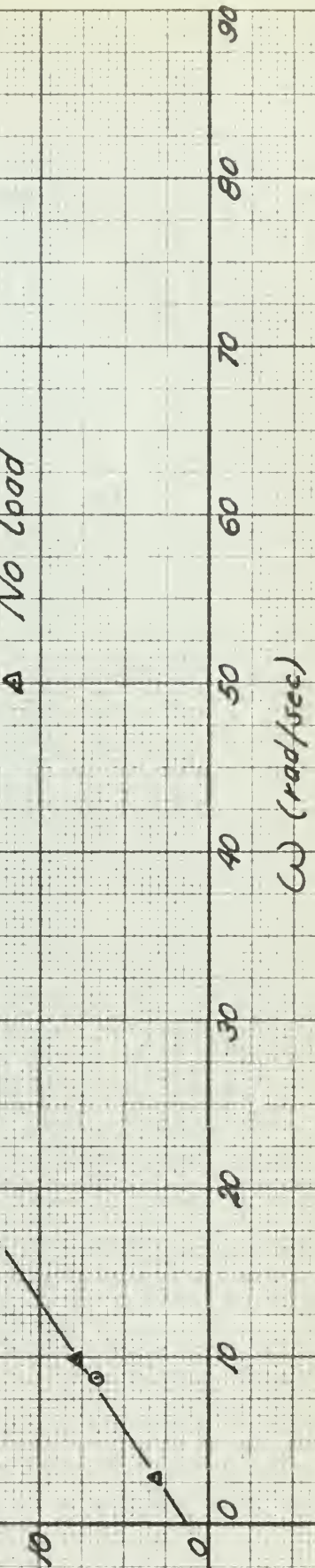


FIG. 4
Motor-Load Combination
 $(E-IR)$ vs. Q

$\bullet \quad k_V = \frac{40.8 - 7.75}{60 - 10} = 0.661 \text{ volt/sec}$

$J = 50 \text{ #-in}^2$

▲ No load



ω (rad/sec)

MOTOR HOUSING

TACHOMETER

SYNCHRO

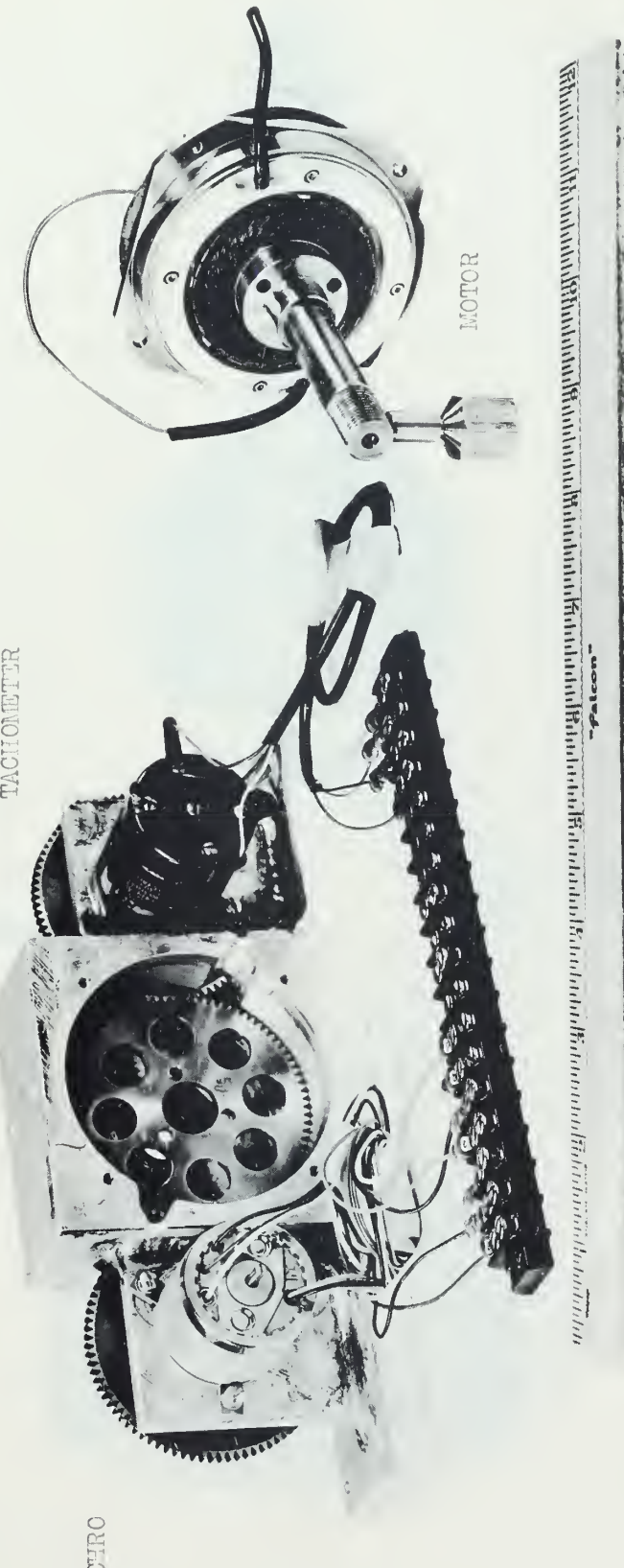
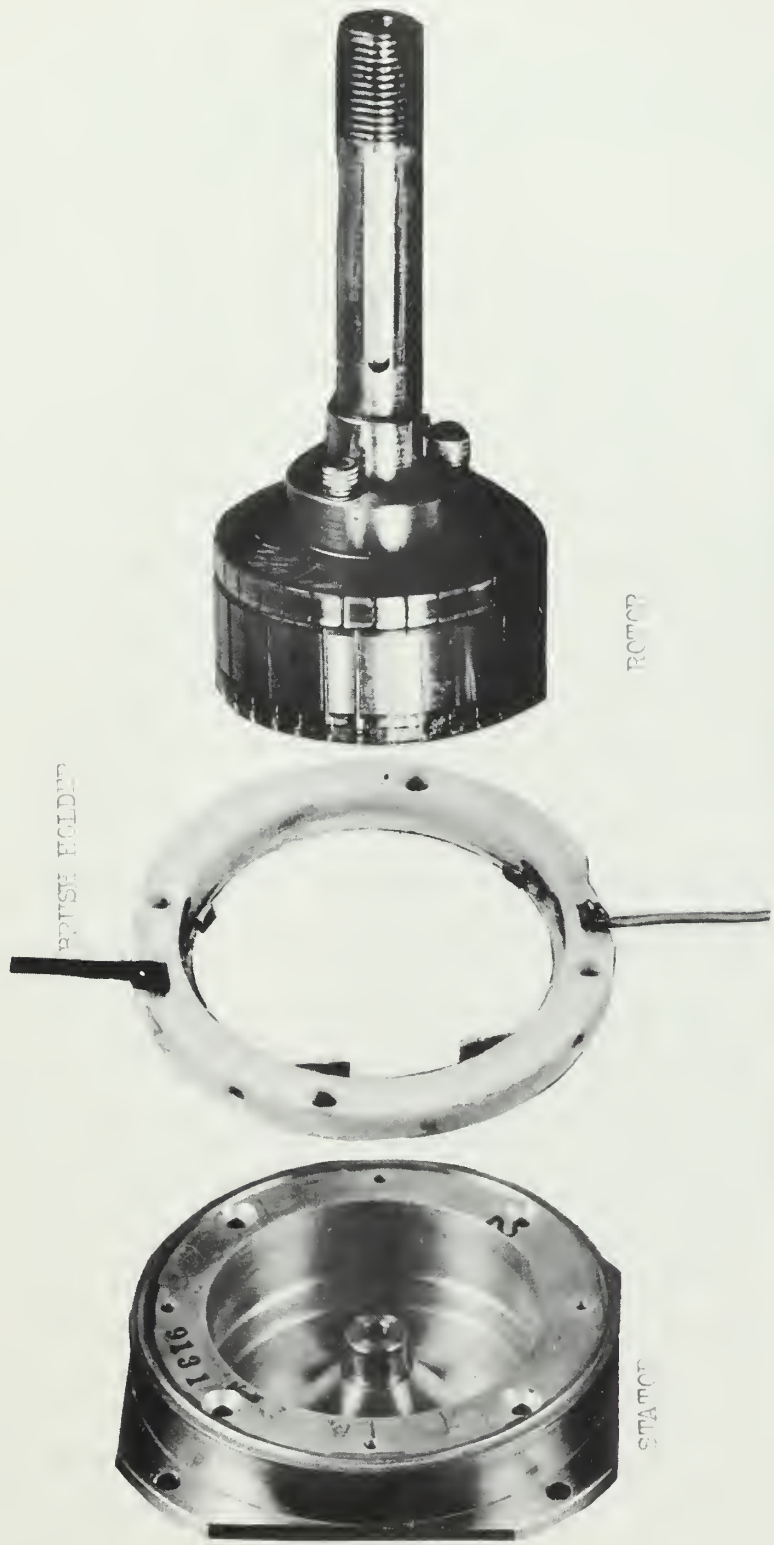


FIG 413 MOUNTING BRACKET FOR MOTOR, TACHOMETER AND SYNCRO "SYNCHRO"



FIG. 4A. MOTOR DISSASSEMBLY



armature resistance of 165 ohms whereas resistance actually varied from 163 ohms to 170 ohms depending on armature position. The Jagabi Chronometric Tachometer is accurate to within 0.5 per cent at speeds over 50 rpm.

Measurement of K_t

The measurement of the motor-torque constant K_t , was made from stalled torque data^{1,4}. As before, several methods of torque measurement were utilized in order to check the validity of the torque constant determined.

The setup of Figures 5 and 6 was used except that the nylon cord from the spring balance was attached to the inertia disk rather than looped around with a suspended weight as shown. Figure 5 is the front and Figure 6 the rear view of the test setup. The inertia disk is the same in both views. In Figure 6 the section of polar coordinate graph paper fastened to the motor housing was used to measure the amount of stator rotation for the ripple torque tests. Armature voltages in increments were applied to the motor while armature current and force on the spring balance were recorded. Two runs were made with the 50 pound-inch² inertia load and two runs were made with the 5 pound-inch² load. The tests with the different inertia loads were run to determine if the increased friction would effect the motor torque constant of the system. The radii of the respective load disks were .25 feet and .1188 feet and torque was calculated by multiplying the spring balance force by the radius of the disk

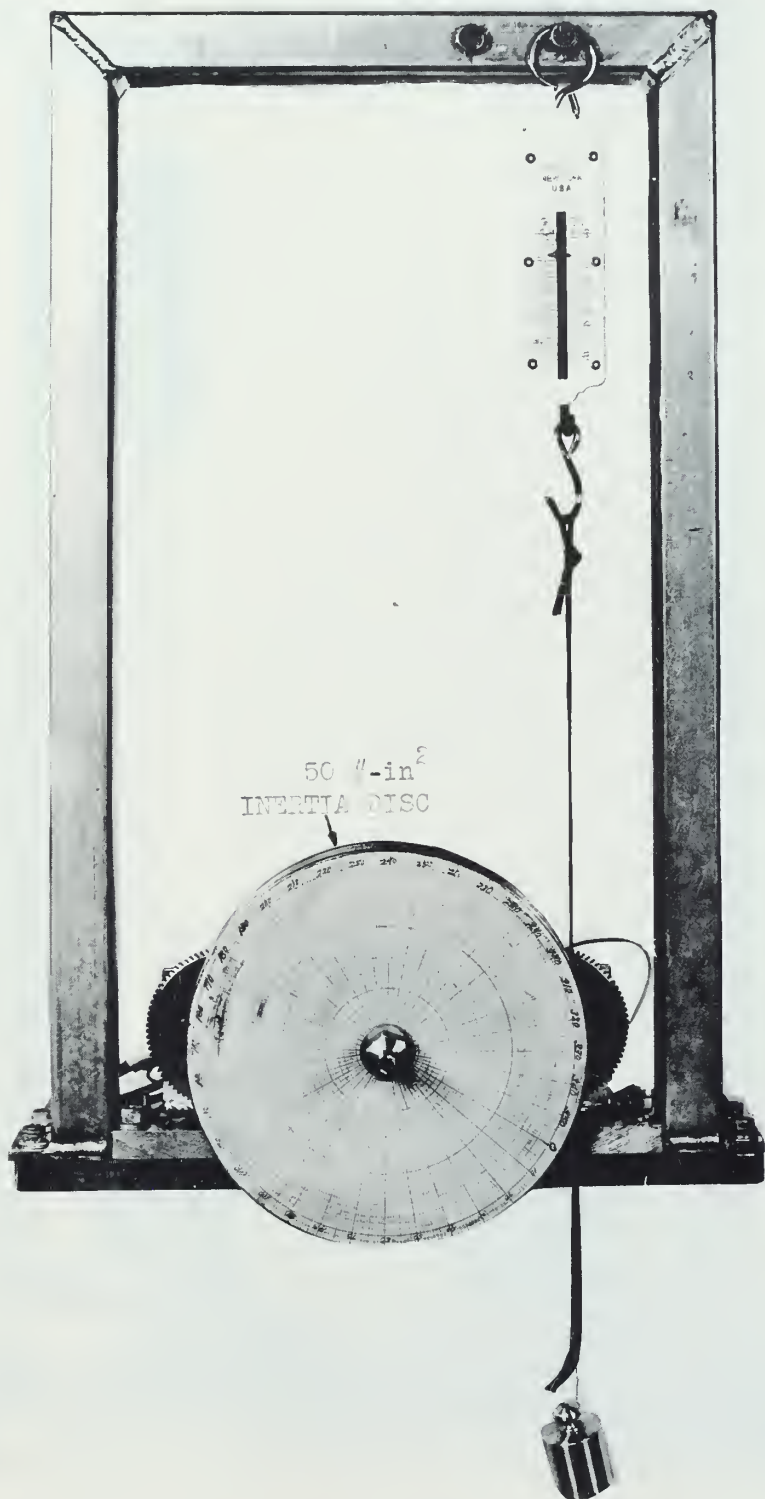


FIG 5 MOTOR BRACKET FOR TOP-PLATE MEASUREMENT
(FRONT VIEW)

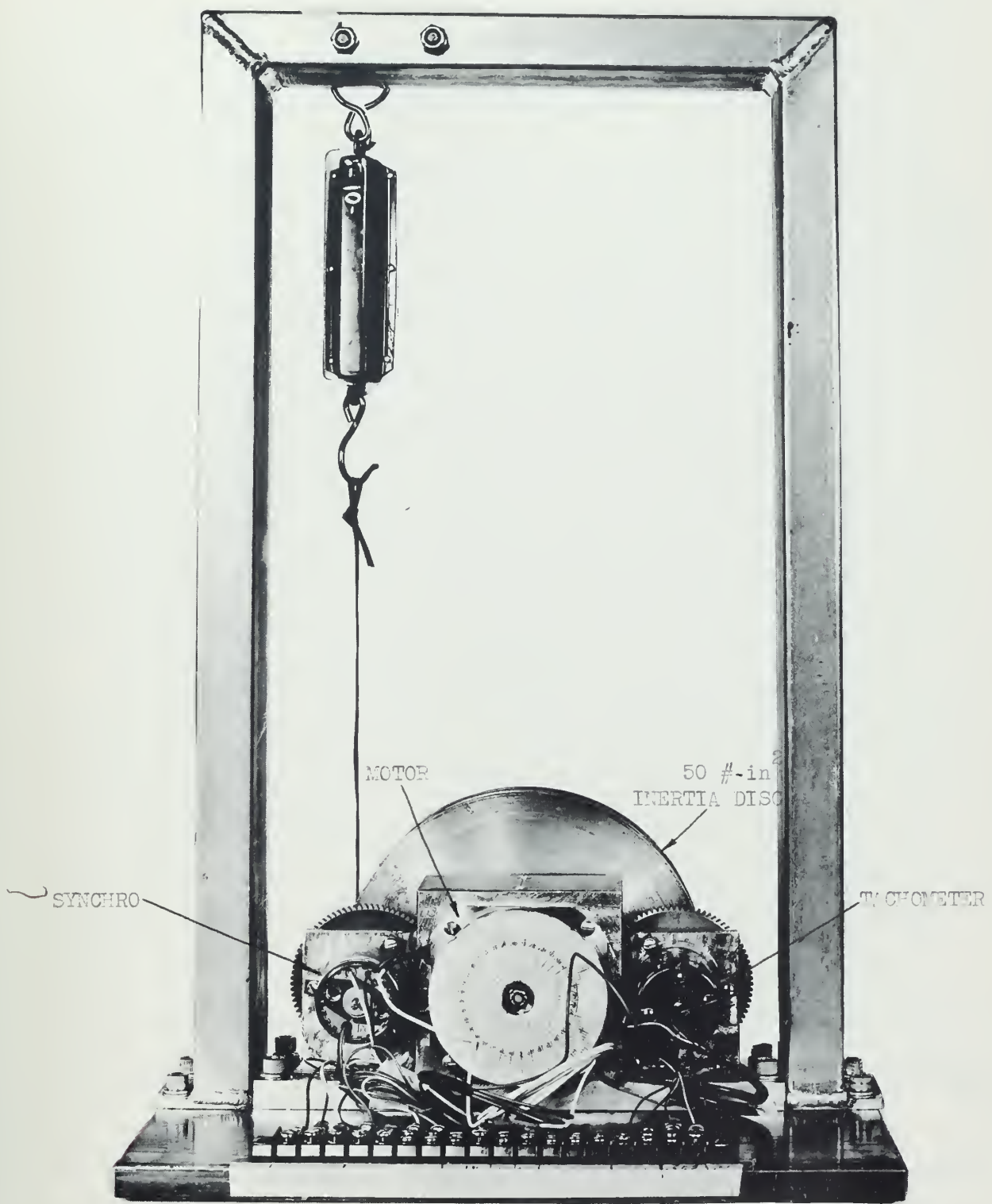


FIG. 6 MOTOR BRACKET (REAR VIEW)

used. At voltages around 75 volts current readings became erratic because of commutation thus limiting the tests. The data is recorded in Table III and the plot of torque versus armature current is plotted on Figure 7. It is noted the data was taken at different times and with different spring balances. It was obvious during these tests that the friction in the spring balance did not give precise repeatable readings. The values for the slopes of the various curves or the motor-torque constant K_t , varied from .463 to .579 foot-pounds per ampere which was not close to the value of .66 pound-feet per ampere given by the manufacturer. The value of .463 was used in the theoretical evaluation of the transfer function and closed loop system since it was the value determined from the latest test which was done with extreme care.

In order to establish confidence in the value for K_t , the test was run again with a torque watch to measure torque. The torque watch has a chuck which fastens to the end of the motor shaft. Fastened to the chuck by a watch spring is a dial calibrated to read torque in inch-ounces. A pointer rigidly attached to the chuck indicates torque as the motor twists the watch spring while the dial is held stationary. The torque watch range of 20 inch-ounces limited the applied voltages to 35 volts as noted in the recorded data of Table IV. The torque versus armature current values are plotted on Figure 8 for the three test conditions of no load, and 5 pound-inch² and 50 pound-inch² inertia disks. There is some vari-

Table III

Determination of K_t from stalled torque data (Spring balance)

Voltage	I	weight ounces	torque in-oz	temp °C
$J = 5 \text{ # - in}^2$ Radius = 1.425				
10	.067	4.0	5.70	23.5
15	.096	6.0	8.55	23.5
20	.158	8.5	12.10	23.5
25	.168	11.5	16.40	23.5
30	.192	12.5	17.82	23.5
35	.208	14.0	19.95	23.0
40	.275	18.0	25.65	23.0
45	.286	19.0	27.06	23.0
50	.300	20.0	28.50	23.0
60	.380	25.1	35.75	23.0
70	.415	28.0	39.90	23.0
80	.417	31.0	44.20	26.0
2nd run				
10	.069	2.70	3.85	
20	.137	6.80	9.68	
30	.205	10.55	15.05	
40	.259	14.90	21.20	
50	.308	17.25	24.55	
60	.367	18.75	26.70	
70	.383	19.75	28.10	
75	.433	24.75	35.25	
$J = 50 \text{ # - in}^2$, Radius = 3"				
10	.065	1.55	4.65	
15	.087	2.50	7.50	
20	.114	3.95	11.85	
25	.172	5.60	16.80	
30	.180	6.55	19.65	
35	.200	7.50	22.50	
40	.225	8.00	24.00	
45	.285	9.60	28.80	
50	.275	10.40	31.20	
60	.303	11.20	33.60	
2nd run				
10	.072	2.70	8.10	
20	.132	3.25	9.75	
30	.203	5.10	15.30	
40	.256	7.75	23.25	
50	.318	8.60	25.80	
60	.353	9.00	27.00	
70	.412	10.20	30.60	

$$\textcircled{O} \quad K_T = 0.496 \text{ ft-lb/amp} \quad 0.75 \text{ in.-oz}$$

$$J = 5 \text{ lb-in}^2$$

$$\textcircled{D} \quad K_T = 0.463 \text{ ft-lb/amp}$$

$$J = 5 \text{ lb-in}^2$$

$$K_T = 0.579 \text{ ft-lb/amp} \quad 20 \text{ in.-oz}$$

$$J = 50 \text{ lb-in}^2$$

$$\textcircled{X} \quad K_T = 0.463 \text{ ft-lb/amp} \quad 23 \text{ in.-oz}$$

$$J = 50 \text{ lb-in}^2$$

$$\textcircled{V} \quad K_T = 0.463 \text{ ft-lb/amp} \quad 1.6 \text{ in.-oz}$$

$$J = 50 \text{ lb-in}^2$$

Torque
(in-oz)

70
30
25
20
15
10
5
0

Fig. 7
Stacked Torque vs. I (arm.)

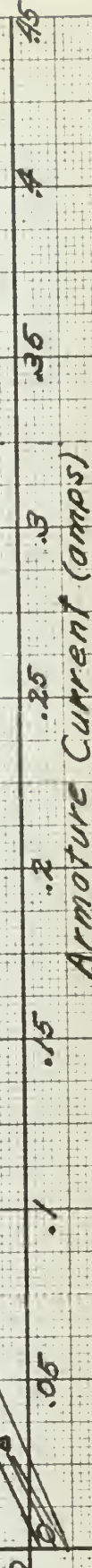


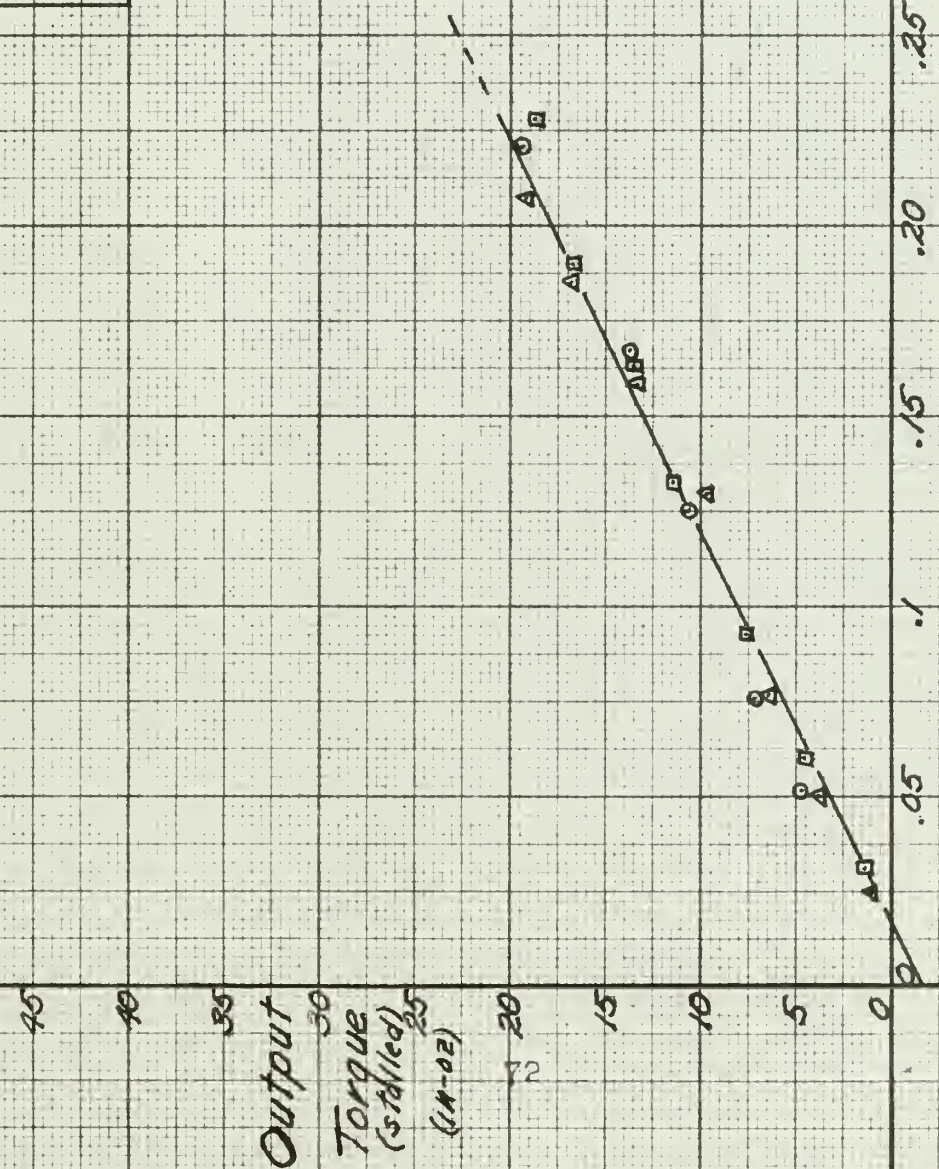
Table IV

Determination of K_t from stalled torque data (Torque watch)

E	I	Torque (in-oz)
$J = 50 \text{ # - in}^2$		
5	.0312	1.4
10	.0605	4.6
15	.0925	7.6
20	.1320	11.3
25	.1620	13.3
30	.1900	16.5
35	.2270	18.8
$J = 5 \text{ # - in}^2$		
5	.024	11.00
10	.051	4.70
15	.0760	7.00
20	.126	10.65
25	.167	13.75
30	.200	15.55
35	.221	19.45
No Load		
5	.0250	1.00
10	.0496	3.75
15	.0766	6.55
20	.1300	9.85
25	.1580	13.30
30	.1850	16.70
35	.2070	19.10



FIG. 8
Output Torque(stalled) vs. I
(Torque match)



Armature Current (amps)

ation in the data, however, a straight line approximation was made and the value of K_t determined as .487 pound-foot per ampere.

The dynamometer² stand was used for measuring the stalled torque in the third test, which was tabulated in Table V. The torque versus armature current data is plotted in Figure 9 and K_t determined as .448 pound-feet per ampere. Although there is variation in the values obtained in the several tests there also appears to be some correlation. The value of .463 pound-feet per ampere falls within the determinations believed to be the more reliable (dynamometer and torque watch), and also obtained in two spring balance tests, therefore, it was used with confidence. The variation with the manufacturer's data is not considered serious in that their values are generalized and may not be based on a wide testing base because of the limited production of these motors. Temperature readings were made as recorded in Table III with negligible temperature raise although the motor was at stall during the entire test.

The back emf constant K_v of any torque motor is related to the torque sensitivity by the relationship⁷, volts per radian per second = $K \times$ (sensitivity in feet-pound per ampere), where $K = 1.356$. This relationship is derived as follows:

Z = number armature conductors

Φ_p = pole flux in webers

l = active length of conductors (meters)

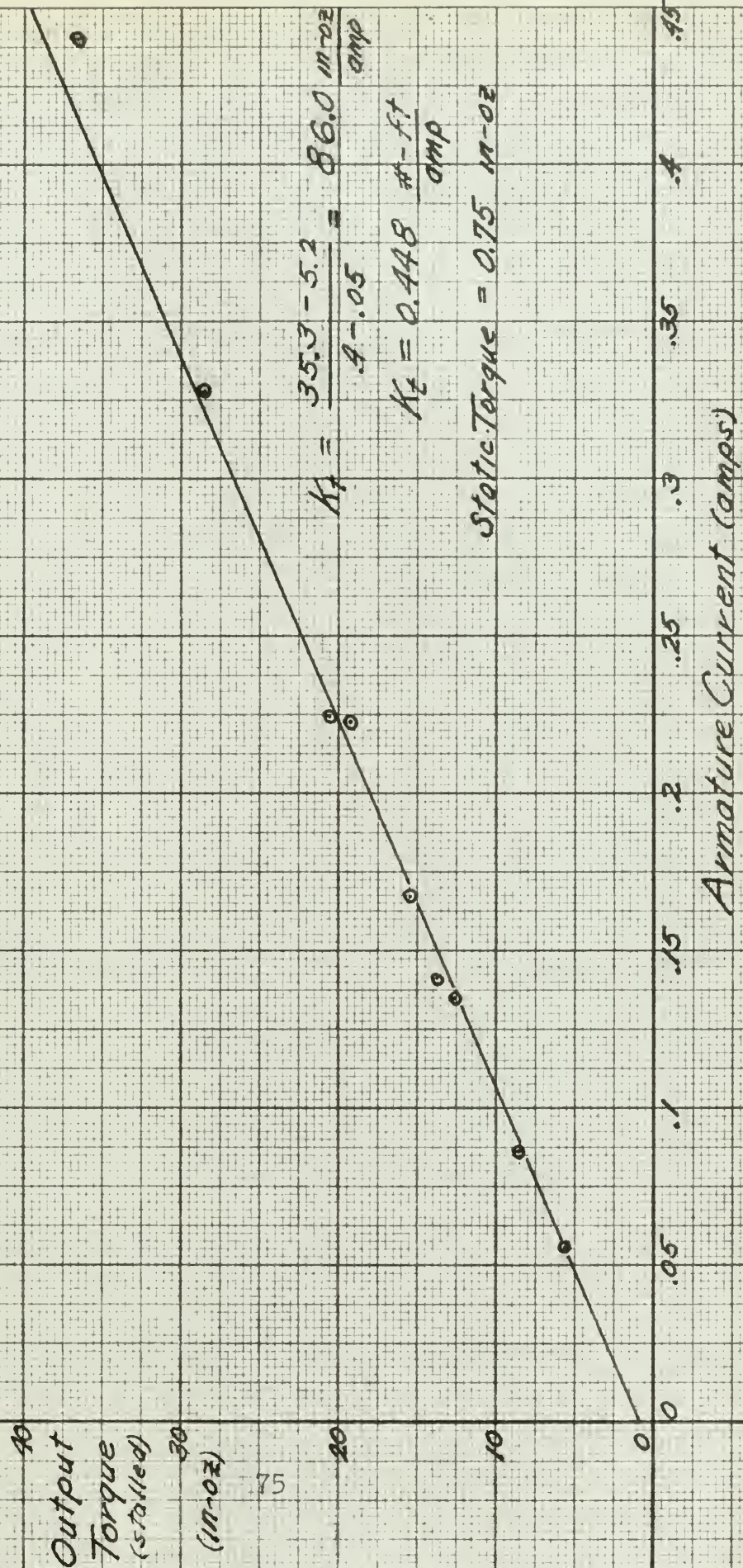
Table V

Determination of K_t from stalled torque data (Dynamometer)

Voltage	I	weight grams	weight ounces	arm inches	torque ounces
10.0	.0556	28.03	.988	5.8	5.74
15.0	.0857	28.03	.988	8.6	8.50
20.0	.1350	56.62	2	6.2	12.40
25.0	.1410	56.62	2	6.8	13.60
29.4	.1670	56.62	2	7.7	15.40
35.0	.2230	56.62	2	9.6	19.20
40.0	.2240	141.98	5	4.1	20.50
43.2	.2280	141.98	5	4.4	22.25
62.0	.3280	141.98	5	5.7	28.50
69.3	.4200	141.98	5	6.5	32.50
88.0	.4400	141.98	5	7.3	36.50

FIG. 9

Output Torque (stalled) vs. I
(Dynamometer)



P = number of poles
 P' = number of parallel paths through armature
 β = flux density under poles = $f (\propto)$ $\frac{\text{webers}}{\text{inch}^2}$
 β_{av} = average flux density for a pole pitch
 T = total torque
 v = velocity in meters per second = $\pi d s$
 ω = $2\pi s$ = radians per second
 s = rps
 i = amperes (current per conductor)
 t = newton-meters (torque per conductor)
 i_a = $i P'$
 d = meters
1 lb. = 4.45 newtons
1 meter = 3.28 feet

$$e_{\text{av/conductor}} = \beta_{av} b v, \quad e_{\text{1 path}} = \frac{Z}{P'} \beta_{av} b v, \quad e_{\text{av/cond}} = \frac{Z}{P'} \beta_{av} b v,$$

$$\phi_p = \beta_{av} b \frac{\pi d}{P}, \quad e_{\text{1 path}} = \frac{Z}{P'} P \phi_p s = K_v s = K_v \omega,$$

$$K_v = \frac{Z}{P'} P \frac{\phi_p}{2\pi} \text{ volts/rad/sec.}$$

$$t_{\text{1 conductor}} = \beta b i \frac{d}{2}, \quad t_{\text{av/cond}} = \beta_{av} b \frac{i_a d}{2P'},$$

$$T = Z \beta_{av} b \frac{i_a d}{2P'} \quad \text{but} \quad \phi_p = \beta_{av} b \frac{\pi d}{P},$$

$$\text{therefore, } T = Z \frac{i_a}{P'} \frac{\phi_p P}{2\pi} \text{ newton-meters or,}$$

$$T = Z \frac{i_a}{P'} \frac{\phi_p P}{2\pi} \frac{3.28}{4.45} \text{ #-ft.}$$

$$T = K_t i_a \quad \text{so} \quad K_t = \frac{Z \phi_p P}{2\pi P'} \frac{3.28}{4.45}.$$

$$K = \frac{K_v}{K_t} = \frac{\frac{Z P \phi_p}{2\pi P'}}{\frac{Z P \phi_p}{2\pi P'} \frac{3.28}{4.45}} = 1.356.$$

Using the value of .463 foot-pounds per ampere as determined in Figure 7, K_v is evaluated as .628 volts per radian per second in the expression above. From the experimental data of Figure 3, K_v was determined to be .661 volts per radian per second which is considered good correlation for experimental data.

Measurement of Friction

As seen from Figure 10, there are three types of friction torque, coulomb, static and viscous, which should be evaluated. The static friction may be evaluated by extrapolating stalled torque versus armature current curves^{1,5}. The coulomb friction which is slightly less than static friction, however, is difficult to measure and was not evaluated. The actual measurement of static friction was made in several ways. Using the setup of Figures 5 and 6 a voltage was applied to the motor while the corresponding current and stalled torque were tabulated in Table III. Two runs were made with the 50 pound-inch squared inertia load and two with a 5 pound-inch squared inertia load. The stalled torque and armature current values of Table III are plotted on Figure 7. By extrapolation the torques at the zero current values are taken as an indication of either coulomb or static torque. These varied from .75 to 2.3 inch-ounces. It is noted that the values were negative, however, the exact interpretation of this intercept is complicated by the fact that friction may either add or subtract from the torque produced by the motor



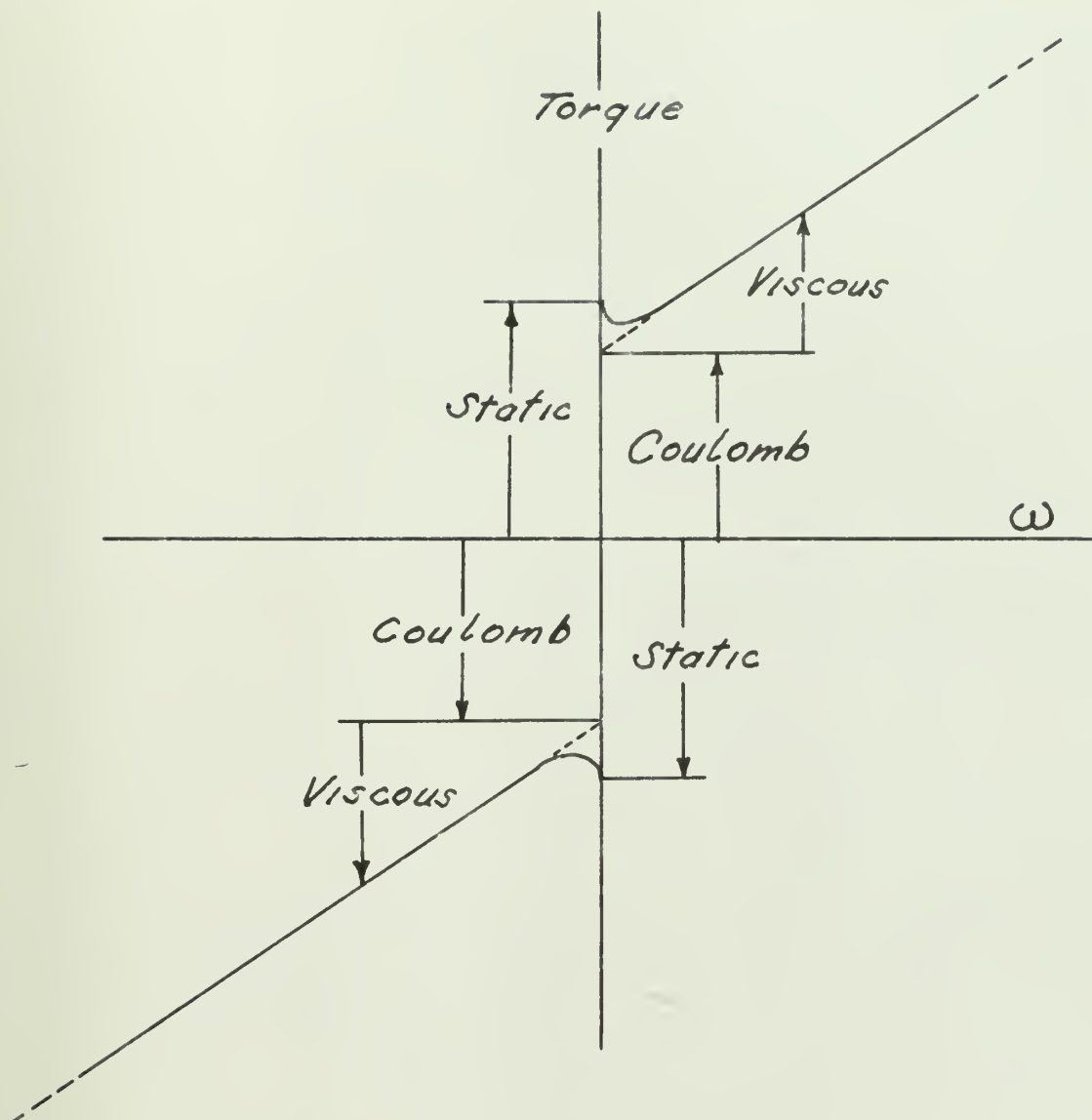


FIG. 10 - Types of friction torque

depending upon the experimental method used.⁵ It was obvious that precise repeatable readings could not be made with the spring balance.

Another set of data was taken utilizing a torque watch for torque measurement under conditions of no inertia load, and 5 and 50 pound-inch squared inertia loads. This data is tabulated in Table IV. The stalled torque versus armature current data is plotted in Figure 8 and it is noted the static torque intercept is + 1.6 ounce-inches and negative⁵.

The torque required to turn the de-energized motor with the torque watch was measured for the conditions of load. The values were respectively 1.9, 2.0, and 1.5 inch-ounces for the 50 pound-inch², 5 pound-inch² and no load conditions. The average value was 1.8 inch-ounces compared with 1.6 inch-ounces from the extrapolated curve.

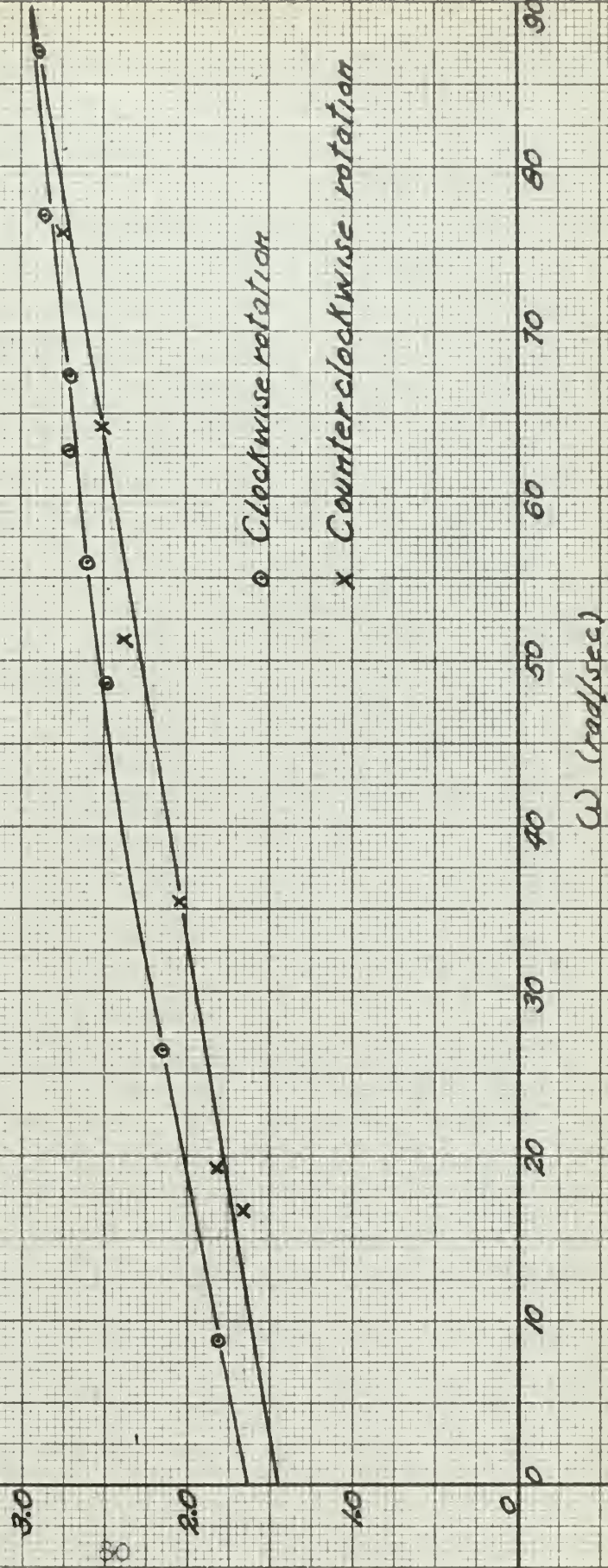
The third static friction measurement utilized the dynamometer previously used for measuring torque. In this test the motor was mechanically driven, with no armature excitation, while torque speed and generated emf were recorded. This data was tabulated in Table I and torque versus speed plotted in Figure 11. By extrapolation the average static friction for clockwise and counterclockwise rotation data was 1.55 inch-ounces.

As with other tests it was felt that the dynamometer tests were the more reliable, therefore, the static friction value of 1.55 inch-ounces was considered to be fairly valid.

FIG. 1/

Coulomb and Viscous
Friction
vs.
 ω (rad/s)

Driving Torque
(motor de-energized)
(in-oz)



The results of the other methods of evaluation⁵ vary about this figure which tends to establish it as a valid average figure.

The viscous friction was measured on the dynamometer while driving the motor as a generator as previously noted. Figure 11 shows viscous friction as a function of motor speed in both the clockwise and counterclockwise directions. From Figure 11 it is seen that at speeds of about 90 radians per second the total friction was 2.95 inch-ounces or assuming a value of coulomb friction of 1.55 inch-ounces the viscous friction was 1.4 inch-ounces. The general shape of the curves of Figure 11 indicate a leveling off at the higher speeds. In the closed loop system, the speeds generally should be much less than 90 radians per second and viscous friction should never be above 1.0 inch-ounces. These values are for the motor, tachometer, synchro pickoff and gears as shown in Figure 4 which was the setup when the loop was closed.

Determining Linearity of the Motor

A DC servomotor is a linear device¹ except for static or coulomb friction effects, therefore, a series of torque versus speed tests were run for various values of applied voltage. It is observed that tests of this kind are for steady state (velocity) conditions but the rate of change of torque with respect to voltage is a constant if the family of curves are parallel straight lines and the partial derivative of torque with respect to speed is constant if the curves are straight lines^{4,6}.

As in other tests two torque measuring methods were employed. In the first test the setup of Figure 5 was used wherein the torque was measured by a spring balance with the nylon cord attached looped around the inertia disk and a weight hung on the end. The expression for determining torque was derived from the two relationships below which are from the Mechanical Engineers Handbook by Marks.

$$HP = \frac{2 RN (w-W)}{33,000}, \text{ where}$$

N is in rpm, R is radius of disk in feet, w is the spring balance reading in pounds and W is the suspended weight in pounds. Also,

$$HP = \frac{T \times RPM}{63,025}, \text{ where}$$

T is in inch-pounds. By equating the two and solving for torque in inch-ounces the following expression was obtained:

$$T = 12.0 R (w-W) \text{ where } R \text{ is in feet.}$$

The radius of the 50 pound-inch squared inertia disk was 0.25 feet and the 5 pound-inch squared disk was 0.1188 feet.

The data obtained for this test is found in Table VI and output torque versus steady state speed data is plotted in Figure 12. Three of the five straight line approximations are based upon two points only but it is observed that all the curves are essentially parallel while still passing through the plotted points.

To correlate these curves, the dynamometer was used to measure output torque¹. Briefly, the motor is driven in the same direction as the developed torque while steady state



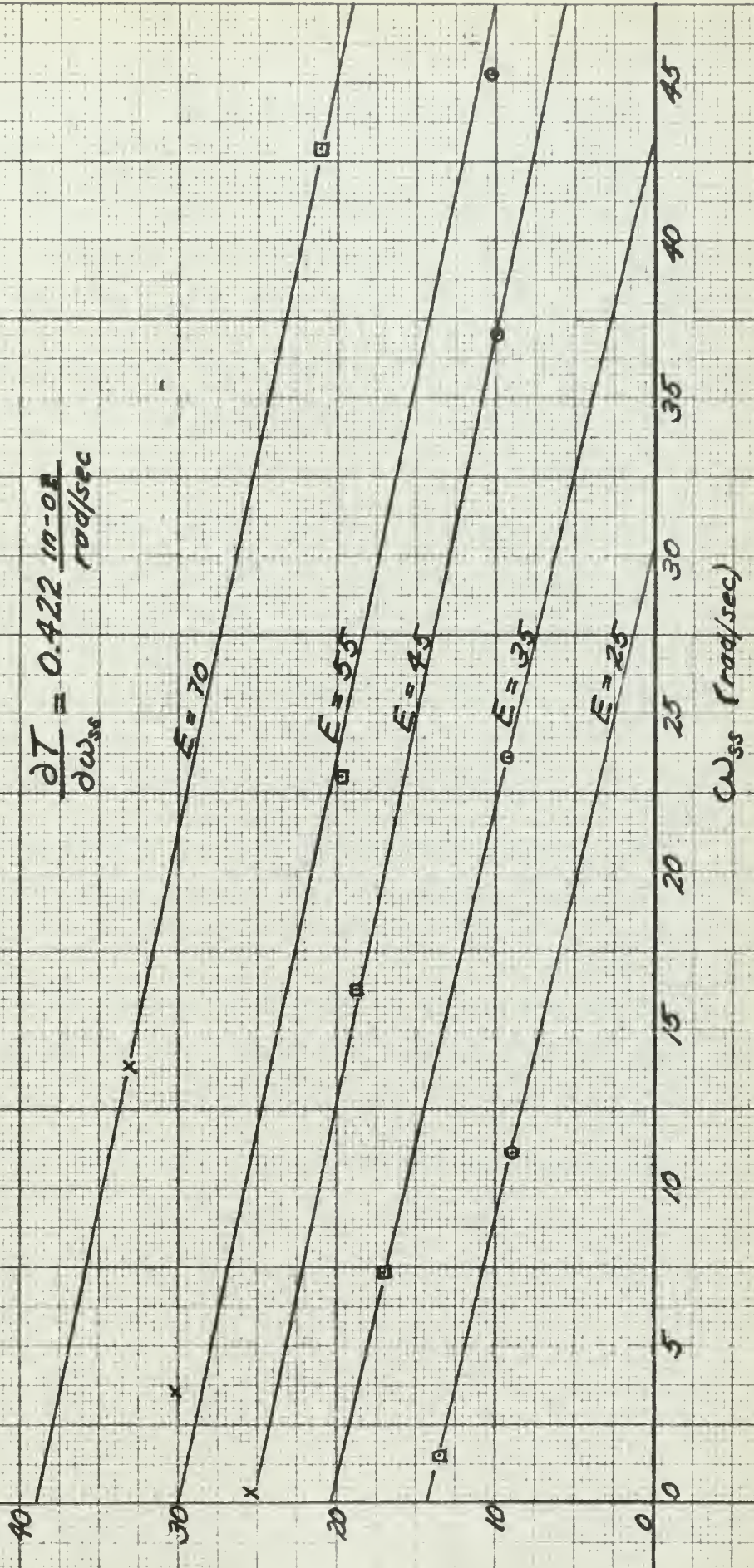
Table VI

Output Torque (Spring Balance)

RPM	ω rad/sec	weight ounces	weight ounces	$W - w$ ounces	Torque in-oz	oE Volts	I Amps
		$J = 50 \text{ lb-in}^2, \text{Radius} = 3"$					
11.0	1.15	3.75	1.0	2.75	8.25	18	.10
106.0	11.10	4.00	1.0	3.00	9.00	25	.11
228.0	23.90	4.12	1.0	3.12	9.36	35	.12
355.0	37.20	4.30	1.0	3.30	9.90	45	.14
432.0	45.20	4.45	1.0	3.45	10.35	55	.15
3.5	.36	12.5	4.0	8.5	25.5	45	.25
34.0	3.56	14.0	4.0	10.0	30.0	55	.29
132.0	13.8	15.0	4.0	11.0	33.0	70	.33
200.0	20.9	15.5	4.0	11.5	34.5	80	.34
3.0	0.31	5.75	2.0	3.75	12.0	20	.12
14.3	1.49	6.50	2.0	4.50	13.5	25	.14
70.5	7.38	7.70	2.0	5.70	17.1	35	.18
155.0	16.22	8.30	2.0	6.30	18.9	45	.20
220.0	23.05	8.60	2.0	6.60	19.8	55	.21
408.5	42.80	9.00	2.0	7.00	21.0	70	.22



Fig. 12

Output Torque vs. ω_{ss} Output Torque
(m-oz)



speed and output torque are measured. The data for several voltages are recorded in Table VII and torque versus speed plotted on Figure 13 where three points for each voltage (except 60 volts) established a line which was considered the straight line approximation. The family of curves are essentially parallel with slopes of .367 inch-ounces per radian per second which gave fair correlation with the previous curves whose slopes were .422 inch-ounces per radian per second.

The curves of Figure 13 are considered more reliable because of the more accurate torque measurements obtainable on the dynamometer, however, the difference may be in the load inertia used in the test of Figure 12 whereas Figure 13 was with no load.

Comparison of the dynamic torque versus armature current curves of the manufacturer with experimental results. The torque and armature current data of the dynamic torque tests tabulated in Tables VI and VII are plotted in Figures 14 and 15 respectively. The points in Figure 14 at torque values around 10 inch-ounces do not lie on the straight line approximation which fairly well passes through the other plotted points. Again this is believed to be caused by insensitive measuring of the torque force with the spring balance. As before, the dynamometer measured torque produced good data at all torque values.



Table VII
Output Torque (Dynamometer)

E Volts	RPM	ω rad/sec	weight grams	weight ounces	arm inches	torque in-oz	I amps
10	170	17.78	28.03	.988	2.1L	2.08	.007
10	250	26.13	28.03	.988	5.3L	5.24	.040
10	337	35.25	28.03	.988	8.7L	8.60	.075
20	339	35.50	28.03	.988	3.3L	3.26	.018
20	461	48.20	28.03	.988	7.9L	7.81	.065
20	562	58.75	56.62	2	5.8L	11.60	.102
30	150	15.67	56.62	2	4.6R	-9.20	-.116
30	356	37.20	56.62	2	0.4R	-0.80	-.032
30	600	62.75	28.03	.988	8.0L	7.91	.062
30	468	48.90	28.03	.988	3.1L	3.06	.012
40	240	25.10	56.62	2	5.6R	-11.20	-.140
40	373	39.00	56.62	2	2.2R	-5.80	-.085
40	510	53.30	28.03	.988	0.5R	-0.49	-.027
60	282	30.20	56.62	2	9.9R	-19.80	-.238
60	195	20.40	141.98	5	4.3R	-21.50	-.253
60	484	50.65	56.62	2	5.7R	-11.40	-.075



Fig. 13

Output Torque vs. ω
(dynamometer)

$$\frac{\partial T}{\partial \omega} = \frac{30.2/17}{75-0} = 0.380 \text{ N-m/sec}$$

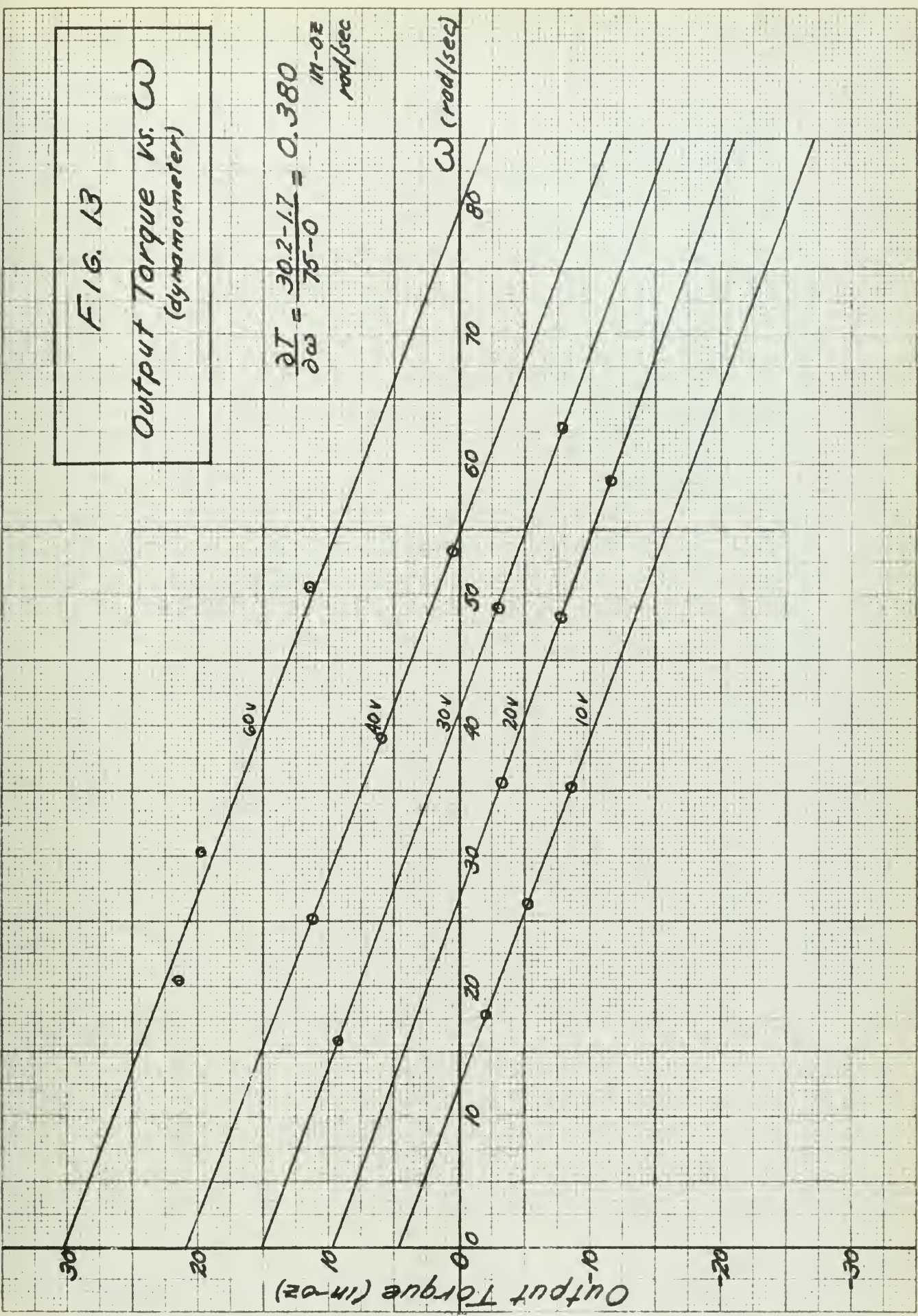
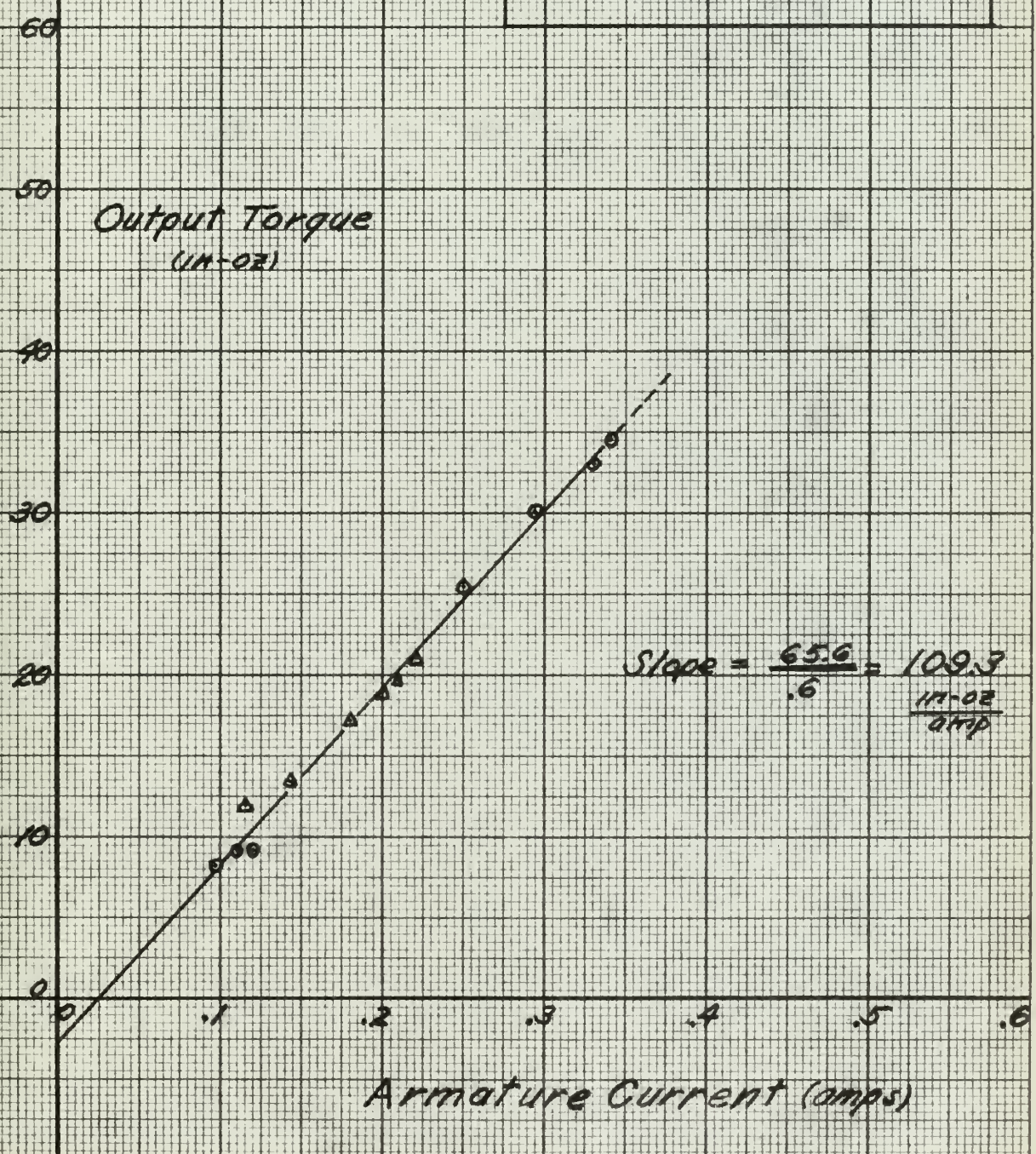


FIG. 14
Output Torque vs. I





30

Output Torque
($N \cdot \text{deg}$)

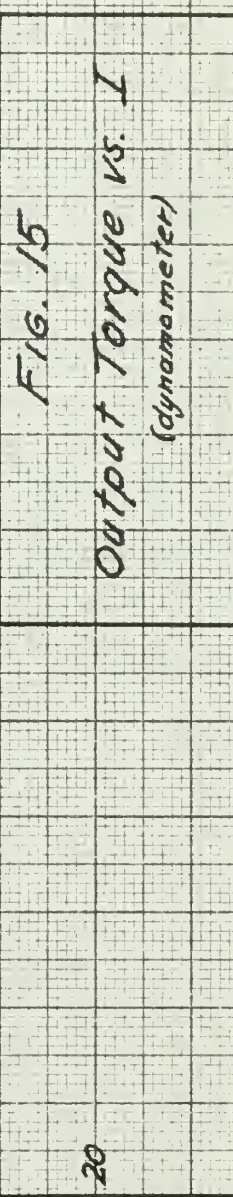
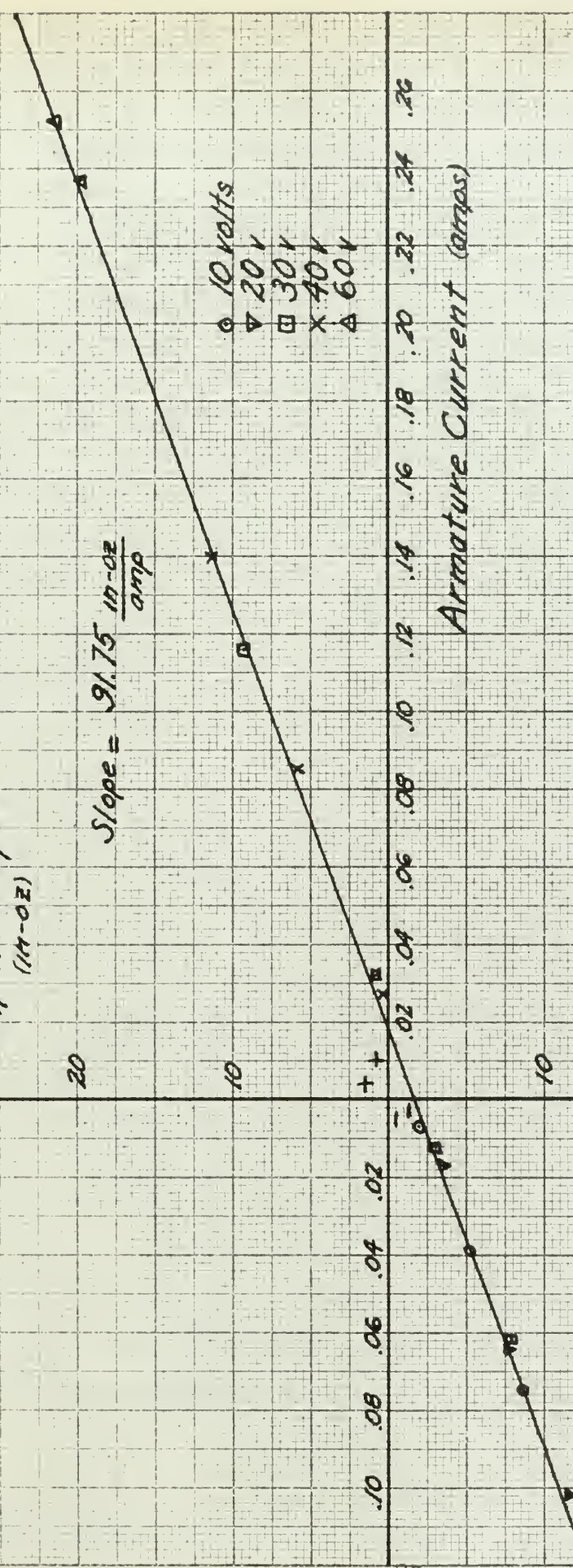
20

$$\text{Slope} = 91.75 \frac{\text{lb-in}}{\text{amp}}$$

10

0

-10



The slopes of the curves are 91.75 inch-ounces per ampere and 109.3 inch-ounces per ampere. The manufacturers data as plotted in Figure 1 gives a slope of 125 inch-ounce per ampere for the linear part of the curve. It is noted here that the slopes of Figures 7 and 8 (K_t values determined for stalled torque versus current) varied from 87.4 to 111.1 inch-ounce per ampere with a value of 88.8 chosen for K_t which correlates with the value obtained in the dynamic torque tests. The variation from the manufacturer's data was not considered serious for the same reason as mentioned previously, therefore, the data obtained in the tests was believed to be reliable. From the dynamic torque test of Figure 15, it is observed that the zero current torque intercept is 1.6 inch-ounce which closely compared with the static torque previously discussed.

Determination of Time Constant, τ .

The time constants for the motor with tachometer, synchro and gears as well as with the inertia load were measured by transient or frequency response or both. The first test was the transient response of the motor with the 50 pound-inch squared inertia load. The circuit for this evaluation is shown in Figure 16. A 100 volt step input was obtained from an electronic power supply. A DC tachometer with disk attached to its shaft was held on the rim of the large inertia disk to give the velocity response of the motor-load combination while the voltage drop across the one ohm resistor was recorded on another Brush amplifier recorder. This transient

response is shown in Figure 16. The average time constant representing 63.2 per cent of the time to reach steady state was approximately 6.0 seconds for two runs. It is recognized that the tachometer rotor also has inertia and friction which would add to that of the motor-load combination to give a time constant greater than the motor-load alone, therefore, the time constant obtained is high. The ammeter of Figure 16A was observed with and without the tachometer and showed a loading effect equivalent to 10 milliamperes at steady state speed.

Another determination of transient response was done utilizing the output torque versus steady speed curves of Figures 12 and 13 with the expression⁶,

$$T = PE - \frac{\partial T}{\partial \omega} \omega ,$$

where T is output torque, E is applied armature voltage, P is a constant of torque over voltage and ω is steady state speed. The constant P is the rate of change of torque with respect to voltage, or,

$$P = \frac{\text{stalled torque at any voltage.}}{\text{voltage producing that torque}}$$

From Figure 12, $P = .561$ inch-ounce per volt and from Figure 13, $P = .496$ inch-ounce per volt for no load dynamic torque. The values of $\frac{\partial T}{\partial \omega}$ were respectively .432 and .380 inch-ounces per radian per second. Neglecting bearing and brush friction⁶, and the electrical time constant which is too small to determine experimentally.

$$J \frac{d^2\theta}{dt^2} = T = PE - \frac{\partial T}{\partial \omega} \omega = PE - \frac{\partial T}{\partial \omega} \frac{d\theta}{dt} , \text{ and}$$

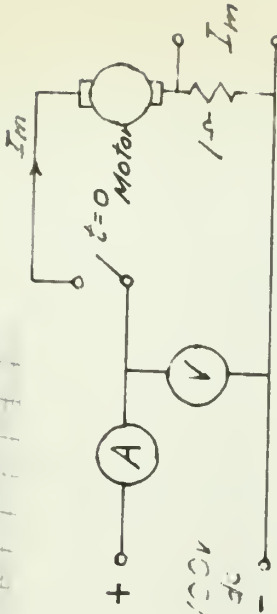


FIG. 16 A
Circuit for Motor Load Transient

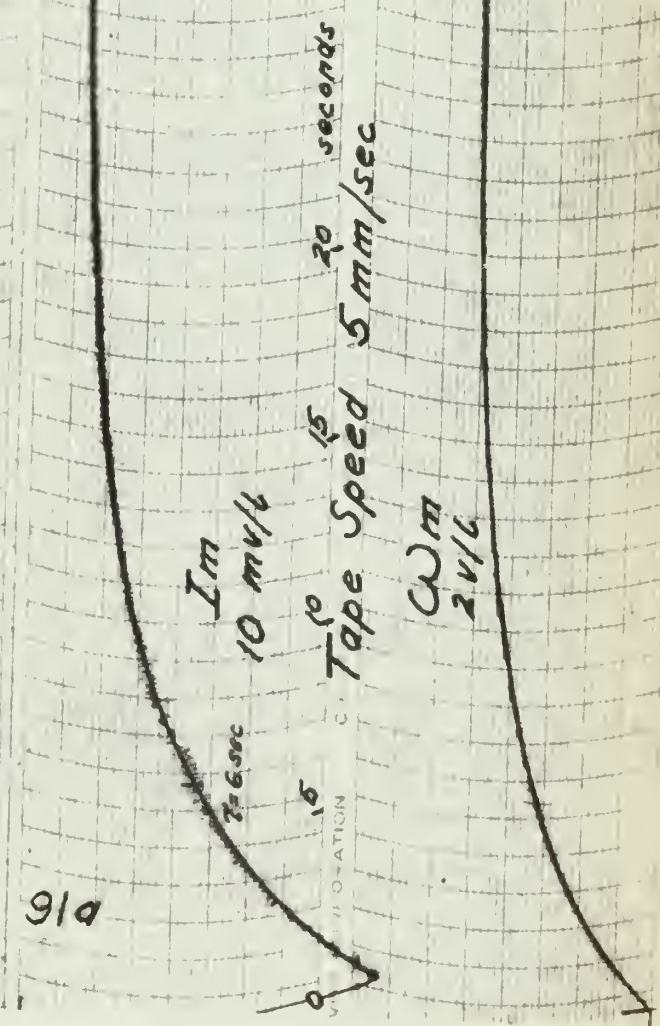
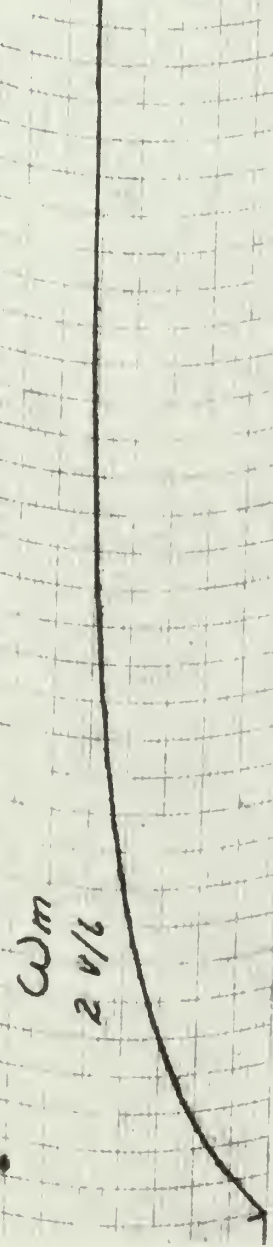
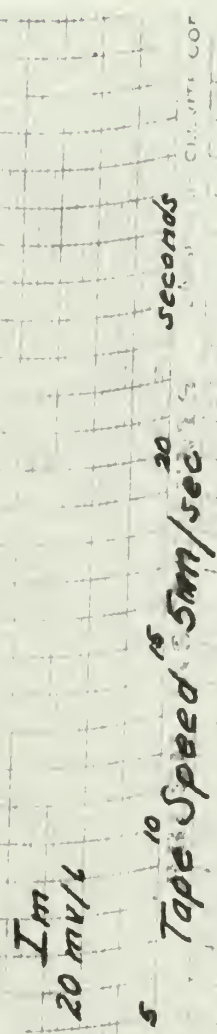


FIG. 16
Determination of Motor and Load Combination Transient

CHART 16-1
MOTOR INSTRUMENT

$$\frac{\theta_0}{E} = \frac{\frac{P}{\partial T/\partial \omega}}{s(s \frac{J}{\partial T/\partial \omega} + 1)},$$

but the approximate transfer function from Chapter II was

$$\frac{\theta_0}{E} = \frac{\frac{1}{K_V}}{s(s \tau + 1)} \text{ and,}$$

$$\frac{1}{K_V} = \frac{P}{\partial T/\partial \omega}, \quad \tau = \frac{J}{\partial T/\partial \omega}$$

Substituting values from the two figures, 12 and 13,

$$\tau_{(m+1)} = 2.37 J_m + 1 \text{ (with inertia load) and,}$$

$$\tau_m = 2.63 J_m \text{ (no inertia load),}$$

where J is in inch-ounce seconds squared. Using $\tau_{(m+1)}$
 $\approx 2.37 J_m + 1$ and a J of 54 pound-inch squared or .224
 inch-ounce second squared calculated in the next section for
 the total inertia of the motor, tachometer, synchro, gears
 and large inertia disk, $\tau_{(m+1)}$ was calculated as 5.3 seconds
 which correlated well with the transient determination of
 6.0 seconds, which was known to be high.

The constant $K_V = \frac{\partial T/\partial \omega}{P}$ was calculated to be .753 and
 .767 volts per radian per second respectively using Figures
 12 and 13, which are compared to the previously experimentally
 determined K_V of .661 and the manufacturers value of .90.

The transient response without the inertia disk was

determined by use of a step input and oscilloscope. The photographs of the transient response for two runs are shown in Figure 17 from which the time constant was determined to be 0.1 second. Figure 17 represents the AC tachometer output for a step voltage applied to the motor.

Using the equation derived from the speed torque curves without load inertia, $T_m = 2.63J$, and a J calculated in the next section of 2.93×10^{-2} inch-ounces second squared, or .707 pound-inch squared, the time constant was calculated at 0.08 seconds.

A third method utilized the frequency response of the motor employing the special mechanical low frequency oscillator of Fig. 18 because of the high current requirements of the motor. (.47 amperes peak). It can be observed in the figure that phase may be read directly on the calibrated dial. In the test setup an oscilloscope was used in conjunction with the phase shifter knob on the mechanical oscillator to read phase shift. Briefly, as the frequency was increased the figure on the scope would shift position thus the phase knob was turned to restore the picture to the index position (the zero or low frequency position) and the phase shift was then read directly.

The mechanical low frequency oscillator was obtained by loan from the University of California. It produces a low frequency sinusoid and square wave from a dc input. The frequency range is .002 cps to 15 cps and the dc output cur-

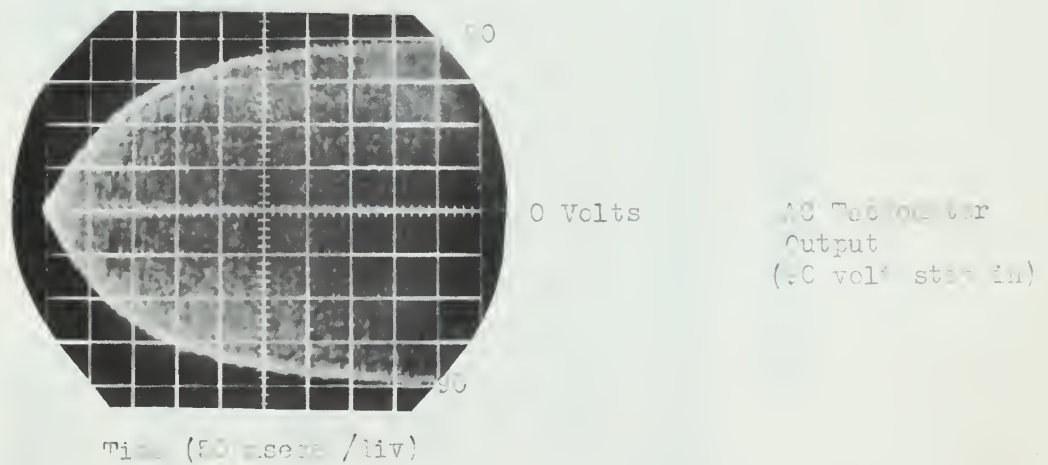
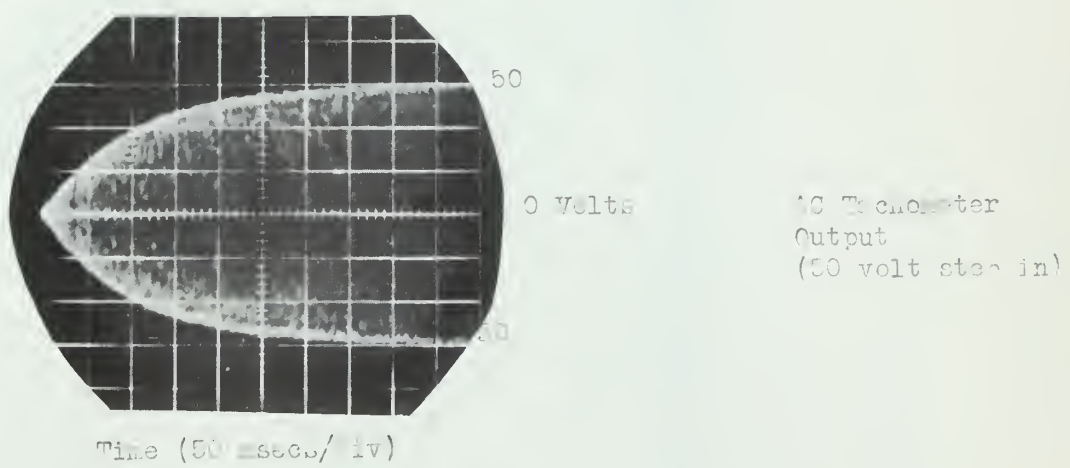


Fig 17 TRANSIENT BEHAVIOR OF MOTOR IN ONE CONDITION (NO LOAD)



FIG. 18. MECHANICAL OSCILLATOR?



rent is limited to 1.5 amperes. The magnitude of the input signal is the magnitude of the sinusoid. The ordinary commercial frequency generators are not suitable for this application because of current limitations.

Two runs were made with the motor and pickoffs but no-load. One at ± 57 volt dc swing and the other at ± 25 volt dc swing. The frequency range at the lower voltage did not provide enough data to determine the corner. Also in a third run with the higher voltage but with the 50 pound-inch squared inertial load the same situation occurred. The plot of Fig. 20 represents the ± 57 volt no-load test of Table VIII. From the figure the corner frequency was determined to be at 14 cycles per second. Taking the reciprocal of this value the time constant was calculated to be .0714 seconds for the motor with tachometer, synchro and gears.

In the three methods used to determine the time constant under no load conditions the values obtained were 0.1, 0.08 and 0.0714 second respectively. The time constant of the motor, tachometer, synchro and gears was considered to be the average value of 0.084 seconds. The electrical time constant of the motor is at 1930 cps and could not be determined experimentally because of frequency limitations.

Calculation of Moment of Inertia, J.

From the dimensions and weights of the inertia disk and gears shown in Fig. 21 their moments of inertias were calculated using the formulas,

$$J_{cyl} = \frac{mr^2}{2} \text{ or,}$$

$$J_{rings} = mr^2.$$

Table VIII

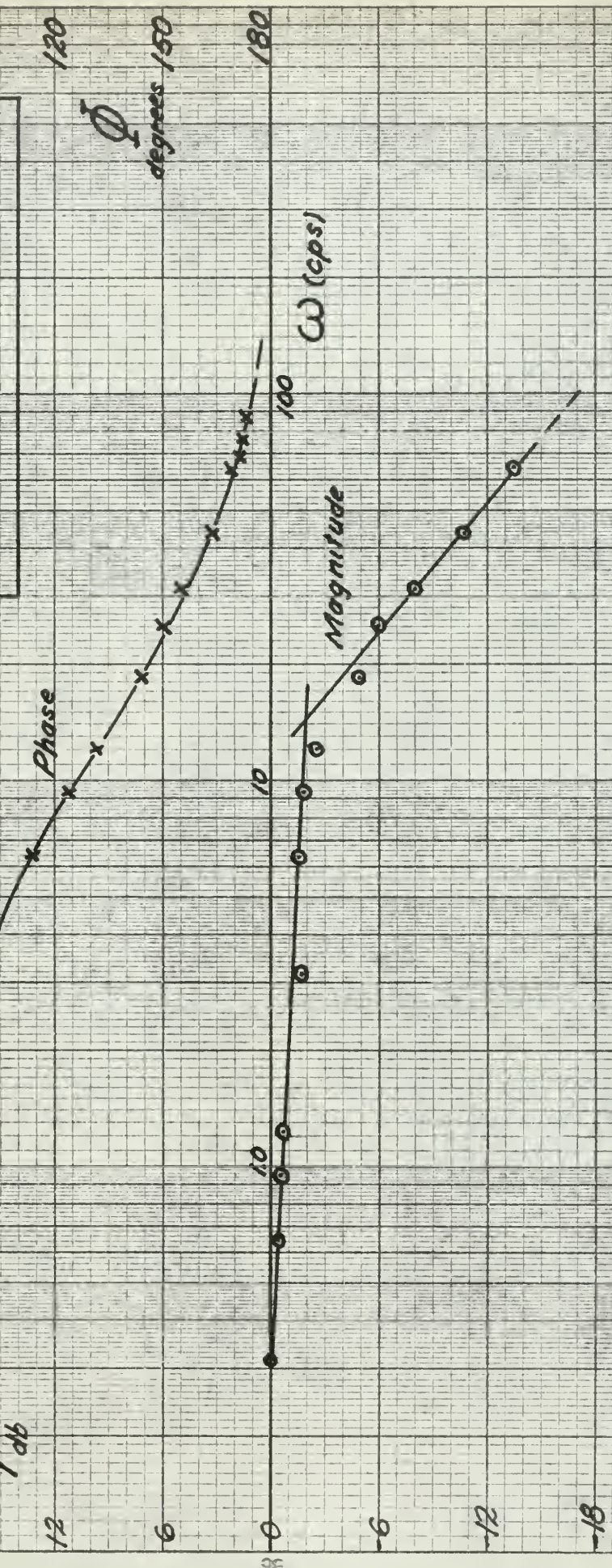
Frequency Response of Motor with Tachometer,
 Synchro and Gears (No load)
 (± 57 V DC Input)

Freq. cps	Magnitude volts	Magnitude Non-dimensional	r db	Phase Shift degrees
.050	7.0	1.00	0.00	0
.100	6.8	0.97	-.27	0
.150	6.6	0.94	-.52	-2
.195	6.4	0.91	-.82	-4
1.00	6.0	0.86	-1.30	-24
1.50	5.6	0.80	-1.92	-33
1.95	5.2	0.74	-2.60	-41
3.00	4.0	0.57	-4.84	-53
4.00	3.5	0.50	-6.00	-59
5.00	2.8	0.40	-7.94	-66
7.00	2.1	0.30	-10.44	-73
10.25	1.5	0.21	-13.54	-78
11.00	1.4	0.20	-14.00	-81
12.20	1.25	0.18	-15.50	-82
14.00	1.12	0.16	-16.60	-83

24

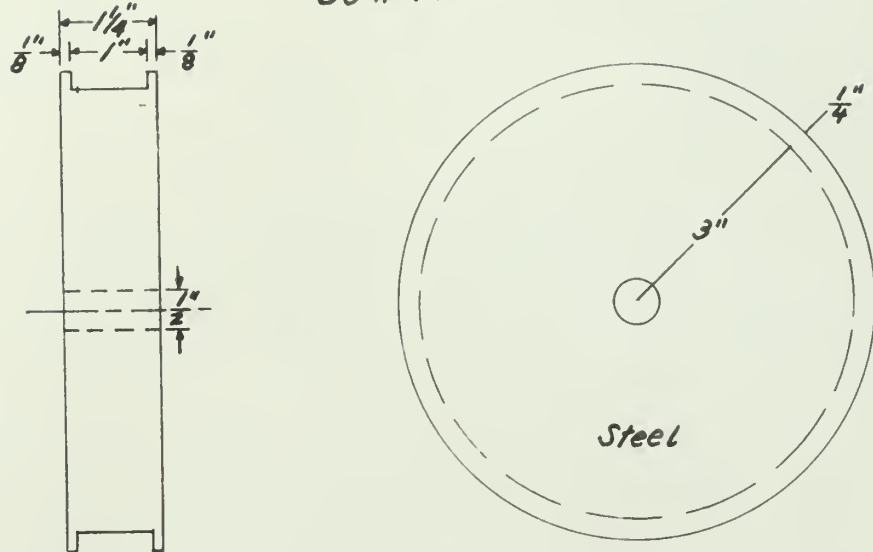
FIG. 20

Frequency Response of
Motor without Load

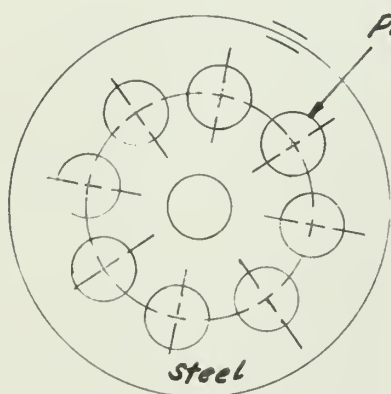


24

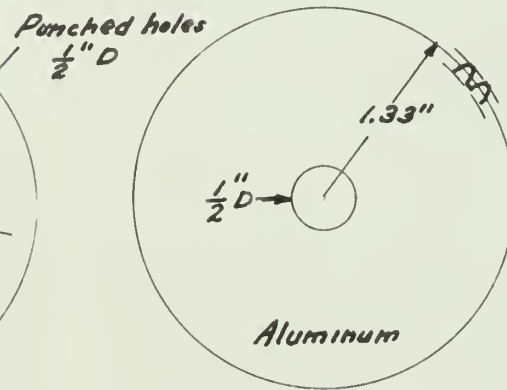
Inertia Disk
50 $\# \cdot \text{in}^2$



Gears



Motor



Tachometer & Synchro
Antibacklash

FIG. 21 - Inertia load and gears

The large inertia disk was calculated to have an inertia of 53.97 pound-inch squared rather than the nominal design value of 50 pound-inch squared. The gears were calculated to have a J of $.9375 \times 10^{-4}$ pound-feet second squared or .434 pound-inch squared. From the manufacturers catalogs, the Bendix Autosyn Resolver (synchro), Model AY-222-S-5-B rotor inertia was 12 gram-centimeter squared and the Kearnott Model R-700-2A Tachometer rotor inertia was 2.1 gram-centimeter squared.



REFERENCES

1. Thaler, G. J. and Stein, W. A., Transfer Function and Parameter Evaluation for DC Servomotors, Proceedings of the AIEE, Applications and Industry, January 1956.
2. Van Wambeck, S. H. and Stein, W. A., A Special Dynamometer for Testing Small Motors, Electrical Engineering, vol. 71, June 1952, pp. 549-51.
3. Saunders, R. M., Measurement of DC Machine Parameters, Electrical Engineering, vol. 70, Sept. 1951, pp. 787-92.
4. Greenwood, I., Holdam, J., and MacRae, D., Electronic Instruments McGraw-Hill Book Co., Inc., New York, 1948, p. 357.
5. Greenwood, I., Holdam, J., and MacRae, D., op. cit., pp. 453-55.
6. Thaler, G. J., Elements of Servomechanism Theory, McGraw-Hill Book Co., Inc., New York, 1955, p. 259.
7. Catalog, Inland Torque Motors and Rotary Amplifiers, Inland Motor Corporation, Pearl River, New York, 1959.



CHAPTER V

INTERMEDIATE ANALYSIS AND DESIGN; TORQUE MOTOR AND SERVO SYSTEM

This chapter is a more accurate analysis of the anticipated response of the system since it incorporates actual experimental data rather than manufacturer's information. Essentially, this Intermediate Analysis is obtained in much the same manner as the Preliminary Analysis.

Proceeding as in Chapter III, Preliminary Analysis, a new motor transfer function and system transfer function was obtained based on the motor characteristics determined by experimentation. This data was summarized in tabular form at the conclusion of Chapter IV. The general motor transfer function was derived in Chapter II:

$$1. \frac{\theta_o}{E} = \frac{1}{K_v S \left[\left(\frac{J R}{K_v K_t} S + 1 \right) \left(\frac{L}{R} S + 1 \right) \right]}$$

Substituting experimental values,

$$2. \frac{\theta_o}{E} = \frac{1}{.665 \left[\frac{(18.4 \times 10^{-4})(165)}{(.66)(5.5)} S + 1 \right] \left[\frac{.15}{165} S + 1 \right]}$$

Which simplifies to:

$$3. \frac{\theta_o}{E} = \frac{1.515}{S(0.083S+1)(9.09 \times 10^{-4}S+1)}$$

Comparing the time constants of this transfer function with equation 13 of Chapter III reveals little correlation.



This, of course, can be attributed to the fact that the results obtained in Chapter III were based on manufacturer's data. In addition, the motor time constant of .083 seconds above includes the effects of the synchro pickoff and tachometer gearing.

Figure 1 represents the logarithmic plot of this motor transfer function. Comparison with Figure 20 of Chapter IV reveals close correlation and indicates that the theoretically obtained data is close to the experimental characteristics. As mentioned in Chapter IV, the second corner (electrical time constant) at 1100 radians per second (176 cycles per second) is not shown on this plot due to its negligible effect on servo performance.

The motor-load combination transfer function was obtained by including the load inertia in equation 1.

$$4. \frac{\theta_o}{E} = \frac{1}{.665 \left[\left(\frac{.14 \times 165}{.66 \times 5.5} s + 1 \right) \left(\frac{.15}{165} s + 1 \right) \right]}$$

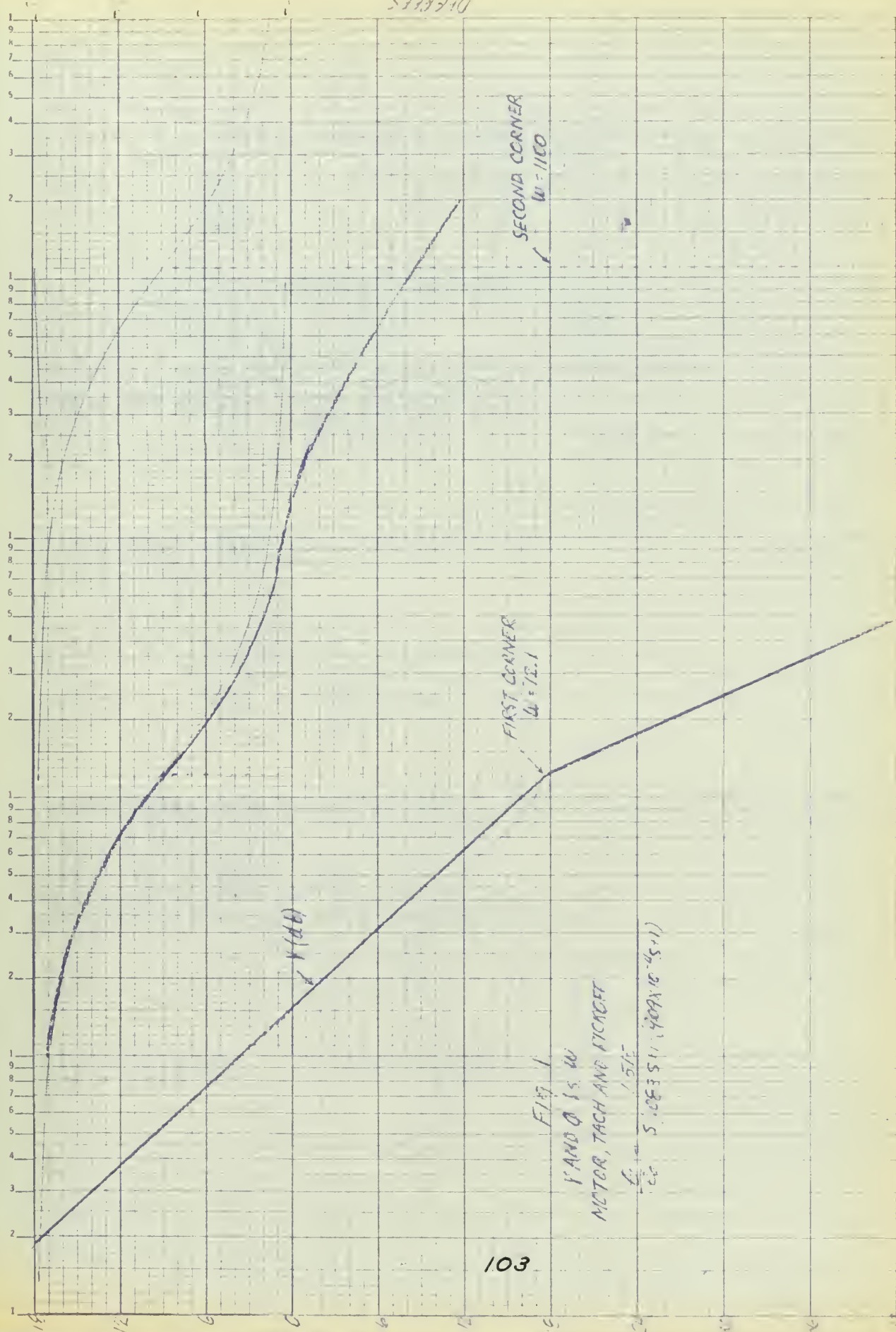
$$5. \frac{\theta_o}{E} = \frac{1.515}{s \left[(6.45 + 1) \left(9.09 \times 10^{-4} s + 1 \right) \right]}$$

Comparing the 6.4 second inertial time constant with Figure 20 indicates a close correlation.

Utilizing this transfer function, the open loop transfer function was obtained. Shaping the resultant locus in such a manner as to meet design and ASME criteria, explained

APR 19 1994

5333270



103

AND O IS IN
NETC TECH AND STCET

15/5

1152-21804:11 \$53.00 23

卷之三

四

160

150

11. *Geologists*

6

1734/73

on page 32 of Chapter III, revealed a requirement for a zero at -60 and a pole at -6. Other poles can be located at any values greater than -1000.

Again both lead and tachometer feedback compensation will be required in order to stabilize the system. Proceeding as in Chapter III many compensation schemes were tried with little success. For the most part, the amount of amplifier gain required was prohibitive. Finally it was determined that a lead network, $\frac{S+60}{S+100}$, would produce a satisfactory system. This network was decided upon by utilizing the same reasoning explained on page 32 of Chapter III.

Using a nominal gain of 1000, the intermediate design was developed in the following manner. The motor transfer function is:

$$6. \frac{\theta_o}{E} = \frac{232}{5(S+139)(S+1100)}$$

Proceeding as on page 36 of Chapter III, the open loop transfer function was obtained in the conventional manner:

$$7. F_o = \frac{\frac{(232)(1000)(S+60)}{5(S^2+1100S+153)(S+100)}}{1+hS \left[\frac{(232)(1000)(S+60)}{5(S^2+1100S+153)(S+100)} \right]}$$

$$8. F_o = \frac{232000 (S+60)}{5 \left[S^3 + 1170S^2 + (110,000 + 232,000h)S + (15,300 + 13,920,000h) \right]}$$

This equation can be factored as:

$$8a. F_o = \frac{23,200 (s+60)}{s(s+a)(s+b)(s+6)}$$

Specifying one root of the characteristic equation at -6 as done in Chapter III to properly shape the locus:

$$a + b + 6 = 1170$$

$$ab + 6a + 6b = 110,153 + 232,000h$$

$$6ab = 2550 + 2,320,000h$$

Solving these simultaneous equations the following values were obtained:

Tachometer constant: .05153

Roots: -6, -117, -1047

Figure 2 is a logarithmic plot of this system, designated the Intermediate Design. Figure 3 represents the M-N chart and Figure 4 is the M-N versus W for this system. No data is presented for frequencies greater than 300 radians per second.

Transient Response

The closed loop transfer function, F_c , is obtained in the following manner:

$$F_c = \frac{F_o}{1+F_o}$$

Thus,

$$9. F_c = \frac{232,000 (s+60)}{s^4 1170 s^3 + 129,483 s^2 + 966,994 s + 13,920,000}$$

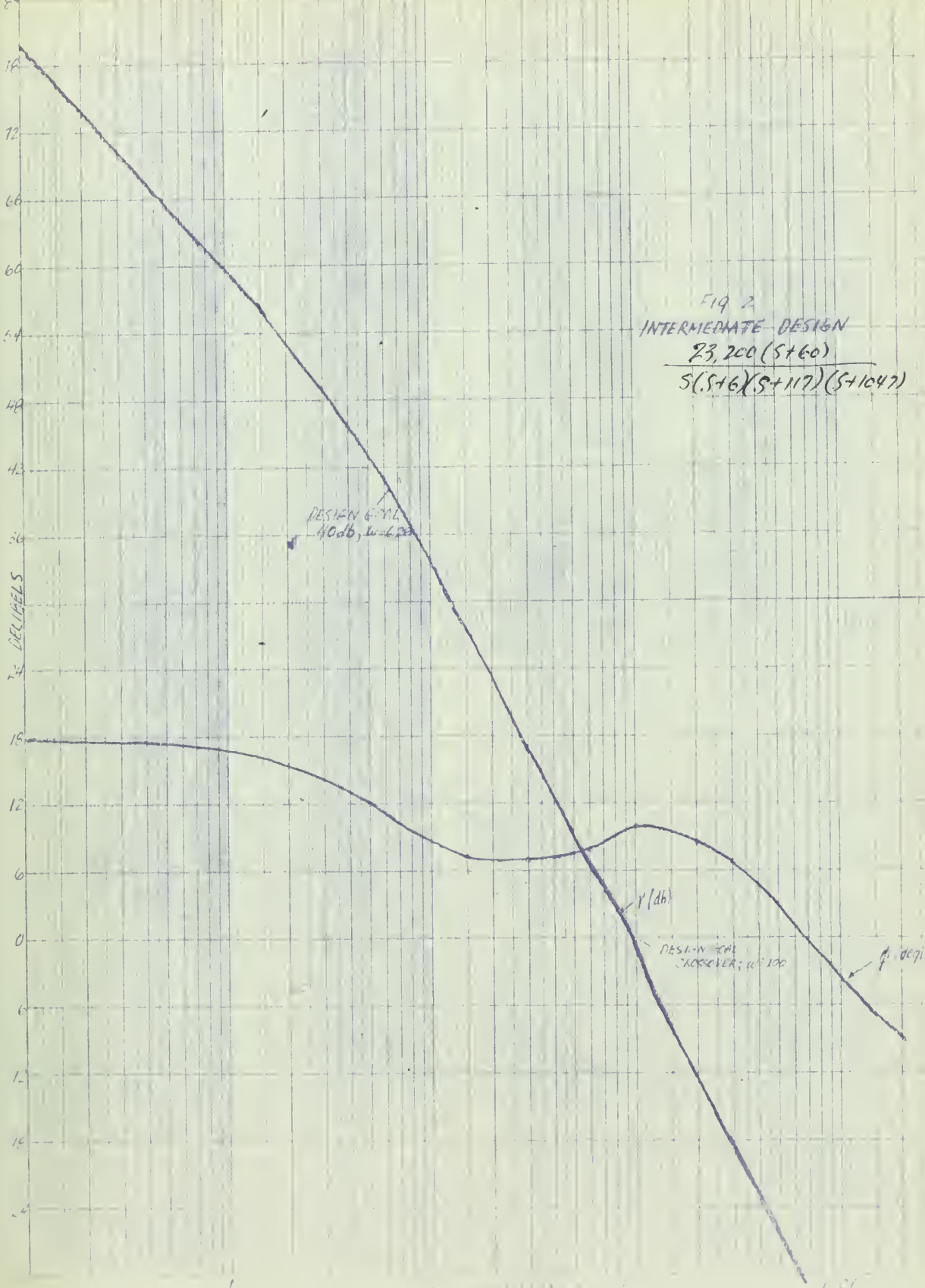
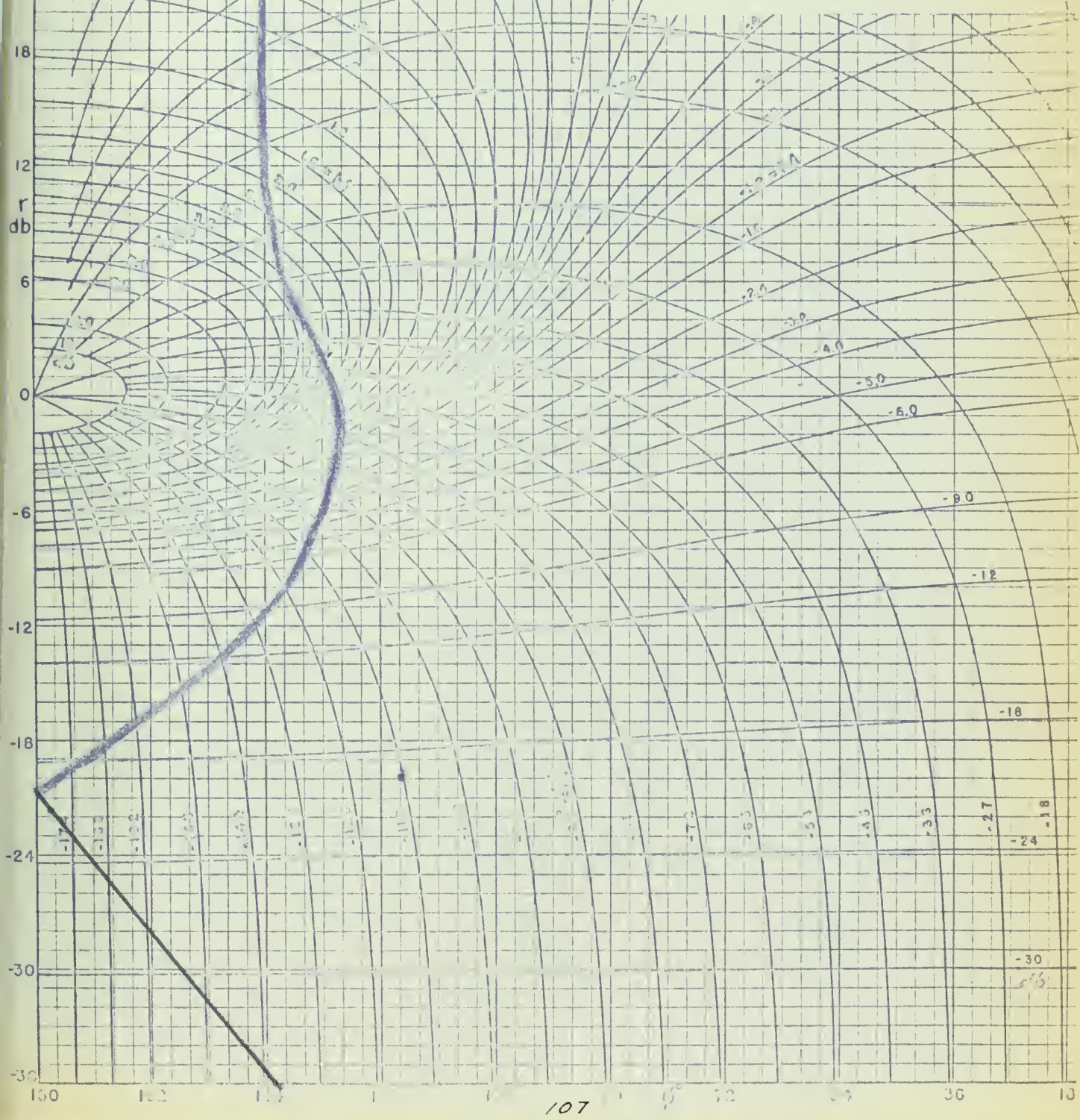




FIG 5
PEN CHART
LEAD-TACHOMETER
SYSTEM
INTERMEDIATE DESIGN



INTERMEDIATE DESIGN

M vs w

FIG 4

25

26

27

28

29

30

31

32

Solving the quartic in the manner prescribed on page 91, Brown and Campbell, the roots of the characteristic equation are:

$$-3.5 \pm j 10.1, -1047, -115$$

Factored, the closed loop transfer function appears as:

$$10. \quad F_c = \frac{232,000 (s+60)}{(s+3.5+j10.1)(s+3.5-j10.1)(s+1047)(s+115)}$$

Calculation of the transient response can be approximated by:

$$\theta_o(t) = 1 + \frac{K}{W_c W_m M_3 M_4} e^{-\alpha t} \sin(\omega_c t - \theta - \psi)$$

$$= 1 + 1.04 e^{-3.5t} \sin(10.1t - 2)$$

11.

Here again the negligible terms have been disregarded for times greater than .01 second.

Figure 5 represents the transient plot for this system. The following is a tabulation of the pertinent data represented by this intermediate system, a system designed to meet all specifications.

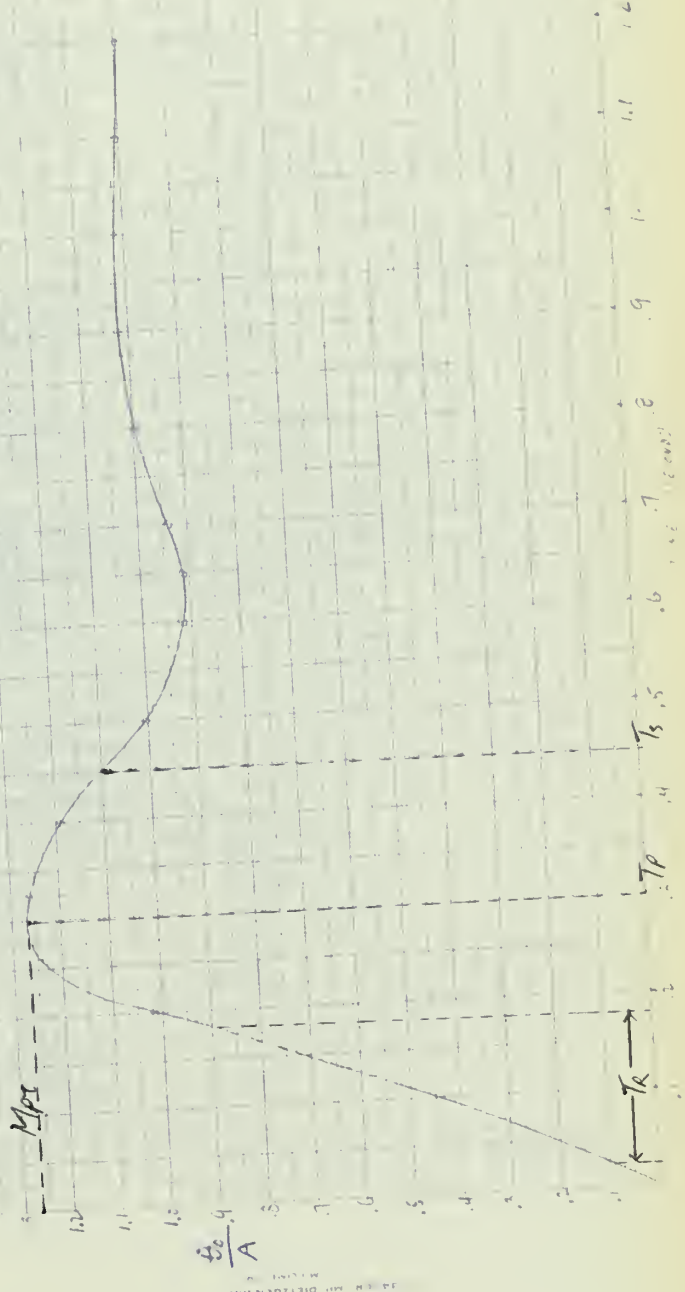
M_{pw} (Magnitude, peak, frequency basis) = 1.43

ω_{pw} (Frequency of M_{pw}) = 66 radians per second

M_{pt} (Magnitude, peak time basis) = 1.26

T_p (Time of M_{pt}) = .3 seconds

FIG. 5
TRANSIENT RESPONSE
INTERMEDIATE DESIGN



W_{BW} (Bandwidth, frequency basis)	= 167 radians per second
T_R (Rise Time)	= .152 seconds
T_D (Settling Time)	= .4 seconds

Chapter VI

This chapter includes the experimental verification of the intermediate design and an analysis and discussion of the results obtained. The chapter also includes a lengthy discussion of the components used in the process of closing the loop of the servo system under investigation in order that the reader may be aware of the complexities involved in summing, modulating and amplifying servo signals in systems of this type.

Of considerable interest in this chapter is the discussion of a servo system similar to the intermediate design, but lacking the lead network. It has been suggested that such a system would function in a satisfactory manner, however, the authors were of the opinion that it would not. Needless to say this system was unsatisfactory, verifying the predictions of the theoretical calculations which indicated that both lead and tachometer compensation was necessary.

Without further discussion of the experimental results it should be mentioned at this time that the final design was identically similar to the intermediate design. This, of course, re-emphasizes the necessity for thorough preliminary calculations utilizing standard analytical methods for predicting servo performance.

Description of components

The components of the closed loop system are shown in detail in the block diagram of Figure 1 and the actual laboratory setup in Figure 2. Inasmuch as the components are generally standard items or circuits the discussion of each will be brief. The critical component in the closed loop was the DC power amplifier because of the particular power requirements of the DC torque motor.

The motor was rated at 0.47 amps and 90 volts which required a DC

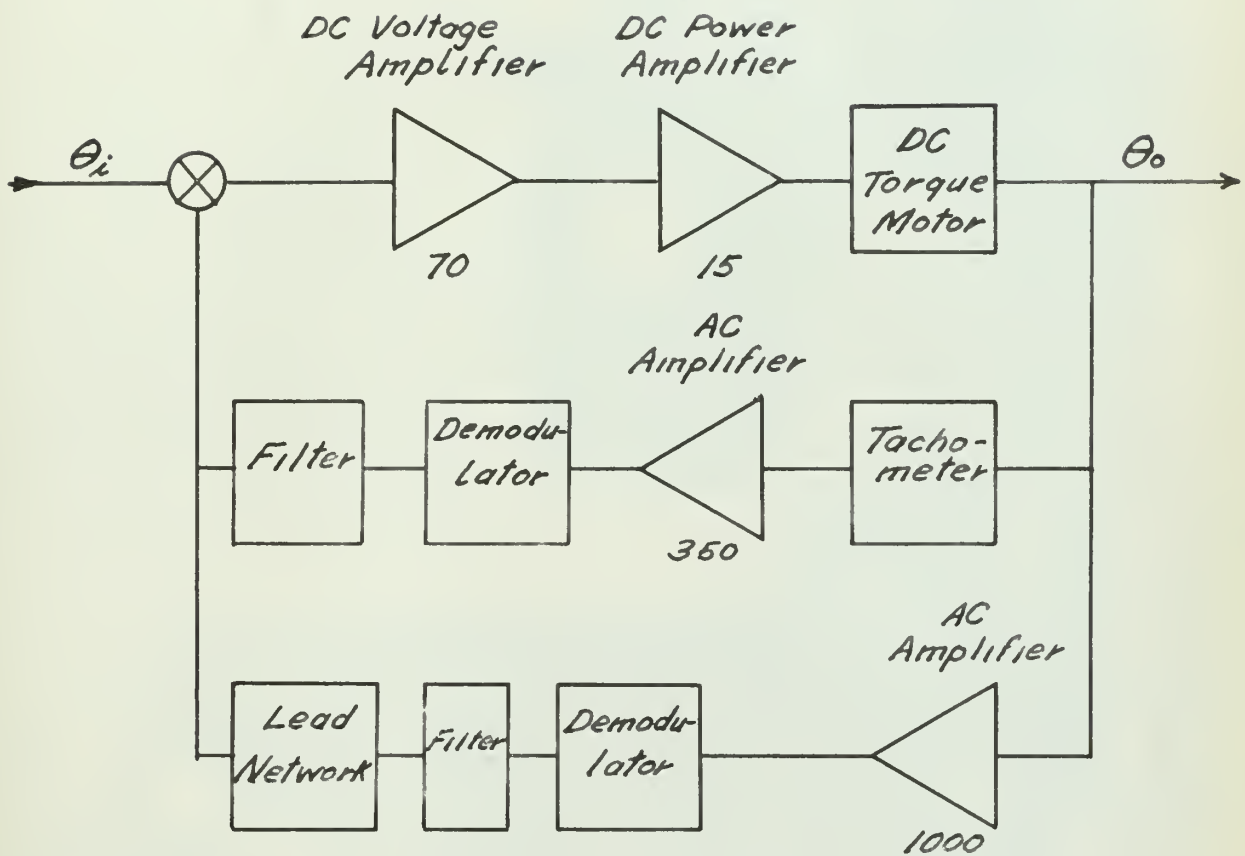
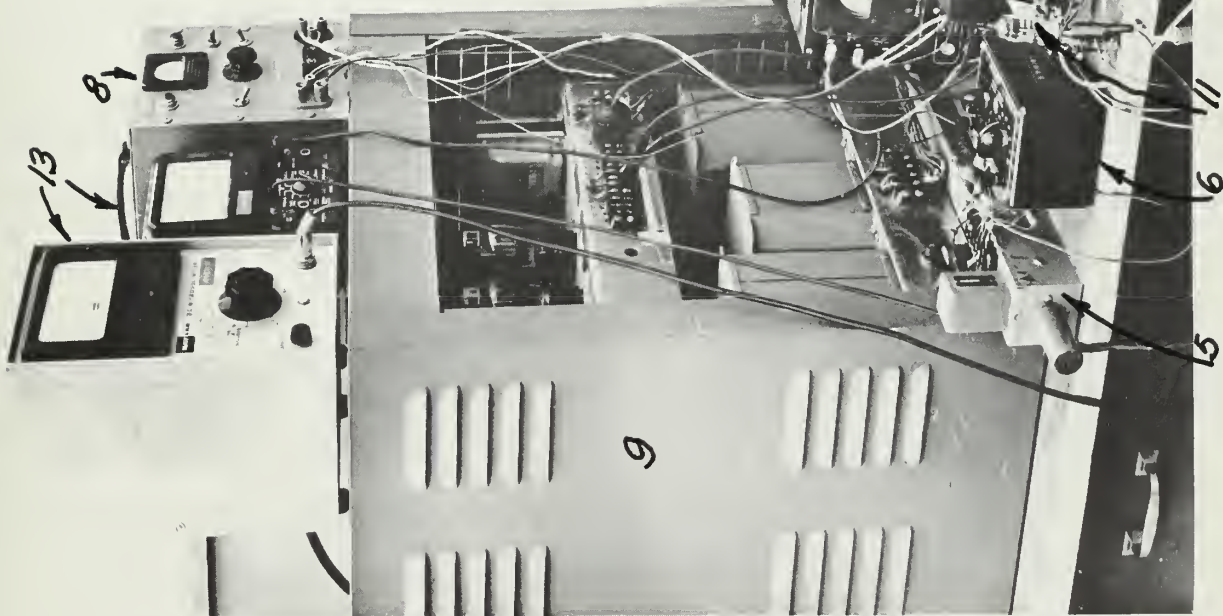


FIG. 1 - Block diagram of closed loop system

- 1 DC power amplifier
- 2 Phase splitter
- 3 AC amplifier in position loop
- 4 AC amplifier in tachometer loop
- 5 Demodulators
- 6 Decade capacitor in lead network
- 7 DC voltage amplifier
- 8 Commercial type DC power supplies (300, 6.3v)
- 9 DC power supply (300 v)
- 10 Transformer for filaments of 6080 tubes in DC power amplifier (110:36v, 3 amps)
- 11 Cathode follower
- 12 Bracket for motor, tachometer and synchro
- 13 Voltmeters



114

amplifier whose capabilities were greater than the common commercial types. By previous arrangement the design and construction of a suitable amplifier was the responsibility of the Dalmo-Victor Company. Some work was done on a transistorized amplifier, however, it was not successful and a vacuum tube amplifier was developed. The complete circuit diagram of the DC power amplifier is shown in Figure 3. The choice of the power tubes was one of economy since there were types available at much higher cost which would have provided the same amplification with fewer tubes.

Briefly, the operation is push-pull to reduce 3rd harmonic distortion and provide a balanced output. The potentiometer in the cathode circuit of the input stage is the balance to insure equal signals to the grids of the first stage power tubes. The zener diodes established the grid signal level at -85 volts for proper operation. The principal of the zener diode is the operation of the diode at the breakdown voltage or back inverse voltage where the voltage remains constant for changes in current.

The input to the power amplifier was double ended, therefore, a phase splitter or DC signal phase inverter was necessary to convert the single ended output of the summing network. The circuit diagram for the phase splitter is given in Figure 4. This circuit is also known as a paraphase amplifier and its operation is described in the literature. The output of the phase splitter is clamped to ground by the zener diodes, glow tube (OB2) and resistances. Several resistances and combinations were tried before this was accomplished.

The AC amplifiers were of different manufacture, however, any number of different types could have been used. The circuit diagram of the AC amplifier in the velocity loop is shown in Figure 5. This circuit is that of an RC amplifier with cathode follower output and feedback and its

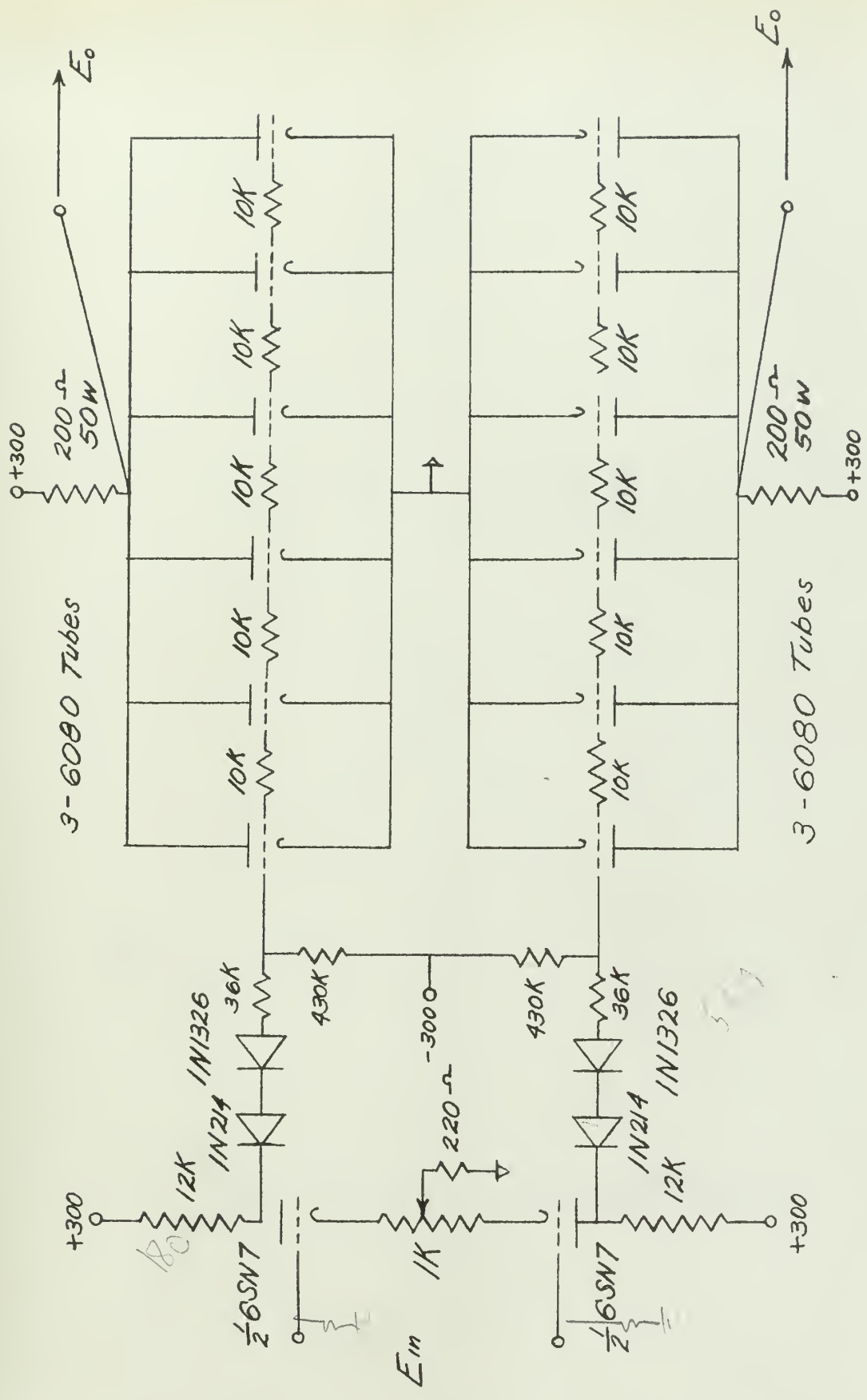


FIG. 3 - DC power amplifier circuit diagram

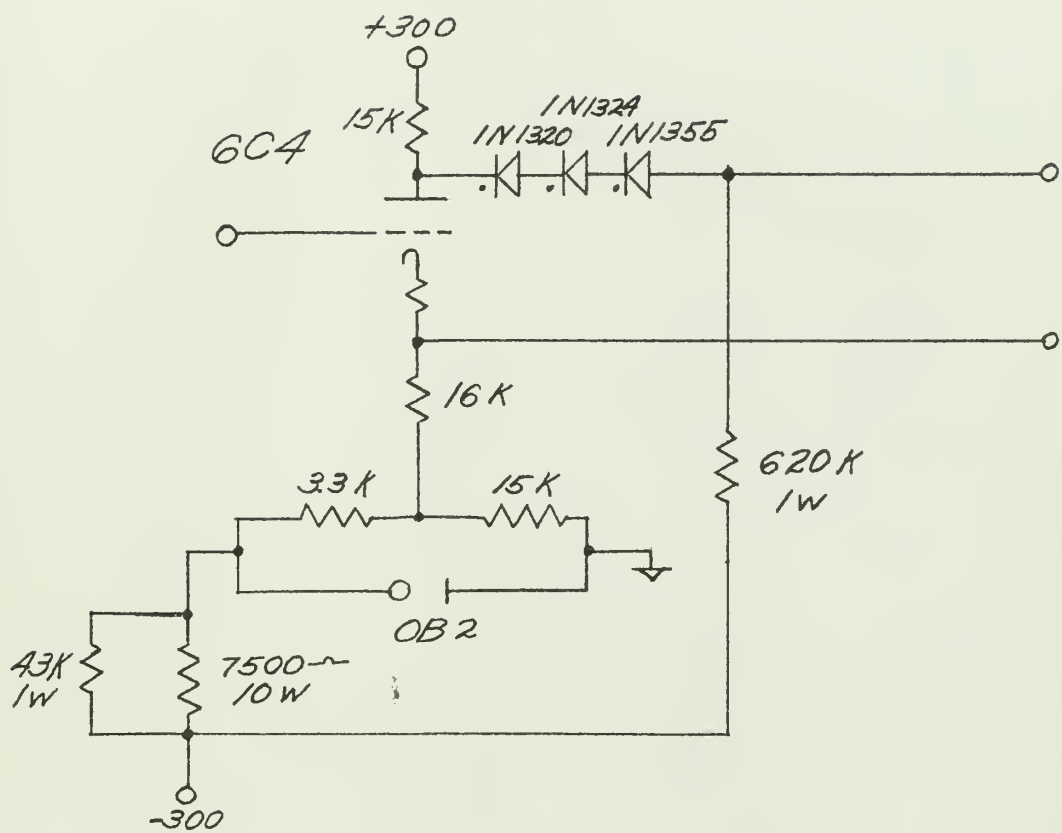


FIG. 4 - Phase Splitter

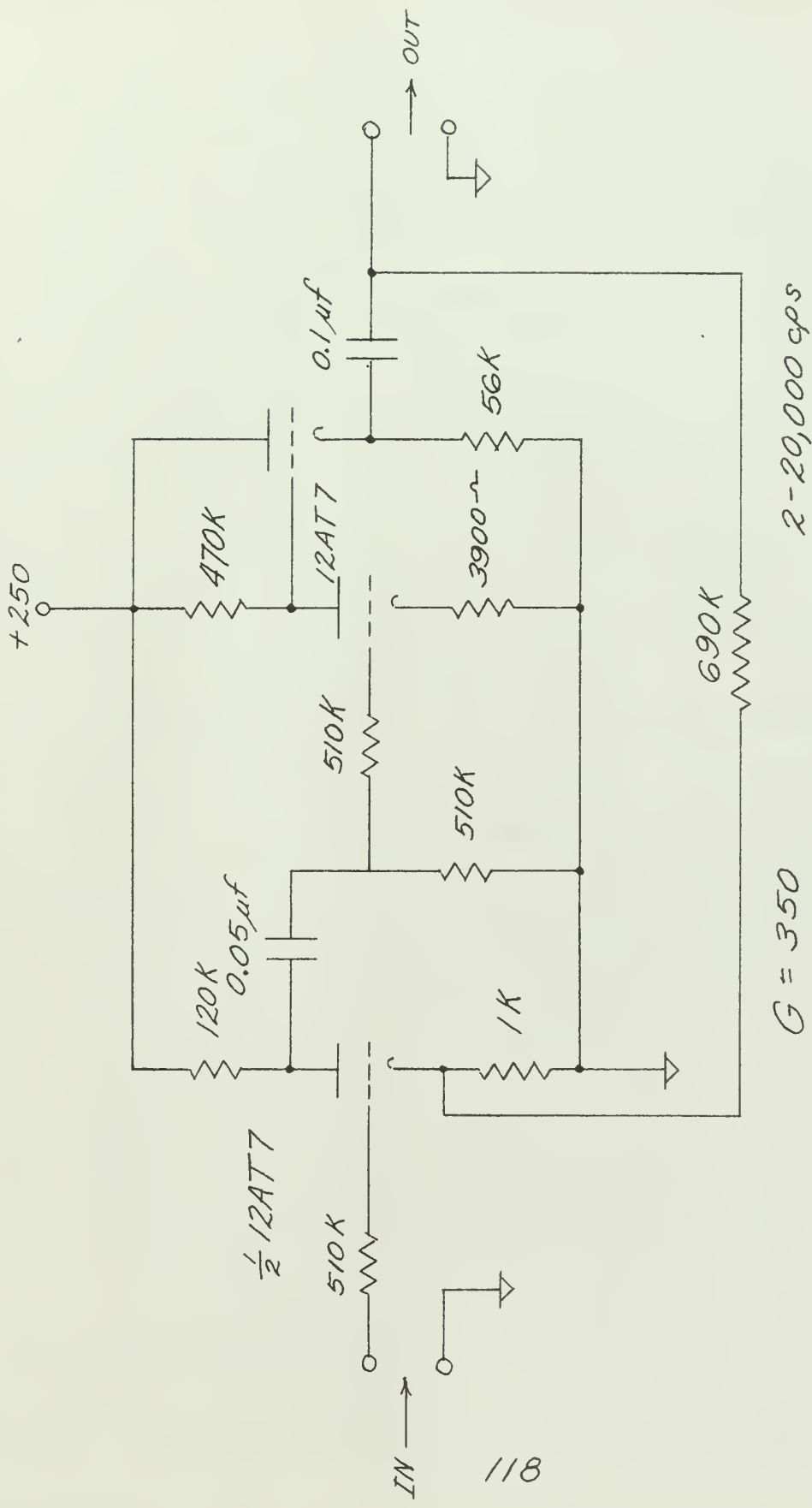


FIG. 5 - AC amplifier in tachometer loop

operation is described in the literature. The AC amplifier in the position loop is shown in Figure 2. It is a commercial type RMS VTVM, Model 320 manufactured by the Ballentine Company.

The demodulator units were both the same. Their circuit diagram is shown in Figure 6. The demodulator is a phase sensitive type described in the literature and utilizes a Sanders, Model 2, Phase Comparator.

A lead network in the position feedback path was combined with filters in both feedback paths to form the summing network shown in Figure 7. It is noted that the decade capacitor of Figure 2 was used to change the lead network until the desired transient response was obtained. The final lead network values are those given in Figure 7.

The DC voltage amplifier was a commercial type manufactured by the Kaylab Company and shown in Figure 2. The gain is variable in steps through 1000 and for the final system the gain was 70.

Additional components not shown in the block diagram of Figure 1 but necessary in the system were the power supplies. Five different supplies were used, two AC and three DC supplies. This was necessary to meet the current requirements of the components other than the power amplifier. They were regulated to $\pm 0.25\%$. The large, locally constructed, DC power supply shown in Figure 2 supplied the 300 volt plate voltages of the power amplifier. The regulation was $\pm 1\%$. Some difficulty was encountered in the closed loop due to inadequate regulation in the power supplies. The filament voltage of the amplifier was supplied by the 36 volt, 3 amp transformer shown in Figure 2. The filaments of the six 6080 tubes were in series and were rated at 2.5 amps each.

The cathode follower shown in Figure 2 was used for isolation in measuring position gain. The motor and bracket is also shown in Figure 2. Shown on top of the large DC supply are the center zero Kaylab DC Micro-

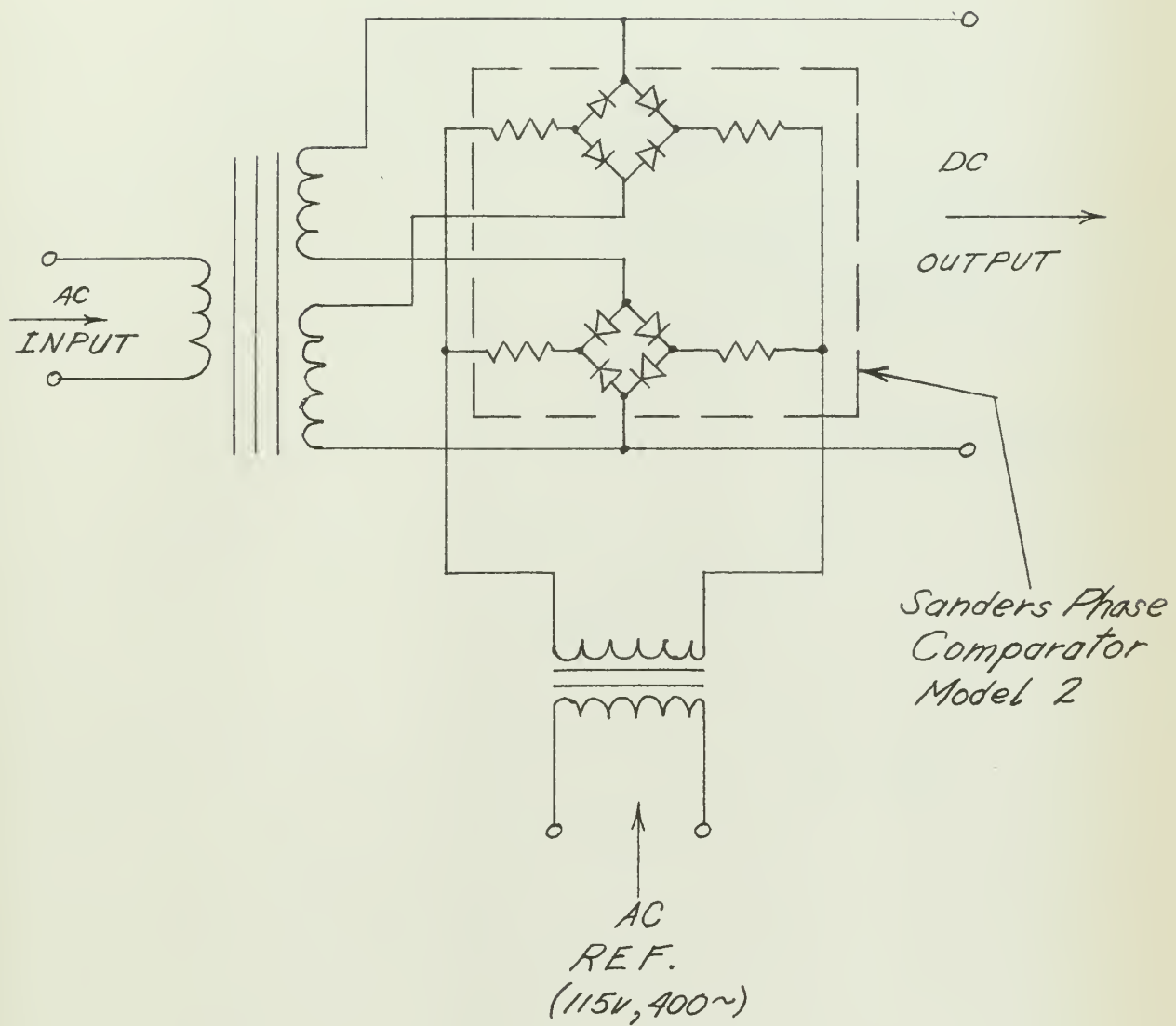


FIG. 6 - Demodulator circuit

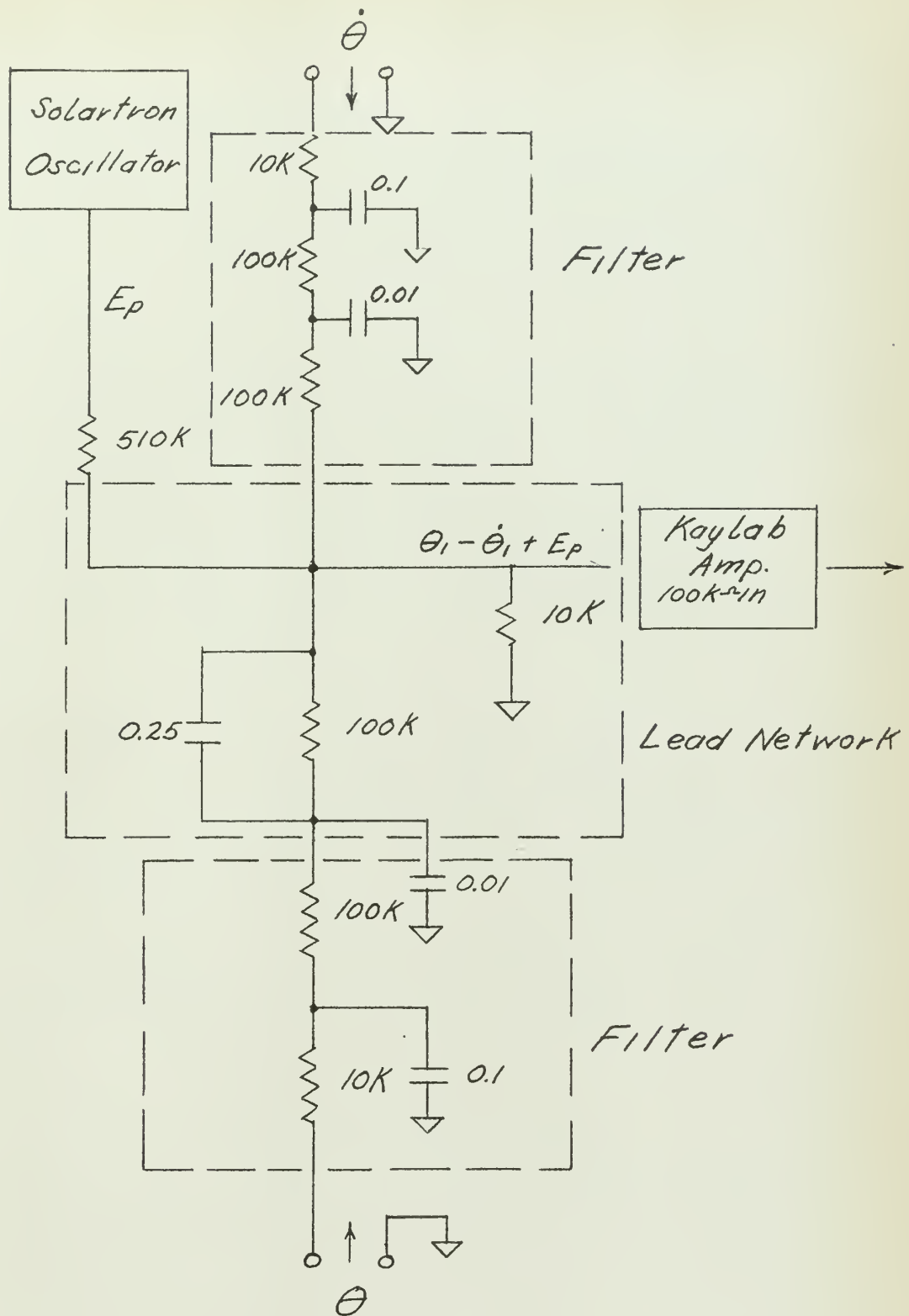


FIG. 7 - Lead network and filters

voltmeter and the Simpson Voltmeter.

Performance of the closed loop components.

With the components described in the previous paragraphs the tachometer and position loops were closed and an evaluation made of components as well as the overall servomechanism to determine if the initial requirements were met.

With the initial closed loop the frequency response determined with the transfer function analyzer (Solartron) showed the crossover frequency to be at 5 cps rather than at 15 cps as stated in the initial design requirements. Nevertheless the evaluation of the electronic position and velocity gain was determined. The block diagram for this test is shown in Figure 8.

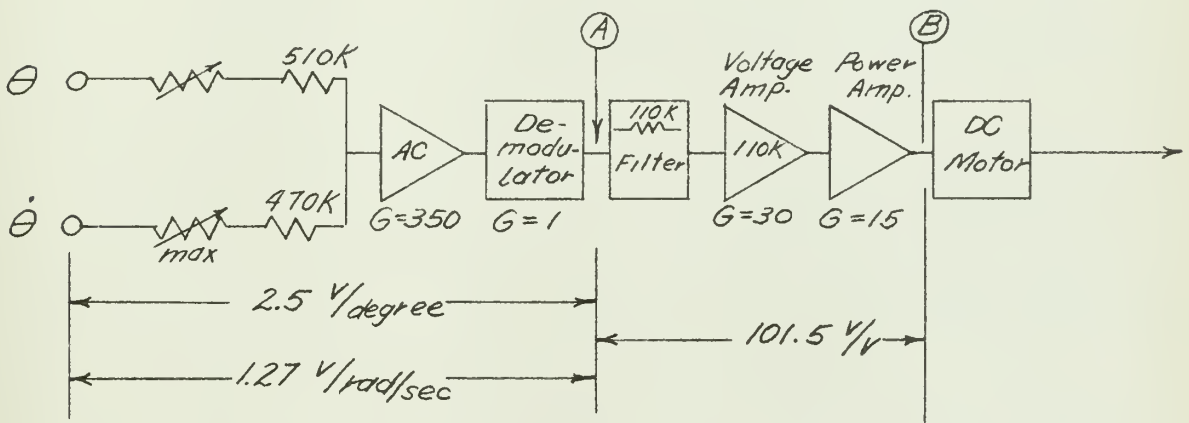


Figure 8 - Block diagram of 5 cps system

The large inertia disk attached to the motor was manually turned in one degree steps while the voltage at point A of Figure 8 was recorded. The polar coordinate paper fastened to the disk as shown in Figure 4 of Chapter V provided an index and convenient measuring device for the one degree increments of rotation. The data obtained from the test is tabulated in Table I. The average number of volts per degree of rotation was

Table I

Disk Position Degrees	Volts
222	-8.30
221	-5.75
220	-2.85
219	-1.00
218	+0.90
217	+3.30
216	+5.75
215	+8.50

2.5 as noted in Figure 8.

To determine the gain from point A to point B in Figure 8 the line at point A was broken and a plus and minus 1.0 volt signal introduced at A while the voltage at B, the plate to ground voltage of the 6080 tubes (see Figure 3) of the power amplifier was measured. The average signal at B for the two different inputs at A was 101.5 volts per volt input as noted on Figure 8.

The velocity gain from θ to point A of Figure 8 was determined by measuring the voltage at A while the load inertia was rotating at 60 RPM. The voltage was 8.0 volts. Converting units the velocity gain was 1.27 volts per radian per second as noted in Figure 8.

To determine the electronic position gain of the position loop an assumed error of one degree was taken. The output function for the position pickoff (synchro) was $17.2 \sin \theta$, or 0.30 volts per degree. Thus the electronic position gain was $(101.5 \times 2.5)/0.30$ or 841 volts per volt.

The minimum usable error signal or static accuracy was required to be 1.5 milliradians or better. Assuming this value or the equivalent, 5.16 minutes, the output of the synchro would be 26 millivolts per degree. That is, the minimum torque at 26 millivolts input should be the friction torque of the system. By measurement, the breakloose voltage across the

motor was 2.5 volts. Therefore, the product of the gain of each component in the position loop times the minimum signal of 26 millivolts must be greater than 2.5 volts. By inspection it can be seen this is the case. An increase or decrease in gain of the voltage amplifier will readily change the product.

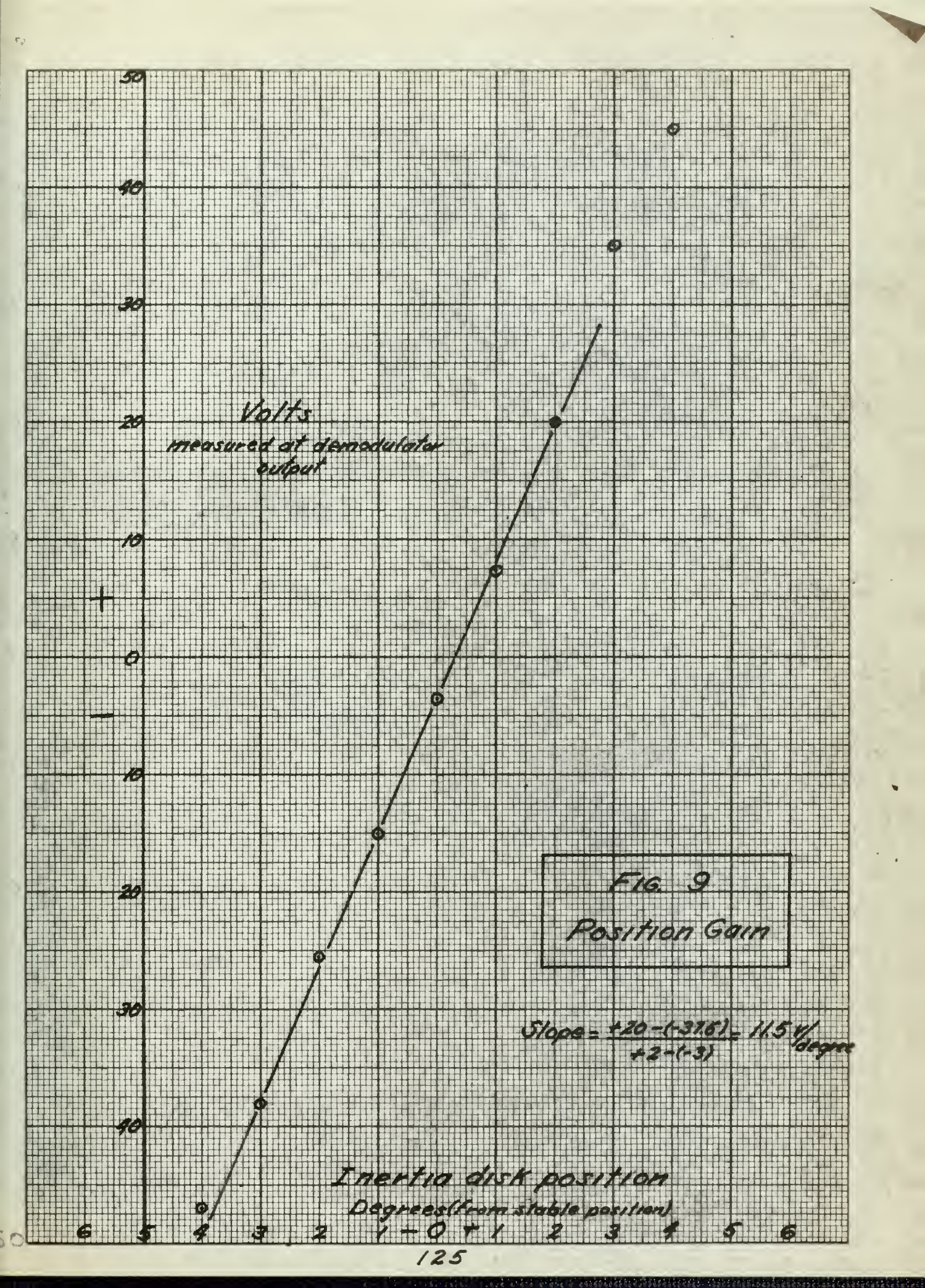
By the addition of a lead network, an AC amplifier in each of the feedback loops and adjustment of the tachometer and position feedback, a closed loop system was obtained whose crossover point was at the desired 15 cps. The following evaluations were on this system.

A requirement of load was a minimum velocity of one milliradian per second as a design goal. To determine if the load would follow at this velocity a function generator was used to provide a sinusoidal error signal of 0.02 cps (1 mr) and the synchro output observed on the scope. The scope presentation was an undistorted sinusoid indicating the system had met the design goal.

The position gain or the gain corresponding to that of Figure 8 from θ to point A was re-evaluated for this system. The data obtained in the same way as before is plotted in Figure 9. The slope of the curve or the position phase detector sensitivity is 11.5 volts per degree. For the static accuracy of 1.5 milliradians or 5.16 minutes the output of the phase sensitive demodulator should not be in error by more than 0.988 volts. ($5.16/60 \times 11.5 = 0.988$ volts). For a periodic 0.1 cps disturbance the maximum amplitude of rotation of the inertia load did not exceed 0.5 degrees, therefore, the peak signal at the output of the demodulator should not exceed ± 5.25 volts.

The velocity gain was determined as before with 40 volts measured at point A of Figure 10 for a 75 RPM rotation of the inertia disk.





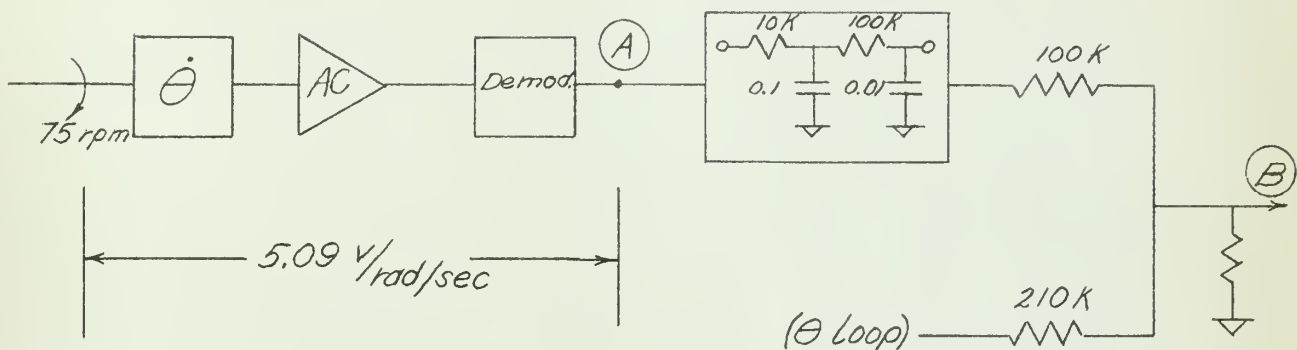


Figure 10 - Velocity gain evaluation

The velocity gain was 5.09 volts per radian per second. The gain at constant velocity and zero frequency from point A to point B in Figure 10 is,

$$\frac{10 \text{ K}}{100 \text{ K}} \times 40 \text{ v} = 1.82 \text{ volts at 75 RPM.}$$

The filter and lead network in the position channel were as illustrated in Figure 11 with the signal value at point A of 11.5

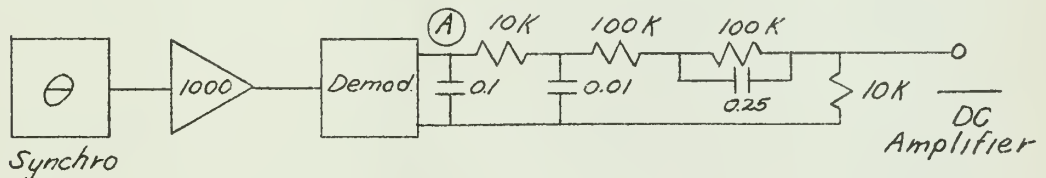


Figure 11 - Filter and lead net gain

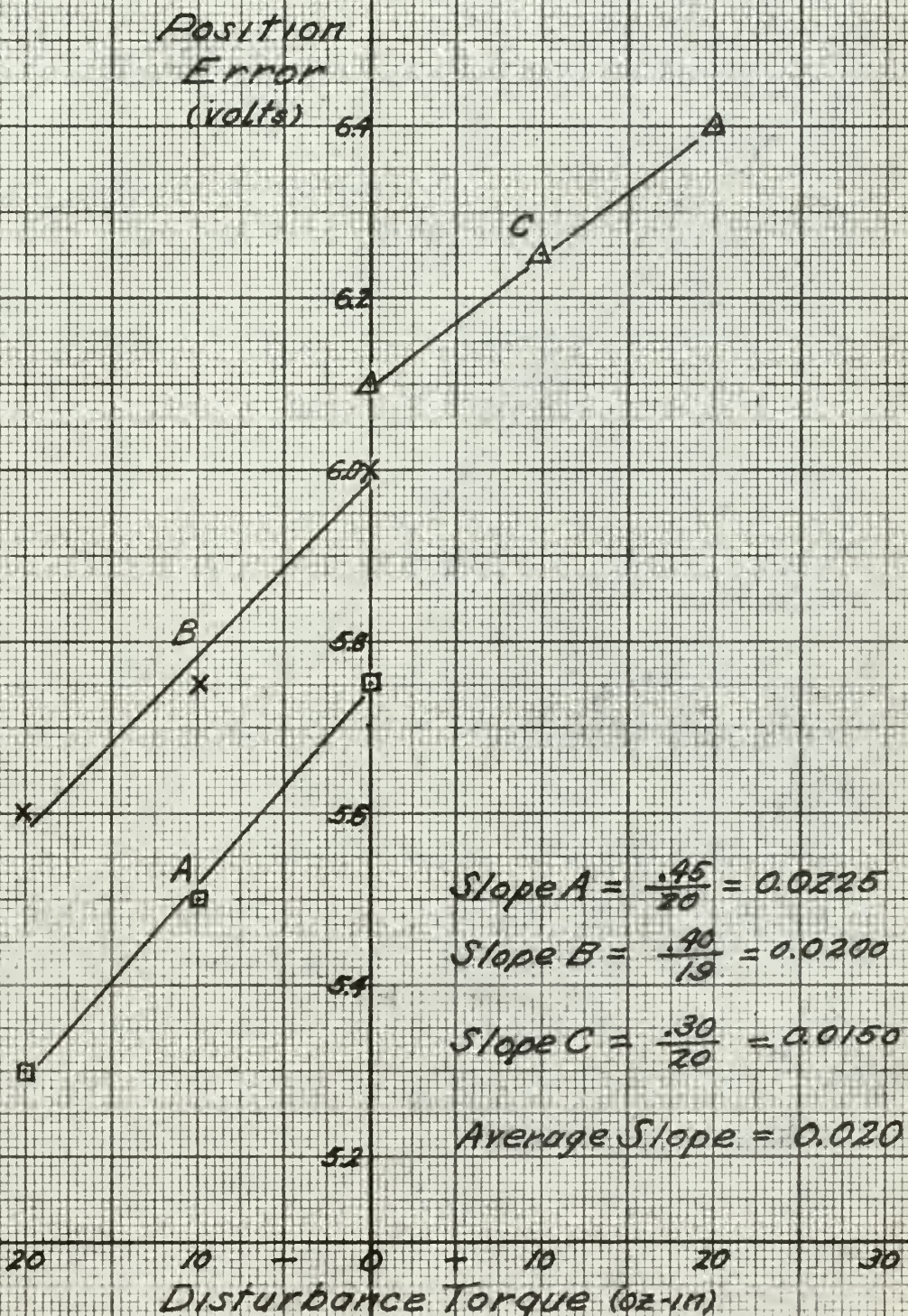
volts per degree. The zero frequency gain at point B is,

$$\frac{10 \text{ K}}{220 \text{ K}} \times 11.5 \frac{\text{volts}}{\text{degree}} = 0.523 \text{ volts/degree.}$$

The torque constant (ounce-inches per volt) was determined by a disturbance torque introduced with a torque watch at the shaft of the inertia disk

FIG. 12

Torque Constant



and observation of the voltage at the output of the position loop demodulator. The data is plotted in Figure 12. The approximate slope is 0.02 volts per ounce-inch. The inverse slope is 50.0 ounce-inches per volt. To determine the closed loop torque gain (ounce-inches per degree) the torque constant determined above was multiplied by the zero frequency gain determined above. The closed loop torque gain is 26.2 ounce-inches per degree.

As determined in Chapter IV the actual static friction of the motor load combination was 1.55 ounce-inches. Therefore, the minimum error in the system necessary to produce motion is,

$$1.55 \text{ oz-in} \times \frac{1 \text{ degree}}{26.2 \text{ oz-in}} = 0.059 \text{ degrees, or}$$

0.942 milliradians. The dead zone is illustrated in Figure 13. The

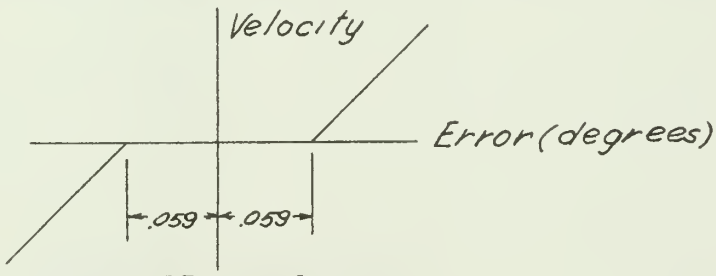


Figure 13 - Dead zone

steady state dynamic error can be less than 0.942 milliradians.

Additional requirements of load were a maximum velocity of 2 radians per second and maximum acceleration of 20 radians per second squared. From Figure 14 the point determined by these requirements is marked A. The corresponding frequency is 1.6 cps and the amplitude ± 12 degrees peak. To determine if these values could be achieved the transfer function analyzer (Solartron) was placed in the position loop as shown in Figure 15. The amplitude of the sinusoidal signal from the Solartron was varied and the error out signal observed on an oscilloscope for distortion. Electronic saturation in the demodulator unit occurred at an amplitude of ± 4 degrees



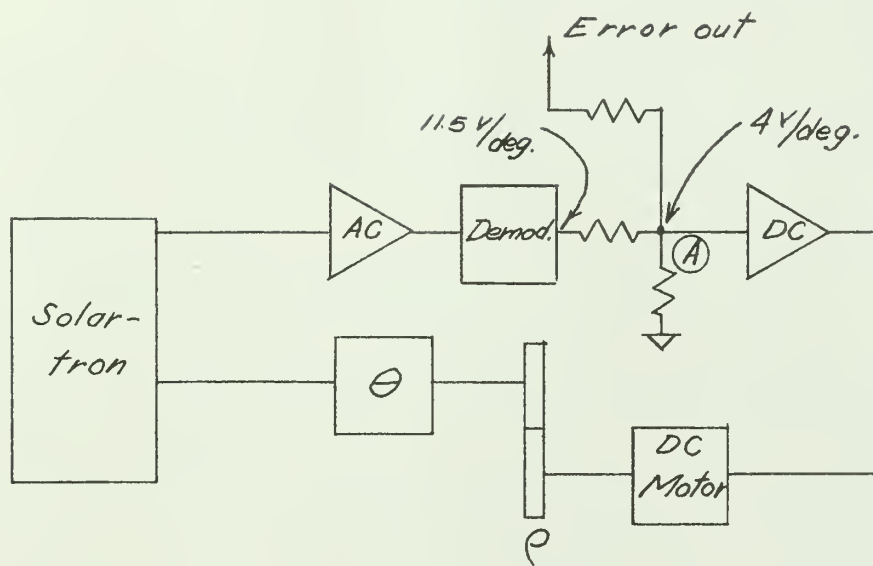


Fig. 15 - Solartron in position loop

peak. At point A of Figure 15 the sensitivity was determined to be 4 volts per degree.

The design requirements were for a 40 db gain (100) at 1 cps thus the maximum error for this gain condition was,

$$4 \text{ degrees} \times \frac{1}{100} \times \frac{60 \text{ minutes}}{\text{degree}} = 2.4 \text{ minutes.}$$

The actual error at point A was 0.7 volt or,

$$\frac{0.7}{4} \frac{\text{volt}}{\text{volt/degree}} \times \frac{60 \text{ minutes}}{\text{degree}} = 10.5 \text{ minutes of}$$

error. The 1 cps gain was,

$$\frac{4 \text{ degree}}{10.5 \text{ minutes}} \times \frac{60 \text{ minutes}}{\text{degree}} = 24 \text{ or } 27.6 \text{ db.}$$

For an assumed -6 per octave slope the gain at one radian per second is 43.6 db (velocity gain).

On Figure 14 the line labeled "electronic saturation" was determined by the ± 4 degree peak amplitude obtained above. The acceleration limit was determined by torque saturation with the 50 pound-inch squared inertia disk. It is noted that these two lines define a region within which any point establishes the velocity and acceleration response of the servo. The intersection establishes the maximum response of approximately 1 radian per second for velocity and 10 radians per second squared for acceleration. The servo did not meet the initial design requirements of 2 radians per second for velocity and 20 radians per second squared for acceleration.

Transient and frequency response of the closed loop system.

The transient response for the closed loop system was obtained in the conventional manner utilizing an oscilloscope, polaroid camera and function generator. A position step input of one volt was applied to the system and the output wave form was observed using the oscilloscope and camera. Figure 16 is the photograph of the transient response so obtained,

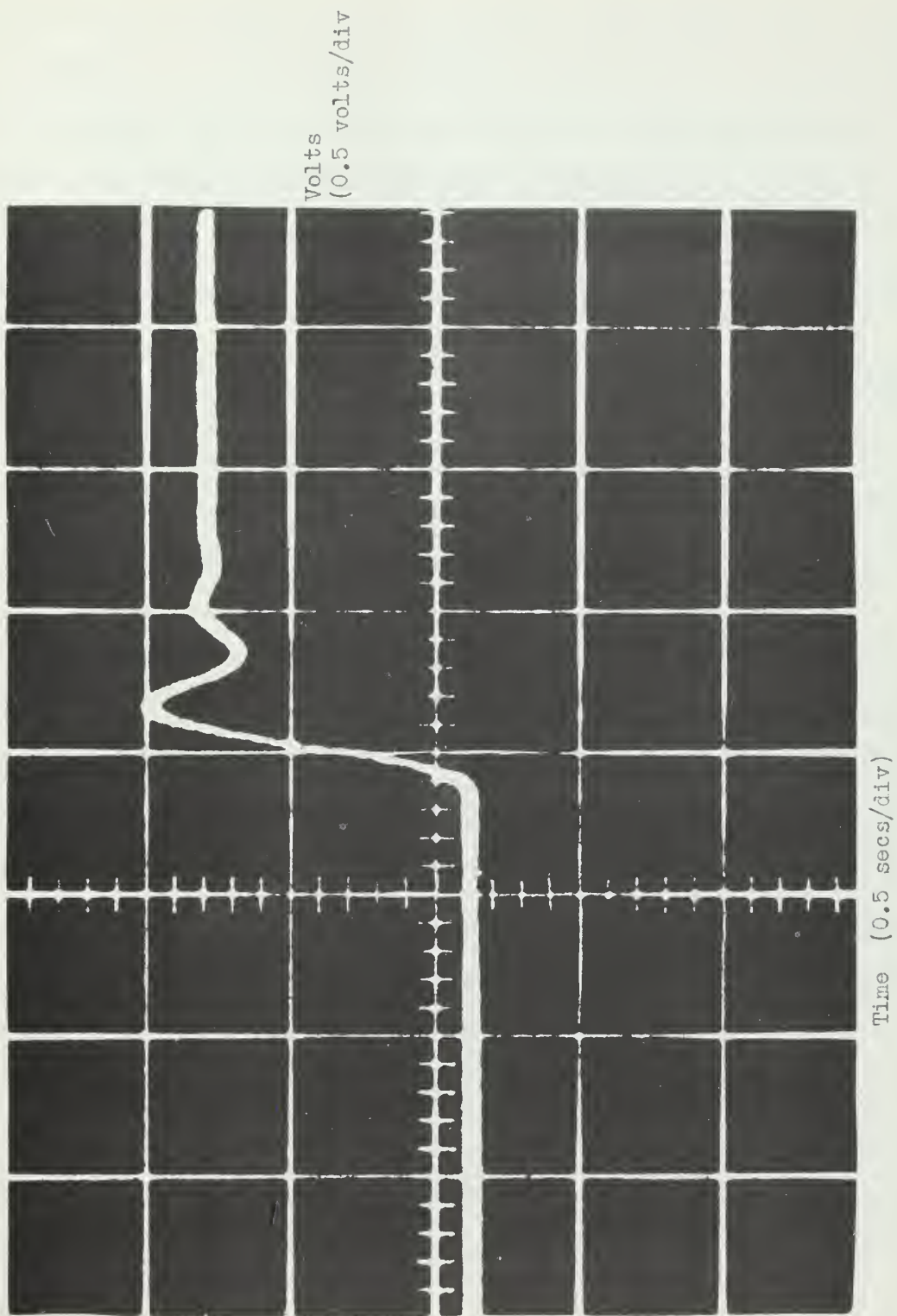


Fig 16 FINAL RESPONSE (TRANSIENT) OF CLOSED LOC SYSTEM

which should be compared with the prediction graphically shown in Figure 5 of Chapter V. Considerable difficulty was encountered in the vertical and horizontal adjustment of the oscilloscope during the operation of the system. The following is a tabulation of the pertinent data represented by this experimental verification of the intermediate design and is compared below with the prediction data of page 109. Close correlation is evident.

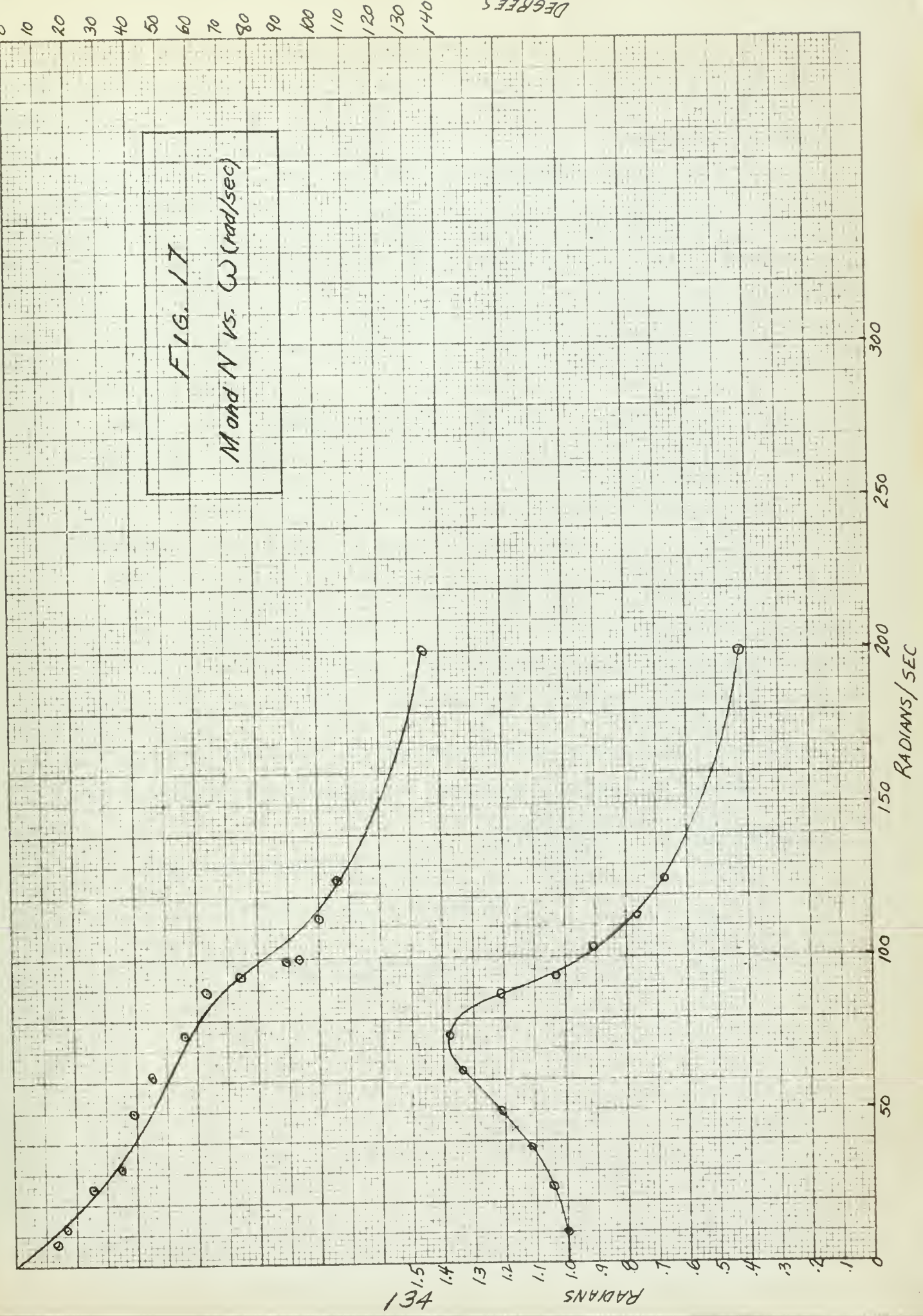
	<u>Theoretical</u>	<u>Experimental</u>
M_{pt} (peak magnitude, seconds)	1.26	1.3
T_p (time of M_{pt} , seconds)	0.3	0.3
T_r (rise time, seconds)	0.152	0.15
T_s (settling time, seconds)	0.4	0.4

The frequency response of the system was obtained by use of the "Solartron", a transfer function analyzer manufactured by the Research and Development Division, Solartron Laboratory Instruments Ltd., Thames Ditton, England. The Solartron has been specially developed for use in testing of servo systems. The phase and amplitude characteristics with frequency may be readily determined under either open or closed loop conditions. The information is provided in a manner such that it may be directly plotted in the form of a Nyquist diagram.

The total equipment comprises a Low Frequency Oscillator OS 103 and a Low Frequency Phase Sensitive Voltmeter VP 253. The nominal frequency range for the overall equipment is 0.5 cps to 1 kcps, but useful measurements can be made down to 0.2 cps or even to 0.1 cps at reduced accuracy.

The basic principle of operation is as follows. The oscillator OS 103 provides a sinusoidal electrical disturbance of known voltage and frequency to the system under test. The resulting signal, at the desired





point of measurement, is then directly indicated by the Low Frequency Phase Sensitive Voltmeter VP 253. This instrument displays the measured signal in the form of two resolved voltage components, utilizing the oscillator output voltage as phase reference. The Low Frequency Phase Sensitive Voltmeter employs the wattmeter principle for phase resolution and, consequently, achieves the greatly desired characteristics that the measurements obtained are unaffected by the presence of harmonics or unrelated frequencies.

In short, this equipment provides the user with the A and B components of the complex number $A + Bj$. When reduced to polar form the data represents M/N where M represents magnitude and N represents phase shift, both referred to a sinusoidal input of one volt RMS.

Using the equipment in the prescribed manner, data was obtained which was resolved and plotted as Figure 17. This figure should be compared with Figure 4 of Chapter V, the theoretically obtained prediction. Close correlation is evident. The following is a tabulation of the pertinent data represented by this experimental verification of the intermediate design and is compared with the prediction data of page 109.

	Theoretical	Experimental
M_{pw} (peak magnitude, radians)	1.43	1.38
ω_{pw} (frequency of M_{pw} , radians/second)	66	75
ω_{bw} (bandwidth, radians/second)	167	122

CONCLUSIONS

It can be concluded from this investigation that the direct drive DC motor provides the servo engineer with a torque producing source which has many important advantages. The elimination of backlash and servo resonance problems are probably the principle advantages although this investigation verified that the DC motor under investigation was essentially a linear device, which is also important.

It is felt that the analytical methods used and the assumptions made in this investigation, insofar as theoretical system performance is concerned, are entirely valid. The authors feel that the transfer functions presented provide the engineer with the tools necessary for the prediction of system performance whenever direct drive DC motors are used in servo control.

Of principle interest in this investigation was the revelation that both lead and tachometer feedback compensation is required to produce a satisfactory system. Further investigation in this field appears warranted.

Finally, it should be mentioned that this investigation involving both theoretical calculations and experimental verification proved conclusively that actual system performance can be closely approximated and predicted by analytical techniques when valid assumptions are made and when individual component characteristics are determined using accurate and reliable methods.





thesP315

Design, analysis and test of a DC servom



3 2768 001 97905 7
DUDLEY KNOX LIBRARY